LEABHARLANN CHOLÁISTE NA TRÍONÓIDE, BAILE ÁTHA CLIATH | TRINITY COLLEGE LIBRARY DUBLIN
Ollscoil Átha Cliath | The University of Dublin

Terms and Conditions of Use of Digitised Theses from Trinity College Library Dublin

Copyright statement

All material supplied by Trinity College Library is protected by copyright (under the Copyright and Related Rights Act, 2000 as amended) and other relevant Intellectual Property Rights. By accessing and using a Digitised Thesis from Trinity College Library you acknowledge that all Intellectual Property Rights in any Works supplied are the sole and exclusive property of the copyright and/or other IPR holder. Specific copyright holders may not be explicitly identified. Use of materials from other sources within a thesis should not be construed as a claim over them.

A non-exclusive, non-transferable licence is hereby granted to those using or reproducing, in whole or in part, the material for valid purposes, providing the copyright owners are acknowledged using the normal conventions. Where specific permission to use material is required, this is identified and such permission must be sought from the copyright holder or agency cited.

Liability statement

By using a Digitised Thesis, I accept that Trinity College Dublin bears no legal responsibility for the accuracy, legality or comprehensiveness of materials contained within the thesis, and that Trinity College Dublin accepts no liability for indirect, consequential, or incidental, damages or losses arising from use of the thesis for whatever reason. Information located in a thesis may be subject to specific use constraints, details of which may not be explicitly described. It is the responsibility of potential and actual users to be aware of such constraints and to abide by them. By making use of material from a digitised thesis, you accept these copyright and disclaimer provisions. Where it is brought to the attention of Trinity College Library that there may be a breach of copyright or other restraint, it is the policy to withdraw or take down access to a thesis while the issue is being resolved.

Access Agreement

By using a Digitised Thesis from Trinity College Library you are bound by the following Terms & Conditions. Please read them carefully.

I have read and I understand the following statement: All material supplied via a Digitised Thesis from Trinity College Library is protected by copyright and other intellectual property rights, and duplication or sale of all or part of any of a thesis is not permitted, except that material may be duplicated by you for your research use or for educational purposes in electronic or print form providing the copyright owners are acknowledged using the normal conventions. You must obtain permission for any other use. Electronic or print copies may not be offered, whether for sale or otherwise to anyone. This copy has been supplied on the understanding that it is copyright material and that no quotation from the thesis may be published without proper acknowledgement.

Computational Investigations of Mesenchymal Stem Cell Ageing in Mechanobiological Simulations of Tissue Differentiation

Feng Xue, B.E., M.Sc.

A thesis submitted to the University of Dublin in partial fulfilment of the requirements for the degree of

Doctor in Philosophy

Trinity College Dublin

Supervisor

Dr. Patrick J. Prendergast

Co-supervisor

Dr. Alexander B. Lennon

External examiner

Prof. Damien Lacroix

Internal examiner

Prof. Daniel J. Kelly

TRINITY COLLEGE
5 JAN 2015
LIBRARY DUBLIN

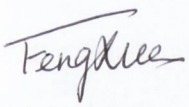
Thesis 10744

Declaration

I declare that this thesis has not been submitted as an exercise for a degree at this or any other university and it is entirely my own work.

I agree to deposit this thesis in the University's open access institutional repository or allow the Library to do so on my behalf, subject to Irish Copyright Legislation and Trinity College Library conditions of use and acknowledgement.

Feng Xue



October, 2013

Abstract

Musculoskeletal health is a major determinant of the quality of life for the increasing aged population groups in our society. Improved healthcare is essential to ensure successful ageing and enhanced musculoskeletal health is pivotal for tackling age-associated diseases such as osteoporosis and osteoarthritis. The primary clinical solutions for treating such diseases are well established for the young population. However, for these therapies to be successful in elder age groups, for whom tissue repair is mostly needed, it is important to understand the influence of mesenchymal stem cell (MSC) ageing to the tissue differentiation.

A predictive computational model was created using finite element models of single cells implemented with the mechanoregulation theory developed by Prendergast et al. (1997). Two mechanobiological events, the gap tissue formation in reconstructive medicine and the MSC differentiation upon substrate stretching in tissue engineering, were simulated to investigate the effects of MSC ageing on cell-tissue differentiation.

The model was able to capture the sub-cellular changes associated with MSC ageing that is without the reach of other mechanoregulation modelling approaches. Simulation results revealed that changes were evident in the predicted tissue differentiation patterns in response to the application of age-related changes in both events, indicating that MSC ageing affects tissue differentiation and therefore should be considered as a factor when performing MSC-based clinical applications.

Most importantly, it was also demonstrated that the presented cell-based mechanoregulation modelling approach is capable of corroborating mechanoregulation theories with basic *in vitro* cell experiments. It could also potentially be used to calibrate well-established mechanoregulation algorithms in the future, to give reliable individual-based, and ultimately, patient-specific predictions prior to operation. Mechanoregulation simulation, or computational mechanobiology as a whole, would then realise its true clinical potential.

Acknowledgements

First and foremost I would like to gratefully thank my esteemed supervisor, Prof. Patrick Prendergast. It has been an honour to be his Ph.D. student. I appreciate all his contributions of time, ideas, and funding to make my Ph.D. experience productive and stimulating. The joy and enthusiasm he has for his research was contagious and motivational for me, even during tough times in the Ph.D. pursuit. I am also thankful for the excellent example he has provided as a successful engineer, scientist and professor.

The members of the Bioengineering group and staff in the department have contributed immensely to my personal and professional time at Trinity. The group has been a source of friendships as well as good advice and collaboration. Sheena in particular, who was always very gracious and helpful for all the administration needs. I would also like to thank Orlagh, Sinead and Helen for their administrative supports. Over the years, Thomas and Iratxe generously advised me on aspects of my project, to whom I am extremely grateful. My postgraduate studies would not have been the same without the social and academic challenges and diversions provided by all my fellow Bioengineers, both past and present –Hanifeh, Katey, Pavel, Stephen, Colin, Colm, Kevin and everyone in the Parsons building.

I would like to acknowledge Dr. Alex Lennon and thank him for his co-supervision, for giving me so much support, even on distance, and for his friendship.

Lastly, I would like to thank my family for all their love and encouragement. For my parents who raised me with a love of science and supported me in all my pursuits. And most of all for my loving, supportive, encouraging, and patient wife Ling whose faithful support during the final stages of this Ph.D. is so appreciated.

Thank you all.

Publications and presentations resulting from this study

Publications

Xue, F., Lennon, A.B., McKayed, K.K., Campbell, V.A., Prendergast, P.J., " The Effect of membrane stiffness and cytoskeletal element density on mechanical stimuli within cells - an analysis of the consequences of ageing in cells", Computer Methods for Biomechanics and Biomedical Engineering (in press), 2013.

Xue, F., McKayed, K.K., Lennon, A.B., Campbell, V.A., Prendergast, P.J., " Computational Investigation of the Influence of Age on Biomechanics of Mesenchymal Stem Cells", 9th International Symposium in Computer Methods in Biomechanics and Biomedical Engineering, proceedings, 2010, pp 121-129.

Lennon, A.B., Khayyeri, H., Xue, F., Prendergast, P.J., Biomechanical modelling of cells in mechanoregulation, Cellular and Biomolecular Mechanics and Mechanobiology (Ed.: Amit Gefen), 2011 (4), pp. 297-329.

Conference contributions

Xue, F., McKayed, K.K., Lennon, A.B., Campbell, V.A., Prendergast, P.J., "Mechanoregulation Simulations using Finite Element Models of Single Cells", 19th Congress of the European Society of Biomechanics, Patras, Greece, 25- 28th August 2013.

Xue, F., McKayed, K.K., Lennon, A.B., Campbell, V.A., Prendergast, P.J., "Computational Investigation of the Influence of Seeding Density on Biomechanics of Mesenchymal Stem Cell During Differentiation", 19th Annual Conference of the Bioengineering Section of the Royal Academy of Medicine in Ireland, Meath, Ireland, 18-19th January 2013.

Xue, F., McKayed, K.K., Lennon, A.B., Campbell, V.A., Prendergast, P.J., "Do Biophysical Stimuli of Mesenchymal Stem Cells Change with Age during Strain-induced Differentiation? ", 6th World Congress of Biomechanics, Singapore, 1-6th August 2010.

Xue, F., McKayed, K.K., Lennon, A.B., Campbell, V.A., Prendergast, P.J., "Computational Investigation of Possible Mechanisms for Changes in Mechanoresponsiveness with Age for Mesenchymal Stem Cells" 17th Congress of the European Society of Biomechanics, Edinburgh, U.K., 5-8th July 2010.

Xue, F., McKayed, K.K., Lennon, A.B., Campbell, V.A., Prendergast, P.J., "Computational investigation of influence of age on biomechanics of mesenchymal stem cells", 9th International Symposium in Computer Methods in Biomechanics and Biomedical Engineering, Valencia, Spain, 25-28th July 2010.

Xue, F., McKayed, K.K., Lennon, A.B., Campbell, V.A., Prendergast, P.J., "Does Age Influence the Mechanoresponsiveness of Mesenchymal Stem Cells? – A Computational Approach", 16th Annual Conference of the Bioengineering Section of the Royal Academy of Medicine in Ireland, Dublin, Ireland, 25-26th January 2010.

Contents

List of Figures i

List of Tables xii

Nomenclature xiv

1. Introduction 1

1.1 General background 1

1.2 Mechanobiology 3

1.3 Objectives of this thesis 4

2. Literature review 7

2.1 Purpose of this Chapter 7

2.2 Mechanobiology of MSCs 7

2.2.1 MSCs 7

2.2.2 Mechanobiology of MSCs 9

2.2.3 MSC ageing 11

2.3 Cell modelling 12

2.3.1 Continuum approach 13

2.3.2 Tensegrity approach 14

2.3.3 Hybrid approach 16

2.4 Mechanoregulation 19
2.4.1 Mechanoregulation theories 19
2.4.2 Mechanoregulation models 24
2.4.3 Corroboration of mechanoregulation theories 26
2.5 Conclusions 28
3. Methods 30
3.1 Overview of methodologies 30
3.2 The effects of MSC ageing on mechanical stimuli within cells 31
3.2.1 General description of the problem 31
3.2.2 Cell geometry 32
3.2.3 Material modelling 34
3.2.4 Modelling of age-related changes of MSCs 36
3.2.5 Loading conditions 37
3.3 Mechanoregulation modelling using whole cell models 38
3.3.1 General background of the problem 38
3.3.2 Finite element model of single cells 39
3.3.3 Establishment of mechanoregulatory boundaries on cellular components 39
3.4 Finite element modelling of gap tissue formation 43

3.4.1 General background of the problem 43
3.4.2 Finite element model of gap tissue 44
3.4.3 Loading conditions 45
3.4.4 Modelling of debonding 46
3.5 Finite element modelling of substrate stretching 47
3.5.1 General description of the problem 47
3.5.2 Finite element model of substrate stretching 49
3.5.3 Modelling of cell-cell interactions 51
3.5.4 Loading conditions 52
4. Results 53
4.1 Finite element modelling of a single adherent cell 53
4.1.1 Cell stiffness 53
4.1.2 Force-displacement curves 54
4.1.3 Biophysical stimuli inside cells 55
4.2 Finite element modelling of gap tissue formation 59
4.2.1 Tissue differentiation under force control 59
4.2.2 Tissue differentiation under motion control 60
4.2.3 The effects of debonding 61
4.2.4 The effects of age-related changes 61
4.3 Finite element modelling of substrate stretching 82

4.3.1 Effects of MSC ageing 82

4.3.2 Effects of seeding density 87

5. Discussion 88

5.1 Introduction 88

5.2 Limitations 88

5.3 Finite element modelling of a single adherent cell 91

5.3.1 Cell modelling approach 92

5.3.2 AFM indentation simulation 93

5.3.3 MSC ageing 95

5.3.4 Main conclusions 96

5.4 Finite element modelling of gap tissue formation 97

5.4.1 The effects of debonding 99

5.4.2 The effects of age-related changes 101

5.4.3 Main conclusions 102

5.5 Finite element modelling of substrate stretching 103

5.5.1 MSC differentiation 104

5.5.2 MSC apoptosis 106

5.5.3 Linkage between cell experiments to mechanoregulation theories 107

5.5.4 MSC ageing 107

5.5.5 Main conclusions 108

5.6 Corroboration of mechanoregulation theories 109

6. Conclusions 111

6.1 Summary of key events 111

6.1.1 Cell modelling 111

6.1.2 Role of MSC ageing in gap tissue differentiation 112

6.1.3 Role of ageing in MSC differentiation subjected to uniaxial loading 113

6.2 Main findings of this work 114

6.3 Future work 116

Bibliography 118

Appendices 139

Appendix A 139

The predicted tissue differentiation patterns under force-control without debonding 139

Appendix B 144

The predicted tissue differentiation patterns under force-control with one debonding surface (debonding case 1) 144

Appendix C 149

The predicted tissue differentiation patterns under force-control with two opposite debonding surface (debonding case 2) 149

Appendix D 154

The predicted tissue differentiation patterns under force-control with two neighbouring debonding surfaces (debonding case 3) 154

Appendix E 159

The predicted tissue differentiation patterns under force-control with three debonding surfaces (debonding case 4) 159

Appendix F 164

The predicted tissue differentiation patterns under motion-control without debonding 164

Appendix G 169

The predicted tissue differentiation patterns under motion-control with one debonding surface (debonding case 1) 169

Appendix H 174

The predicted tissue differentiation patterns under motion-control with two opposite debonding surfaces (debonding case 2) 174

Appendix I 179

The predicted tissue differentiation patterns under motion-control with two neighbouring debonding surfaces (debonding case 3) 179

Appendix J 184

The predicted tissue differentiation patterns under motion-control with three debonding surfaces (debonding case 4) 184

List of Figures

1.1 General scheme of the proposed approach for the validation of mechanoregulation theories with basic *in vitro* cell experiments (indicated by orange downwards arrows). The inverse process (indicated in solid blue upwards arrows) could potentially be used to calibrate well established mechanoregulation algorithms to perform accurate individual-specific simulations. The specific procedures of each step will be explained in details throughout this thesis..... 6

2.1 The mesengenic differentiation process. Multipotent MSCs derived from bone marrow are capable of proliferating and differentiating into different musculoskeletal tissue types by committing, differentiating, and maturing in a lineage specific fashion. This figure is adapted from Firth and Yuan (2012)..... 9

2.2 Tensegrity structures consist of tensional cables and compressive struts (A). They have been widely used in architectural building blocks (B) since their recognition by the modern and futurist architect R. Buckminster Fuller. Tensegrity structures exist within biological systems in various forms (C) and were introduced into cell mechanics by Donald E. Ingber and utilised to model the CSK of a cell (D). This figure was adapted from The Ingber Lab..... 15

2.3 Figure 2.3. FE models based on the hybrid approach. (A) FE models of McGarry and Prendergast (2004), including discrete elements for MTs (red) and AFs (light blue), and continuum components, including the nucleus, cytoplasm and cell membrane. (B) FE model of De Santis et al. (2011), including MTs (blue), AFs (red) and continuum components (green)..... 18

2.4 Figure 2.4. Schematic representation of Pauwels' hypothesis of the mechanoregulatory tissue differentiation. Modified by Weinans and Prendergast (1996) from Pauwels (1960)..... 20

2.5 Perren and Cordey's ideas were based on how much elongation each tissue type can tolerate. This figure is created based on Perren and Cordey (1980)..... 21

2.6 Mechanobiological model as proposed by Carter et al., (1998). Two lines separate the different predicted tissue types, one line based on tensile strain and one line based on hydrostatic pressure. This figure is created based on Carter et al. (1998).... 21

2.7 Figure 2.7. A schematic representation of Claes and Heigele's hypothesis of the mechanoregulatory tissue differentiation. Modified by Isaksson (2007) form Claes and Heigele (1998)... 22

2.8 Figure 2.8. A schematic representation of mechanoregulatory tissue differentiation (Prendergast et al. 1997)..... 24

3.1 (A) The formation of the CSK network. It is formed by 3 sets of 6-strut flattened tensegrity structures, with the identical second and third set rotated along y-axis by 40 and 80 degrees clockwise, respectively, with struts (red lines) representing MTs and cables (blue dotted lines) representing actin bundles. (B) The formation of the NSK network. The same method shown in applies to 3 sets of round-configuration tensegrity structures, with nuclear lamina and chromatin modelled by struts and cables, respectively. (C) NSK is then placed at the centre of the CSK and the two structures are connected by direct linkages representing IFs (shown in green lines)..... 33

3.2 Schematic representation of the standard linear solid model that was used to characterise the viscoelastic behaviours of the cytoplasm and nucleus. It consists of a spring k1 paralleled with a series of another spring k2 and a dashpot η..... 35

3.3 AFM indentation simulations were performed at two positions on the cell membrane: the apex and one of the receptor sites.... 38

3.4 (A) The formation of CSK-NSK network using multiple sets of regularised tensegrity structures. Each tensegrity structure consists of 6 identical beams and 24 cables of the same dimension (B) A finite element model of a single cell (left) was placed at the centre of a block of a granulation tissue (right). Shear strains that are equivalent to the boundaries expressed

in terms of octahedral shear strain used in mechanoregulation diagram were applied on the top surface of the tissue block..... 42

3.5 Simulation setup of bone/implant gap tissue (shown in green boxes) with a cell placed in each tissue block. The implant is located at the centre (shown in grey)..... 45

3.6 There are four possible debonding case in the current simulation setup. The red lines indicate the surface where debonding occurs. Debonding case (1) denotes there is one debonding surface between implant and gap tissue, whereas Debonding case (2), (3) and (4) indicate debonding occurs at two opposite surfaces, two neighbouring surfaces and three surfaces, respectively 47

3.7 A cell model resided on a substrate. The cell-substrate interactions between the cell basal area and the top surface of the substrate are modelled by direct linkers shown in red..... 50

3.8 Simulation setup for substrate stretching with (A) 5 cells and (B) 4 cells. The interactions between each neighbouring cells are shown in red lines. Note that the distances between each cells are exaggerated for simplification and clarification purposes..... 51

4.1 Force-displacement curves from indentation at two different indenting locations (apex and a receptor site), with the stiffness of cell membrane varying from 0.1 time (x0.1) to 10

times (x10) of the original value for a normal (young) cell. The experimental data are taken from a study measuring the stiffness of bovine chondrocytes using AFM indentation (Ng et al. 2007) and shown in the figure as dotted black curves..... 55

4.2 (A) Contour plots of Von Mises stress during indentation with different indenting locations, at apex (A, B) and a receptor site (C, D) of young cells (A, C) and aged cells (B, D). Cut-views are shown for visual comparison of Von Mises stress inside the cells..... 56

4.2 (B) Area of membrane within a given strain range. Aged cells have smaller membrane area under high strain and correspondingly have greater membrane area under low strain, than young cells subjected to indentation..... 56

4.3 (A) Volume of nucleus within a given strain range (hydrostatic strain). The slim green line indicates zero strain location. Little difference can be seen between the aged and young cells..... 57

4.3 (B) Volume of nucleus within a given strain range (deviatoric strain). The slim green line indicates zero strain location. Differences are seen between aged and young cells at mid-low strain ranges, particularly in the negative region..... 58

4.4 Displacements of the implant when loaded with a vertical downward force of 0.48 μN. Debonding greatly alters the implants' behaviour. However, little change can be seen between

young and aged cells. Debonding 1 – 4 denotes different debonding cases shown in Figure 3.6..... 62

4.5 Reaction force from the implant when loaded with a vertical downward displacement of 12 μm. Debonding greatly alters the implants' behaviour. However, very small changes can be seen between young and aged cells..... 63

4.6 Tissue differentiation patterns of young (A) and aged (B) cells under force-control with a loading magnitude of 0.48 μN. Four different debonding scenarios were simulated and compared with un-debonded case..... 64

4.7 Tissue differentiation patterns of young (A) and aged (B) cells under force-control with a loading magnitude of 0.36 μN. Four different debonding scenarios were simulated and compared with un-debonded case..... 65

4.8 Tissue differentiation patterns of young (A) and aged (B) cells under force-control with a loading magnitude of 0.24 μN. Four different debonding scenarios were simulated and compared with un-debonded case..... 66

4.9 Tissue differentiation patterns of young (A) and aged (B) cells under force-control with a loading magnitude of 0.12 μN. Four different debonding scenarios were simulated and compared with un-debonded case..... 67

4.10 Tissue differentiation patterns of young (A) and aged (B) cells

under motion-control with a loading magnitude of 12 μm. Four different debonding scenarios were simulated and compared with un-debonded case..... 68

4.11 Tissue differentiation patterns of young (A) and aged (B) cells under motion-control with a loading magnitude of 9 μm. Four different debonding scenarios were simulated and compared with un-debonded case..... 69

4.12 Tissue differentiation patterns of young (A) and aged (B) cells under motion-control with a loading magnitude of 6 μm. Four different debonding scenarios were simulated and compared with un-debonded case..... 70

4.13 Tissue differentiation patterns of young (A) and aged (B) cells under motion-control with a loading magnitude of 3 μm. Four different debonding scenarios were simulated and compared with un-debonded case..... 71

4.14 Tissue differentiation patterns under force-control with a loading magnitude of 0.48 μN without debonding. The stiffness of cell membrane was altered from 10% (x0.1) to 10 times (x10) of the original young cell. The high-lighted two lines, i.e. Emem x1 (3T) and Emem x2 (2T) are the young and aged cells, respectively, according to the descriptions in the Methods in this study..... 72

4.15 Tissue differentiation patterns under force-control with a loading magnitude of 0.48 μN with one debonded surface

(Debonding case 1). The stiff-ness of cell membrane was altered from 10% (x0.1) to 10 times (x10) of the original young cell. The highlighted two lines, i.e. Emem x1 (3T) and Emem x2 (2T) are the young and aged cells, respectively, according to the descriptions in the Methods in this study..... 73

4.16 Tissue differentiation patterns under force-control with a loading magnitude of 0.48 μN with two opposite debonded surfaces (Debonding case 2). The stiffness of cell membrane was altered from 10% (x0.1) to 10 times (x10) of the original young cell. The highlighted two lines, i.e. Emem x1 (3T) and Emem x2 (2T) are the young and aged cells, respectively, according to the descriptions in the Methods in this study..... 74

4.17 Tissue differentiation patterns under force-control with a loading magnitude of 0.48 μN with two neighbouring debonded surfaces (Debonding case 3). The stiffness of cell membrane was altered from 10% (x0.1) to 10 times (x10) of the original young cell. The highlighted two lines, i.e. Emem x1 (3T) and Emem x2 (2T) are the young and aged cells, respectively, according to the descriptions in the Methods in this study..... 75

4.18 Tissue differentiation patterns under force-control with a loading magnitude of 0.48 μN with three debonded surfaces (Debonding case 4). The stiffness of cell membrane was altered from 10% (x0.1) to 10 times (x10) of the original young

cell. The highlighted two lines, i.e. Emem x1 (3T) and Emem x2 (2T) are the young and aged cells, respectively, according to the descriptions in the Methods in this study..... 76

4.19 Tissue differentiation patterns under motion-control with a loading magnitude of 12 μm without debonding. The stiffness of cell membrane was altered from 10% (x0.1) to 10 times (x10) of the original young cell. The highlighted two lines, i.e. Emem x1 (3T) and Emem x2 (2T) are the young and aged cells, respectively, according to the descriptions in the Methods in this study..... 77

4.20 Tissue differentiation patterns under motion-control with a loading magnitude of 12 μm with one debonded surface (Debonding case 1). The debond stiffness of cell membrane was altered from 10% (x0.1) to 10 times (x10) of the original young cell. The highlighted two lines, i.e. Emem x1 (3T) and Emem x2 (2T) are the young and aged cells, respectively, according to the descriptions in the Methods in this study..... 78

4.21 Tissue differentiation patterns under motion-control with a loading magnitude of 12 μm with two opposite debonded surfaces (Debonding case 2). The stiffness of cell membrane was altered from 10% (x0.1) to 10 times (x10) of the original

young cell. The highlighted two lines, i.e. Emem x1 (3T) and Emem x2 (2T) are the young and aged cells, respectively, according to the descriptions in the Methods in this study..... 79

4.22 Tissue differentiation patterns under motion-control with a loading magnitude of 12 μm with two neighbouring debonded surfaces (Debonding case 3). The stiffness of cell membrane was altered from 10% (x0.1) to 10 times (x10) of the original young cell. The highlighted two lines, i.e. Emem x1 (3T) and Emem x2 (2T) are the young and aged cells, respectively, according to the descriptions in the Methods in this study..... 80

4.23 Tissue differentiation patterns under motion-control with a loading magnitude of 12 μm with three debonded surfaces (Debonding case 4). The stiffness of cell membrane was altered from 10% (x0.1) to 10 times (x10) of the original young cell. The highlighted two lines, i.e. Emem x1 (3T) and Emem x2 (2T) are the young and aged cells, respectively, according to the descriptions in the Methods in this study..... 81

4.24 Contour plots of cell membrane strain of young and aged cells from top view (A) and bottom view (B) when loaded with 10% uniaxial substrate stretching..... 83

4.25 The membrane stain of young and aged cells subjected to uniaxial stretching of different magnitudes. The value 0.027

shown on the Y-axis is the index for cell-tissue differentiation between bone and cartilage regions as shown in Table 3.5..... 84

4.26 The peak strain of cell membrane when subjected to uniaxial stretching with different magnitudes. The red markers on the Y-axis indicate the strains at which the probabilities of the opening of mechanosensitive, strain-activated ion channels are 100%, 50% and 0%, as demonstrated by Lunze et al. (2009).... 85

4.27 The equivalent membrane strain of a single cell, four cells and five cells, with or without cell-cell interactions when loaded with 10% uniaxial stretching..... 86

List of Tables

3.1 Viscoelastic properties of cellular components..... 36

3.2 Elastic and geometric properties of CSK-NSK components..... 36

3.3 The computed boundaries on cell membrane strain (on the right) as apposed to the mechanoregulatory boundaries (on the left) proposed by Prendergast et al. (1997)..... 43

3.4 Material properties of different tissue types and the implant..... 43

3.5 Mechanoregulatory indexes established on cell membrane strain. The calculation and conversion were explained in details in Chapter 3.3..... 50

4.1 Experimentally measured cell stiffness using AFM from previous studies..... 54

Nomenclature

Variables

G	Shear modulus
K	Bulk modulus
τ	Relaxation time
v	Poisson's ratio
α	a half of opening angle of the indenter tip
δ	Indentation depth
E	Stiffness
S	mechanoregulatory stimulus
γ_{oct}	octahedral shear strain
υ	fluid velocity
ε	Normal strain
γ	Shear strain
k	Spring constant
η	Viscosity
σ	Stress

Acronyms

3D	Three-dimensional
AF	Actin filament
CSK	Cytoskeleton
ECM	Extracellular matrix
IF	Intermediate filament
MT	Microtubules
NSK	Nucleoskeleton
THA	Total Hip Arthroplasty

Chapter 1

1. Introduction

1.1 General background

Musculoskeletal health is a major determinant of the quality of life for the increasing aged population group in our society. The proportion of aged population has been expanding rapidly for the past decades and is expected to increase with an even faster pace for the incoming century, according to the United Nations Statistics. As the life expectancy increases, tackling the age-associated musculoskeletal diseases, such as osteoporosis and osteoarthritis, becomes one core task to ensure a successful ageing.

Traditionally, Total Hip Arthroplasty (THA) was the primary solution for treating osteochondral defects. The surgical procedure involves the implantation of an artificial replacement joint, made by combinations of engineered metals and plastics, into the defected bone cavity and the integration of the implant and the bone by a fixation process. The optimal method of fixation for primary total joint replacements, particularly fixation with or without the use of cement is still controversial (Abdulkarim *et al.*, 2013). While better short-term clinical outcome, particularly in terms of recovery time and pain reduction, can be obtained with cemented fixation, the cement itself tends to deteriorate progressively over time and is considered as a cause of

loosening (Amstutz *et al.*, 1988; Hozack *et al.*, 1990). On the other hand, cementless fixation which allows bone to grow into or onto the implant offers great clinical and functional potential outcomes regarding long-term survival rates. It has been implied that once stable fixation occurs in the cementless implant, it does not deteriorate with time (Engh *et al.*, 1987). However, to achieve such potentials of cementless fixation, it is essential to gain a better understanding of the underlying mechanisms by which bone ingrowth phenomenon initiated by MSCs occur. Furthermore, it remains to be investigated whether or not the ageing of MSCs influences this ossification process.

Tissue engineering approaches offer the potential of avoiding long-term implantation of reconstructive implants by using autologous MSCs seeded in a three-dimensional (3D) scaffold and implanted into the patient. MSCs are undifferentiated progenitor cells that can differentiate into specialised skeletal cells such as osteocytes, chondrocytes, adipocytes and tendon cells (Pittenger *et al.* 1999). Under the appropriate conditions, these cells can be manipulated *in vitro* for the development of skeletal tissue for the application of regenerative medicine. To date, the majority of successes in tissue engineering research have been restricted to young patients, particularly those with degenerative diseases as a result of sporting injuries (Gudas *et al.,* 2003; Saris *et al.,* 2009). For this to be successful in elder age groups, for whom tissue repair is mostly needed, the difference in mechanoresponsiveness of MSCs induced by age-related changes at cellular level must be systematically studied, as MSCs are always subjected to mechanical stimulation, either immediately upon implantation or by *in vitro* mechanical conditioning in a bioreactor prior to implantation.

1.2 Mechanobiology

The idea that mechanical factors can influence tissue growth seems to have been accepted from the earliest times that accounts for the ancient Chinese custom of binding the feet of aristocratic girls. This produced a marked reduction in both longitudinal and lateral growth, as an aid to beauty and denoting social status (Golding, 1993). It remains evident after thousands of years' civilisation as the Padaung women of the Kayan people still wear neck coils from an early age to elongate their necks. The length of the coil is gradually increased with age and could eventually reach as long as a surprising 40 centimetres (Guinness World Record book). It has been shown that wearing the neck coils does not contribute to increasing the overall body height, but rather puts an excessive load on the collarbone and ribs, forcing them to deform (Swanson, 1960). While the true historical incentives and social impact of such historical heritages are still in dispute the consequential biological changes made to the body parts clearly depict the influences of mechanical stimuli on biological systems.

The systematic study of the interactions between mechanical stimuli and biological processes at molecular, cellular, tissue and organ levels is referred to as mechanobiology. One core concept within mechanobiology is that the differentiation of mesenchymal stem cells (MSCs) is modulated by external mechanical stimulation. A number of mechanoregulation theories have been proposed that relate the differentiation pathways of MSCs to their local biomechanical environment. Researchers were able to demonstrate the biological relevance and predictability of these models using computational simulations. One of the most prevailing core theories in mechanoregulation was proposed by Prendergast *et al.* (1997), that relates tissue differentiation to local octahedral shear strain and fluid velocity. Based on this theory, sev-

eral researches have since focused on different aspects in extending this modelling approach, proving it is well suited to modelling mechanoregulation at tissue level in various applications (Lacroix and Prendergast, 2001; Checa and Prendergast, 2010; Nagel and Kelly, 2010; Khayyeri *et al.*, 2012). However, changes at cellular level could not be captured using the present approaches as cells are seen as lattice points within defined tissue boundaries without any cellular composition and structure taken into consideration. Therefore, the author believes that mechanoregulation theories have not been adequately corroborated and must be further developed to capture changes occurs at sub-cellular level, in order to collaborate with basic *in vitro* experimental observations of MSCs differentiation, for validation and calibration purposes. Mechanoregulation would then realise its true potential in reconstructive surgery and regenerative medicine without the immense criticisms in its existence in the first place (Jacobs and Kelly, 2011).

1.3 Objectives of this thesis

In this study, it is aimed to demonstrate that mechanoregulation simulations can be performed using finite element models of single cells implemented with mechanoregulation theories. Additionally, it is also the author's intention to show that the cell-based mechanoregulation modelling approach developed in this work widens the range of mechanoregulation prediction capacity to single MSCs where no tissue formation is necessary, e.g. substrate stretching, and most impotently, mechanoregulation theories can potentially be validated from basic cell experiments using the presented approach (illustrated in Figure 1.1).

To demonstrate the practicality of the proposed cell-based mechanoregulation modelling approach, the influence of MSC ageing to cell-tissue differentiation is investigated by applying it to two biomechanical events, the gap tissue formation in reconstructive medicine and the MSC differentiation upon substrate stretching in tissue engineering. Specifically, it is hypothesised that MSC ageing affects cell-tissue differentiation in both events.

This leads to the objectives of the thesis:

- To create a finite element model of a single cell that is capable of capturing the sub-cellular changes associated with MSC ageing
- To establish mechanoregulatory boundaries on cellular components
- To test if MSC ageing affect the tissue differentiation of gap tissue with biologically relevant loading conditions
- To test if ageing affect MSC differentiation subjected to uniaxial stretching.

If the aims of this thesis are met, the model can be further developed and incorporated into the mechanoregulation algorithm to capture sub-cellular changes. More importantly, this modelling technique provides a possible means of corroborating mechanoregulation theories with basic *in vitro* cell experiments and potentially could be used to calibrate well established mechanoregulation algorithms to give reliable individual-based, and ultimately, patient-specific predictions. Mechanoregulation simulation, or computational mechanobiology as a whole, would then realise its true clinical potential in the field of biomedical engineering.

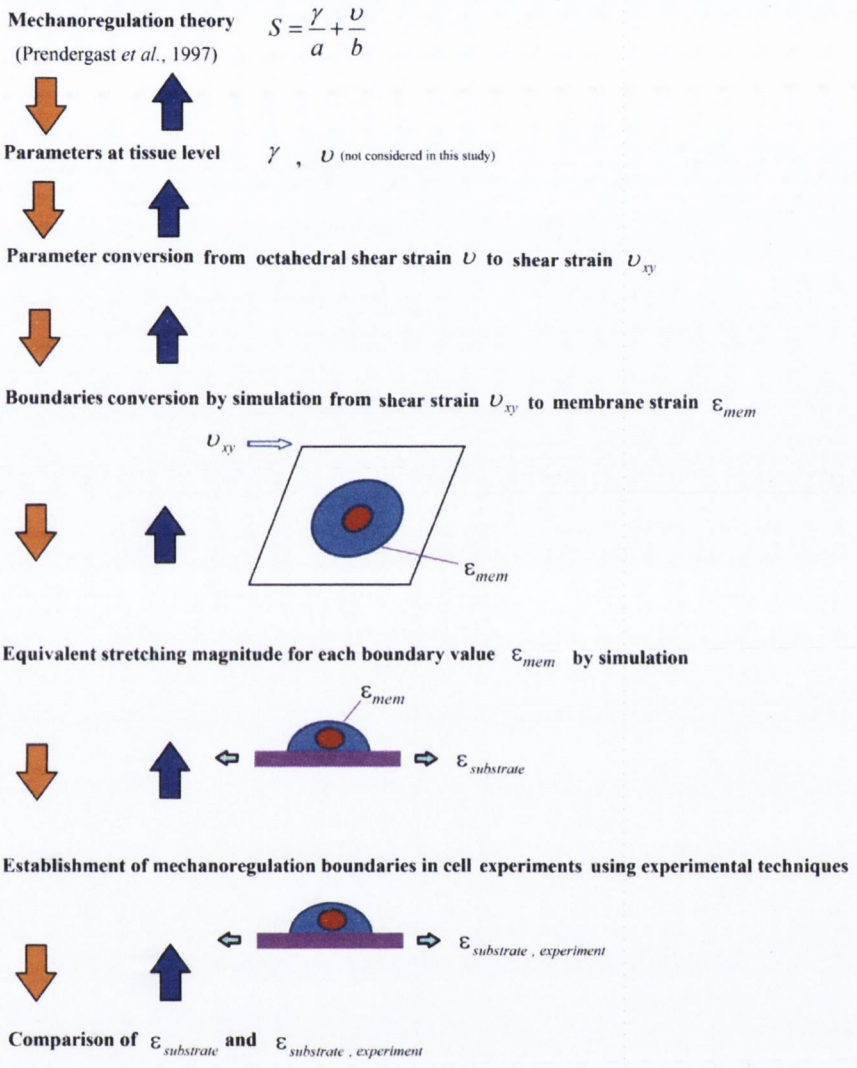


Figure 1.1. General scheme of the proposed approach for the validation of mechanoregulation theories with basic in vitro cell experiments (indicated by orange downwards arrows). The inverse process (indicated in solid blue upwards arrows) could potentially be used to calibrate well established mechanoregulation algorithms to perform accurate individual-specific simulations. The specific procedures of each step will be explained in details throughout this thesis.

Chapter 2

2. Literature review

2.1 Purpose of this Chapter

Issues relevant to MSCs, and in particular the differentiation and ageing , are reviewed first. Next, a survey of computational modelling approaches for single cells and mechanoregulation is presented as a background to the modelling methods to be developed later. Finally, an assessment of mechanoregulation theories and predictive modelling approaches in the literature for mechanoregulation simulations is presented, and the areas that require further development regarding mechanoregulation simulations, particularly, the corroboration of mechanoregulation theories are also identified.

2.2 Mechanobiology of MSCs

2.2.1 MSCs

The presence within bone marrow of a population of MSCs was first suggested by Friedenstein nearly 40 years ago (Friedenstein *et al.*,1966). Since then MSC have been demonstrated in a variety of fetal and adult tissues, including bone marrow,

fetal blood and liver, cord blood, amniotic fluid and, in some circumstances, in adult peripheral blood (Postacchini *et al.*, 1995; Iwaki et al., 1997; Gerstenfeld *et al.*, 2003b). MSCs have generated a great deal of excitement and promise as a potential source of cells for cell-based therapeutic strategies, primarily owing to their intrinsic ability to selfrenew and differentiate into functional cell types that constitute the tissue in which they exist. MSCs can differentiate towards several highly different cell phenotypes, including osteoblasts, chondrocytes and fibroblasts (Figure 2.1). These differentiated cells begin to synthesize the extracellular matrix (ECM) of their corresponding tissues. Several factors influence which lineage pathways the cell and tissue differentiation will take. These factors include biochemical signaling molecules and mechanical conditions (Ashhurst, 1986; Sandberg et al., 1993).

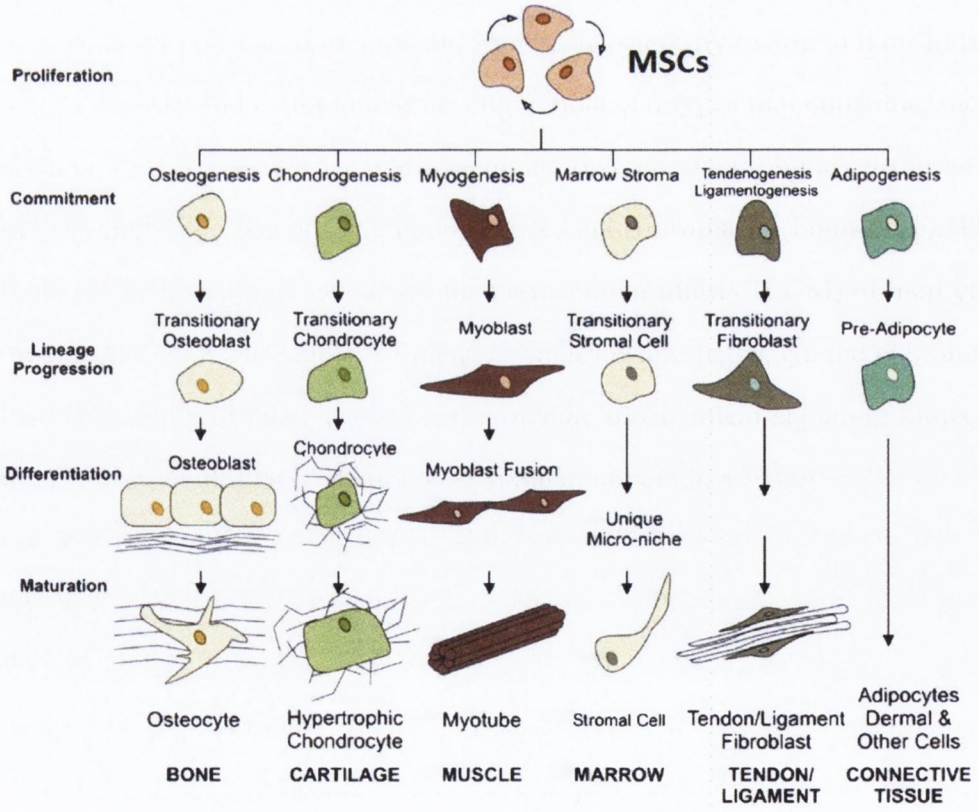


Figure 2.1. The mesengenic differentiation process. Multipotent MSCs derived from bone marrow are capable of proliferating and differentiating into different musculoskeletal tissue types by committing, differentiating, and maturing in a lineage specific fashion. This figure is adapted from Firth and Yuan (2012).

MSCs are considered a readily accepted source of stem cells because such cells have already demonstrated efficacy in multiple types of cellular therapeutic strategies, including applications in treating children with *osteogenesis imperfecta*, hematopoietic recovery, and bone tissue regeneration strategies (Horwitz, *et al.*, 2002; Koc, *et al.*, 2000; Petite, *et al.*, 2000). More importantly, these cells may be directly obtained from individual patients, thereby eliminating the complications associated with immune rejection of allogeneic tissue.

2.2.2 Mechanobiology of MSCs

Human beings experience diverse mechanical forces from a wide variety of sources. Gravity, tension, compression, fluid shear stress, and hydrostatic pressure are just a few examples of the forces that constantly act on cells within organs and tissues (Davies *et al.*, 1995; Grodzinsky *et al.*, 2000; Kakisis *et al.*, 2004; Lehoux *et al.*, 2006; Silver *et al.*, 2003; Wang, 2006). Besides these external mechanical forces, cells also generate their own mechanical forces, known as cell traction forces (CTFs). Cells use CTFs to migrate, maintain their shape, and generate mechanical signals. Different types of cells in the body are subjected to various levels of mechanical forces. All types of cells that are subjected to large mechanical forces, or loads, and are referred to as mechano-responsive cells. Cellular responses to loads depend on loading conditions; they also depend on cell type, cell source, developmental stage,

and cell microenvironment, such as surrounding matrix proteins as well as soluble factors (Frangos, 1993; Grinnell, 2003; Vandenburgh, 1992). Cells use multiple sensing mechanisms to detect mechanical loads and transduce them into intracellular signals that lead to modulation of many vital cellular functions, such as proliferation, differentiation, migration, adhesion, apoptosis, and gene and protein expression (Bartling *et al.*, 2000; Chien *et al.*, 2005; Geiger and Bershadsky, 2002; Hsieh and Nguyen, 2005; Pradhan and Sumpio, 2004; Sarasa-Renedo and Chiquet, 2005; Wang *et al.*, 2007). In addition, intracellular tensile forces resulting from cytoskeletal reorganization play an equally important role in regulating cell function (Matthews, *et al.*, 2006; Ruiz and Chen, 2008). The ability of cells to respond to mechanical cues is governed by mechanosensitive receptors or structures that sense and convert mechanical signals into biochemical signaling events, a process known as mechanotransduction which have been under intensive investigation for the past two decades. Highly coordinated extensive cellular components including the cytoskeleton (CSK), adhesion complexes, and ion channels have been implicated as the predominant mediators of mechanotransduction (Burridge and Chrzanowska-Wodnicka, 1996; Ingber, 1991; Sadoshima and Izumo, 1997).

Mechanobiology is defined as the study of mechanisms by which cells detect and respond to mechanical stimuli. It aims to determine how loads are transferred to the tissues, how the cells sense these loads, and how the signals are translated into the cascade of biochemical reactions that stimulate cell expression and cell- or tissue differentiation (van der Meulen and Huiskes, 2002). The mechanical forces imposed on the growing and differentiating fetal tissues play an increasingly critical role in the developmental process, effectively guiding the development of the functional organism. Mechanobiology contributes first to the understanding of the hierarchical

mechanical properties at the tissue, cellular and subcellular levels and the inter-relationship between these properties. Moreover, mechanobiology reveals fundamental processes associated with development, normal physiology and pathology, through elucidation of mechanotransduction pathways, by which mechanical perturbation is transduced into a biological response. Furthermore, it is fundamental to tissue cell-based regenerative strategies, particularly for load-bearing tissues.

Computational mechanobiology attempts to determine the quantitative rules that govern the effects of mechanical loading on tissue differentiation, growth, adaptation and maintenance by trial-and-error. From a mechanics point of view, the task is considered a 'boundary value problem', whereby the boundary loads of a domain are translated into local mechanical variables within the domain, depending on the geometry and mechanical properties of its materials. Such problems are usually solved with finite element analysis (FEA). Modeling considerations include force application at the boundary, force transmission through the tissue matrix, mechanosensation and transduction by cells, cell gene expression, and transformation of ECM characteristics. All these parts are combined in a computer simulation model. These processes must be represented by variables, parameters and mathematical relationships. Some of these are known, or can be measured, whereas others have to be estimated (van der Meulen and Huiskes, 2002).

2.2.3 MSC ageing

Ageing of adult stem cells may contribute to the fact that body's regenerative potential decreases with age, since age markers have been found in MSCs, including morphology, proliferation, division and differentiation (Sethe *et al*, 2006). While there is

no solid evidence suggesting that adult stem cells undergo functional and molecular changes with age *in vivo* (Wagner *et al.*, 2009), intrinsic alterations occurring in MSCs with ageing, including reduced differentiation potential, increased oxidative damage and an altered response to mechanical stimulation, have been revealed by a number of *in vitro* studies (Mueller and Glowacki, 2001; Zheng *et al.*, 2007; Zhou et al., 2008; Stolzing and Scutt, 2006). There are also reports showing that MSCs from aged donors display typical biomarkers of ageing. For example, a quantitative study (McKayed *el al.*, 2010) revealed that there is a decrease of approximately 35% in the expression of actin and integrin alpha, and an increase of 50% in lipid peroxidation in MSCs from aged rats. Typically, in an aged cell membrane, the accumulation of lipid oxidation products in the cell membrane and growth of the domains with polysaturated fatty acids and cholesterol with age leads to an increase in average stiffness and viscosity of the lipid bilayer (Morris *et al.*, 2004; Staroddubtseva, 2011). Recently, Hale *et al.* (2011) has demonstrated that the amount of lipid peroxidation products found in cell membrane is approximately proportional to the membrane elasticity. Literature also suggest that as much as a 450% increase in membrane stiffness is possible when doubling the amount of lipid peroxidation products (Ajmani *et al.*, 2000).

These pieces of evidence indicate that MSC ageing induces structural changes to cellular components, leading alterations in the mechanics inside a cell. This in turn could affect the biophysical stimuli under loading conditions, and potentially influence the differentiation of MSCs.

2.3 Cell modelling

Cell modelling is an interesting, though challenging topic. There is no such a single correct model in the field of cell modelling. Rather, the simplest model that captures the phenomenological aspects of cell mechanics under the investigated circumstance, without conflicting the biological order, is considered a good model. In general, there are three main approaches in modelling a single cell.

2.3.1 Continuum approach

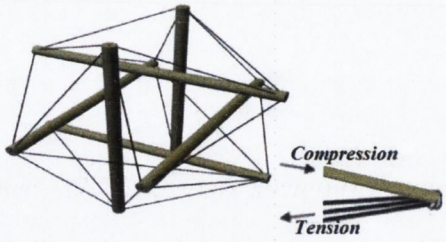
A cell was considered as a homogenous continuum structure that was capable of displaying the distribution of stress and strain from early studies of cell mechanics. The Newtonian liquid drop model developed by Evens and Yeung (1989) was used to simulate blood cells. The model was defined as a viscous fluid surrounded by a cortical membrane, without a presence of any other cellular component. A cell model of similar structure, but with the addition of nuclear membrane, was developed by Dong *et al.* (1991) to explain the experimental observations of micropipette aspiration. Kamm *et al.* (2000) developed a biomechanical model for the investigation of the effects of pressure applied to the apical surface of an adherent epithelial cell. The model consists of a membrane, nucleus, the cytoplasm. More recently, Slomka and Gefen (2010) developed a continuum cell model to demonstrate the difference between global stretching magnitudes and local membrane strain of myoblasts resided on a substrate. Cytoskeletal fibres were introduced in the cell model to capture the direct stimulation on cell nucleus in response to external stimuli, as observed experimentally. Aiming to indentify the role of different cellular components under external mechanical stimulation, Bareto *et al.* (2013) created a 3D continuum cell model with an addition of prestressed actin bundles and microtubules

(MTs), modelled by discrete star-shaped fibres initiated at the centrosome, spreading to the cortex.

While the continuum approach suits for describing whole-cell deformations, a shortcoming of the approach is that the role of individual cytoskeletal components (such as MTs, actin filaments (AFs) and intermediate filaments (IFs)) in maintaining cell structure and stiffness under external mechanical forces is not accounted for. Also, it does not capture the changes induced by MSC ageing and therefore could not be used in this study.

2.3.2 Tensegrity approach

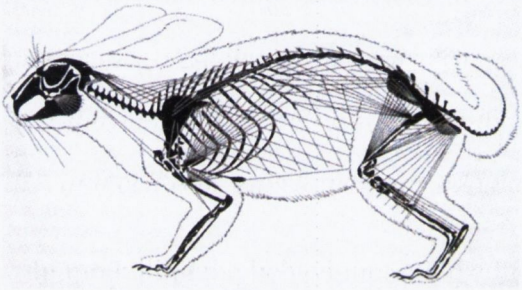
Recognising the role of CSK in cell mechanic in providing structural stability and transmitting chemical signals and mechanical loads from the ECM, several attempts have been made to explicitly address the importance of the CSK with the most successful one being the tensegrity approach (Ingber, 1993). A tensegrity structure is a structural entity that is capable of self-stabilising through the internal arrangement of tensional and compressive elements. The structural stability is maintained by a prestress created in the tensional elements, without which the structure would lose the stabilising ability. Introduced by the modern architect Buckminster Fuller in the 1960s as a portmanteau of "tensional integrity", and later widely used by the contemporary sculptor and photographer Kenneth Snelson, defined as "The Architecture of Life" by Donald E. Ingber, Tensegrity is a discrete structural cell model that has gained a certain traction in the literature due to the close resemblance of its predictions to various experimental observations (see Figure 2.2) (Ingber, 1997, 2003).



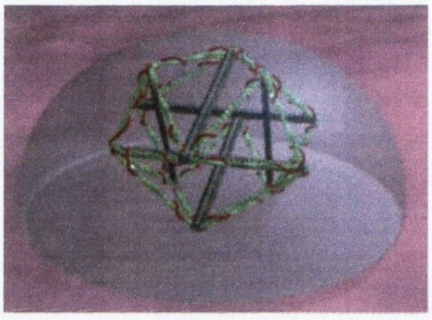
(A)



(B)



(C)



(D)

Figure 2.2. Tensegrity structures consist of tensional cables and compressive struts (A). They have been widely used in architectural building blocks (B) since their recognition by the modern and futurist architect R. Buckminster Fuller. Tensegrity structures exist within biological systems in various forms, involving unique arrangements of skeleton and muscles connected by ligaments and tendons, (C) and were introduced into cell mechanics by Donald E. Ingber and utilised to model the CSK of a cell (D). This figure was adapted from The Ingber Lab.

In modelling the behaviours of an adherent cell, it was proposed that the AFs play the role of the tensional elements, while MTs can represent the compress bearing rods (Ingber, 1997). The tensegrity model had been extensively used to investigate cellular deformability as a mean to represent the various structural elements of the CSK and its adhesion to the ECM. Researchers have demonstrated that the tensegrity model can replicate a number of behaviours observed in living adherent cells

under external mechanical stimulation, that support the concept of the utilisation of tensegrity structures in cell mechanics. It was found that stiffness of cells increases directly proportional with increasing contractile stress (Stamenovic and Coughlin, 1999; Wendling *et al.*, 1999; Hu *et al.*, 2003). Pulling and pushing with an integrin coated micropipette showed the coordinated deformation of the CSK and the nucleus, indicating connectivity of cytoskeletal filaments from the cell surface to the nucleus (Maniotis et al., 1997). MTs can carry large compressive loads (Brangwynne *et al.*, 2006) that balance a substantial portion of the cytoskeletal prestress, together with IFs, the key players in cell-cell interactions, are important contributors to cell contractility under application of large forces and facilitate the transfer of loads between the cell surface and the nucleus (Wang *et al.*, 2001). Other key experimental observations that support tensegrity modelling approach in cell mechanics include observations of the 'action at a distance' phenomenon, whereby cell probing causes movement of cytoskeletal components away from the site of manipulation as reported by Ingber *et al.* (2000).

Despite all these pieces of experimental evidence that supports the existence of tensegrity modelling approach in cell mechanics, tensegrity does not take into account the continuum components that are equally important to the mechanics of a cell, for example, the membrane, cytoplasm and nucleus that are influential to the cells mechanical behaviour. This also eliminates the use of this approach in investigating the effect of cell ageing, since no age-related changes could be captured by using this modelling approach alone.

2.3.3 Hybrid approach

First introduced by McGarry and Prendergast (2004) the hybrid continuum-tensegrity approach combines the features of the two approaches, with CSK modelled by a 6-strut tensegrity structure and the rest of cellular components modelled as continuum. It was used to simulate the effects of each cellular components on the overall cell stiffness. This model incorporates the cellular components considered structurally significant: the cytoplasm, nucleus and membrane, with MTs and AFs modelled as a tensegrity structure (Figure 2.3 (A)). The simulation results showed that indentation location influenced the predicted cell stiffness. The model was also sufficient enough in complexity to capture the non-linear structural behaviours, such as cell stiffening and effects of prestress. Parametric studies revealed that material properties of the cytoplasm and nucleus were the most influential continuum components to the overall cellular stiffness (McGarry & Prendergast, 2004). This model was further developed to make qualitative and quantitative predictions of the differences in cellular deformation caused by fluid shear stress and substrate strain at magnitudes commonly applied in vitro (McGarry *et al.*, 2005a), and for cell-substrate contact during cyclic substrate deformation (McGarry *et al.*, 2005b). More recently, a similar approach was used by De Santis *et al.* (2011), with an improvement of implementing a 12-strut tensegrity structure representing the CSK, to demonstrate that adherent cells can sense the stiffness of substrates (Figure 2.3 (B)).

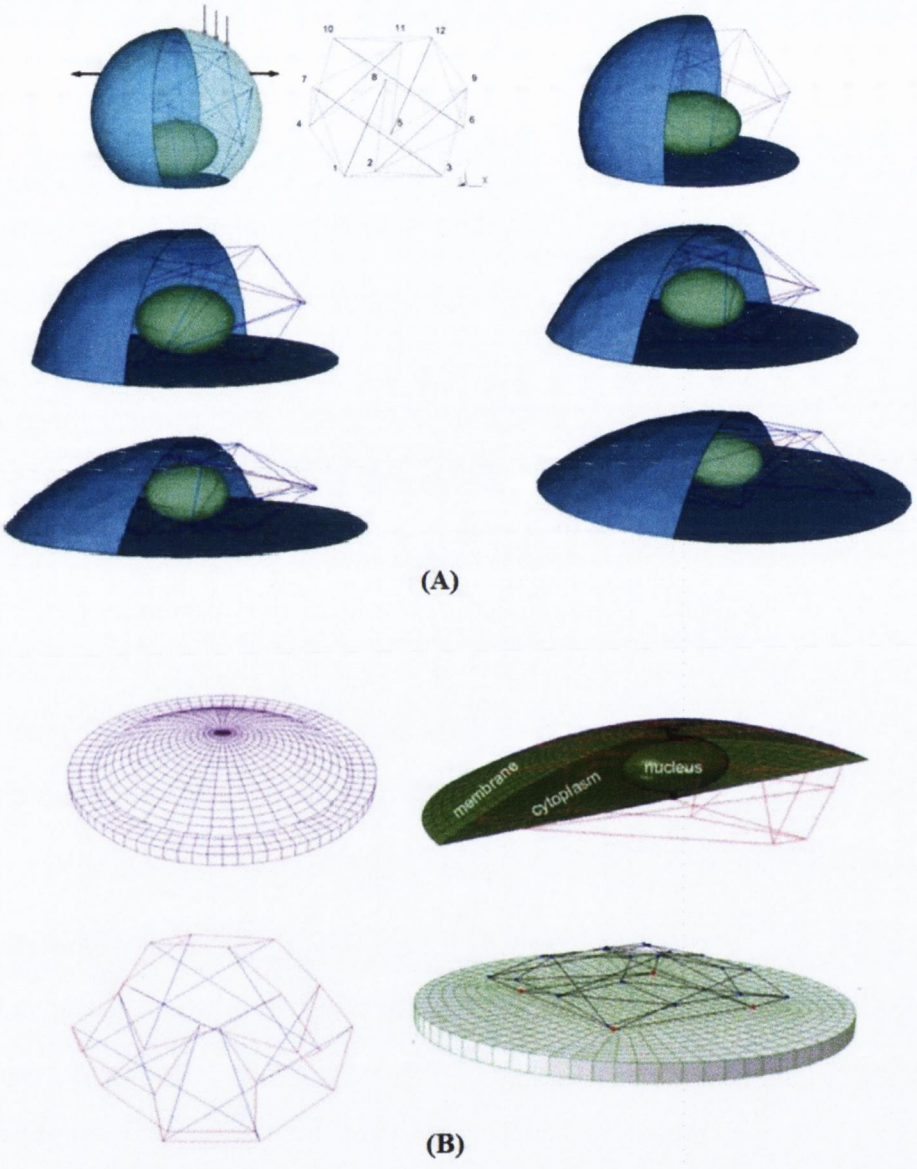


Figure 2.3. FE models based on the hybrid approach. (A) FE models of McGarry and Prendergast (2004), including discrete elements for MTs (red) and AFs (light blue), and continuum components, including the nucleus, cytoplasm and cell membrane. (B) FE model of De Santis et al. (2011), including MTs (blue), AFs (red) and continuum components (green).

2.4 Mechanoregulation

2.4.1 Mechanoregulation theories

Mechanical forces that originate externally from the environment influence many aspects of human health and disease (Banes *et al.*, 1990). In fact, it is the cells in tissues that are responsible for this remodeling in response to mechanical forces. Conversely, abnormal mechanical loading conditions alter cellular function and change the structure and composition of the ECM, eventually leading to tissue or organ pathologies (Ross 1986; Chicurel *et al.* 1998; Riley *et al.* 2002; Ingber 2003; Lammerding *et al.* 2004). Although it is clear that cell response to mechanical stimulations is closely related to tissue physiology and pathology, it remains unclear how the cells sense mechanical stimuli and convert such "mechanical signals" into biological responses. This is further complicated by the fact that cells are highly dynamic and their complex structure changes in response to mechanical forces.

One of the first theories for tissue differentiation was proposed by Pauwels (1960) whose hypothesis revealed that bone could only form after the soft tissue stabilized the mechanical environment sufficiently to reduce the magnitude of these two stimuli. He later (1980) postulated the idea that the differentiation pathway is regulated by the mechanical stress and strain invariants of hydrostatic (dilatational) stress and octahedral shear (distortional) stress through the observation of differentiation pattern and mechanical loading in the fracture callus. The conclusion of his finding can be schematically illustrated in Figure 2.4 which suggests high hydrostatic stress favors the development of cartilage, while the fibrous tissue is the product of high shear.

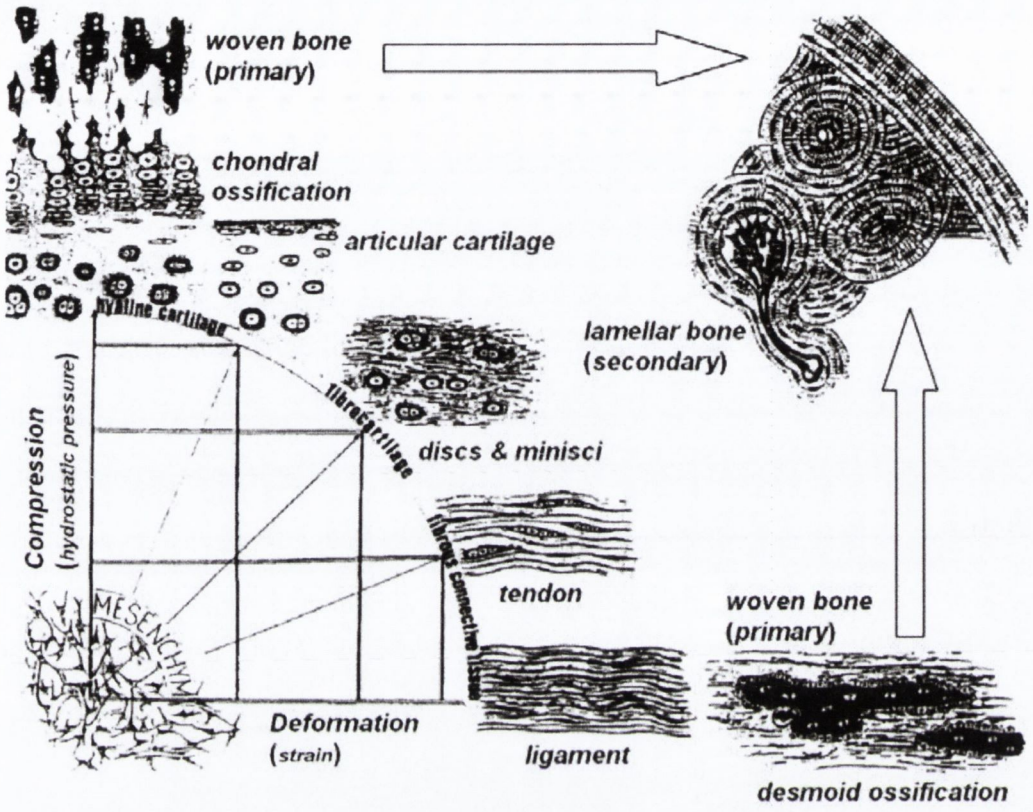


Figure 2.4. Schematic representation of Pauwels' hypothesis of the mechanoregulatory tissue differentiation. Modified by Weinans and Prendergast (1996) from Pauwels (1960).

The interfragmentary strain theory proposed by Perren and Cordey (1979) in a simpler way, as tissue type was determined by its ability not to rupture under the local strain induced by the interfragmentary displacement. Their main idea was that a tissue that ruptures or fails at a certain strain level cannot be formed in a region experiencing strains greater than this (Figure 2.5).

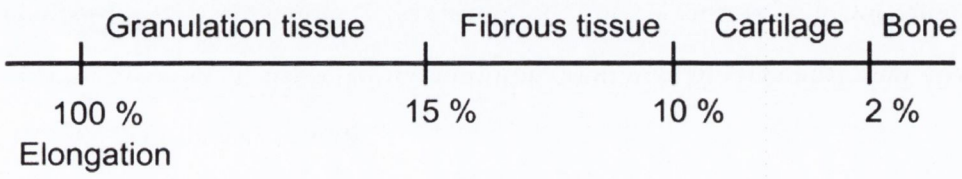


Figure 2.5 Perren and Cordey's ideas were based on how much elongation each tissue type can tolerate. This figure is created based on Perren and Cordey (1980).

Carter *et al.* (1988, 1998) expanded on this idea and used hydrostatic stress and maximum principle strain as regulators, with quantitative boundaries of the mechanoregulation scheme (Figure 2.6). When the tissue is subjected to high tensile strains fibrous matrix is produced. Production of cartilaginous matrix is predicted to occur under high pressure, i.e. to the left of the pressure line, since this tissue can support and resist hydrostatic pressure. When the hydrostatic pressure is very low, i.e. to the right of this line, formation of bone occurs. No quantitative limits were set for when the various tissues were to form.

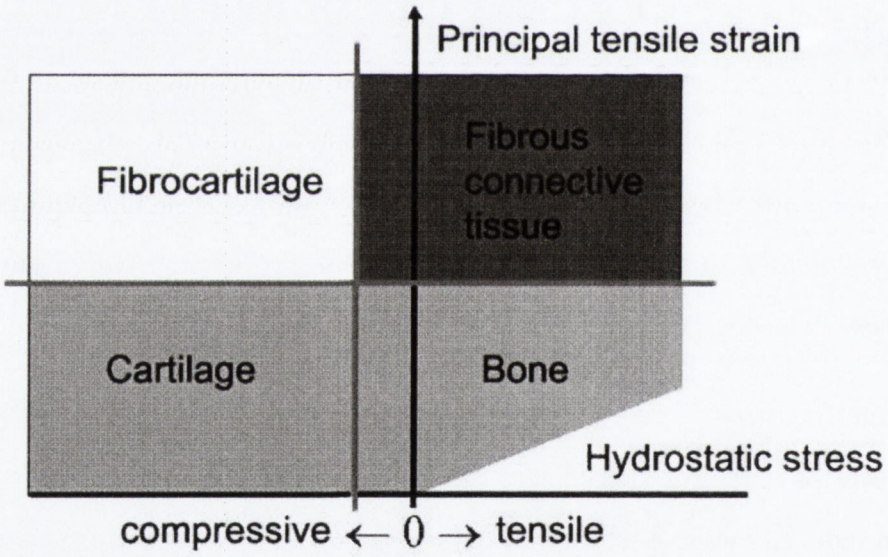


Figure 2.6. Mechanobiological model as proposed by Carter et al., (1998). Two lines separate the different predicted tissue types, one line based on tensile strain and one line based on hydrostatic pressure. This figure is created based on Carter et al. (1998)

Claes and Heigele (1999) put forth mechanoregulation theories based on hydrostatic stress and tensile strain. They presented the first model that quantified the thresholds (Figure 2.7) of various tissue formation in terms of local stress and strain by comparing the experimental data from animal histology and finite element analysis, which simulated fracture callus as a hyperelastic material. Their hypothesis suggests that intramembranous bone formation occurs as strains smaller than approximately 5% and hydrostatic pressure smaller than • 0.15MPa. Compressive pressure that is greater than -15MPa and strains smaller than • 15% stimulates endochondral ossification. All other conditions lead to the development of fibrous tissue or fibrocartilage.

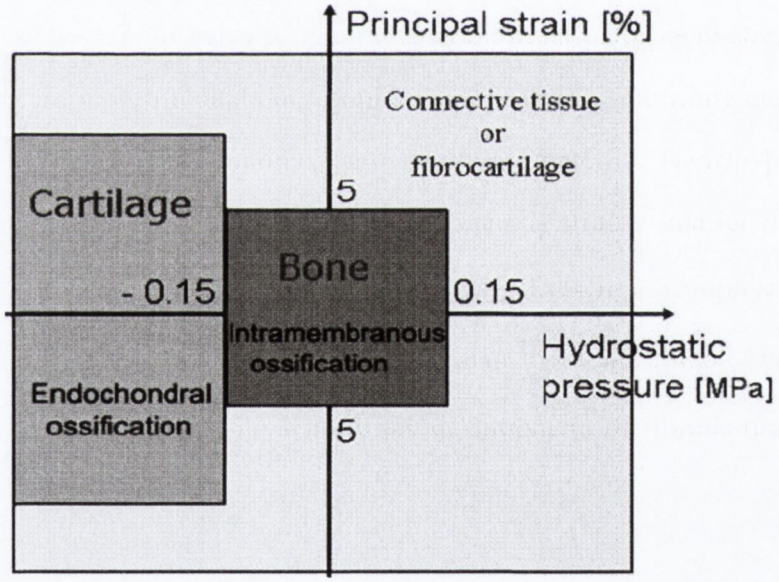


Figure 2.7. A schematic representation of Claes and Heigele's hypothesis of the mechanoregulatory tissue differentiation. Modified by Isaksson (2007) form Claes and Heigele (1998).

For axial loading of a transverse osteotomy, these latter three theories predicted very similar patterns of tissue formation, and these patterns that were in general agreement with histological observations (Carter *et al.* 1998; Isaksson *et al.* 2006b; Lacroix and Prendergast 2002a).

Prendergast et al. (1997) proposed that combinations of interstitial fluid velocity and octahedral shear strain govern the course of tissue differentiation where high magnitudes of either favors fibrous tissue, and only when both stimuli are low enough, can ossification occur. High level of this stimulus is associated with the fibroblast differentiation, intermediate stimulus is in favor of chondrocyte differentiation and low stimulus promotes the osteoblast differentiation as shown in Figure 2.8. This model accurately predicted tissue differentiation at implant/bone interfaces (Huiskes *et al.*, 1997; Prendergast *et al.*, 1997) and was further developed and adapted to simulate tissue differentiation during fracture healing (Lacroix and Prendergast, 2002a; Lacroix *et al.*, 2002). Mechanoregulation theories are already being applied to the design of tissue engineering scaffolds (Byrne *et al.* 2007; Kelly and Prendergast 2006; Lacroix et al. 2006).

These mechanoregulation proposals (Carter *et al.*, 1998; Claes and Heigele, 1999; Lacroix and Prendergast, 2002a), although different in theory, were consistent with the actual tissues formed during fracture healing. A subsequent study that investigated torsional loading of a transverse osteotomy indicated that the Prendergast theory yielded much more accurate predictions than those resulting from theories based on hydrostatic stress and tensile strain or on shear strain alone (Isaksson *et al.* 2006a). The Prendergast theory has also been applied to distraction osteogenesis, healing of an osteochondral defect, and healing at a bone-implant interface (Isaksson *et al.* 2007; Kelly and Prendergast 2005;Prendergast *et al.* 1997). Further, in com-

paring these three theories, Isaksson et al. (2006b) demonstrated that an algorithm based solely on shear strain resulted in predictions very similar to those of the Prendergast theory. The algorithms of Carter and Claes both predicted changes in tissue phenotype at specific time points, but their simulations were not continued over the complete healing period.

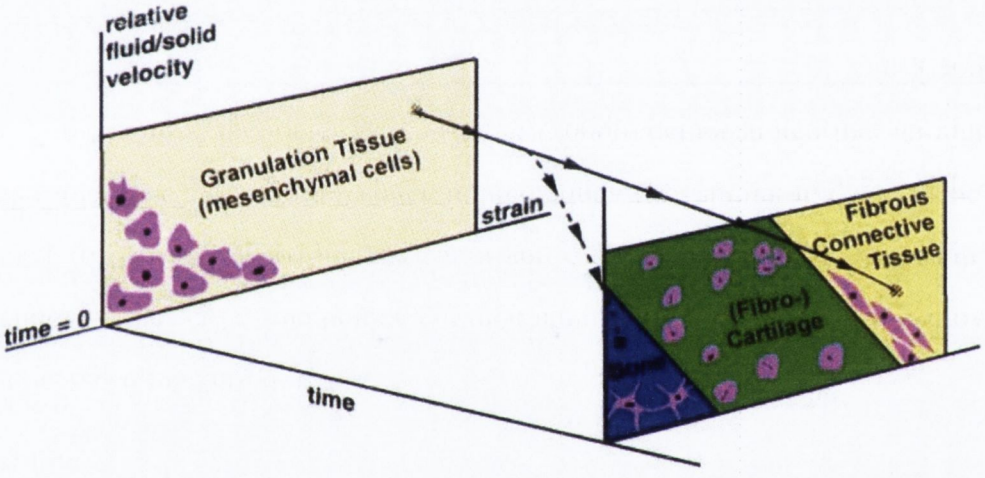


Figure 2.8. A schematic representation of Prendergast's hypothesis of the mechanoregulatory tissue differentiation (Prendergast et al. 1997).

2.4.2 Mechanoregulation models

Many biological processes are so complex that physical experimentation is either too time consuming, too expensive, or impossible. As a result, in mechanobiology, these computational models have been developed and used together with *in vivo* and *in vitro* experiments to quantitatively determine the rules that govern the effects of

mechanical loading on cells and tissue differentiation, growth, and adaptation and maintenance of bone (Isaksson, 2007). It has gone from single phase linear elastic models which were evaluated at only one time point (Carter *et al.*, 1988; 1998) via hyperelastic (Claes and Heigele, 1999) to poroelastic material descriptions implemented in models that adapt tissue distributions over time (Huiskes *et al.*, 1997; Prendergast *et al.*, 1997). Over the last couple of years, the focus has shifted from pure mechanical analyses, towards implementing more mechanobiological aspects, initially only including stem cell concentrations (Lacroix and Prendergast, 2002a), as well as solely biological models (Bailon- Plaza and van der Meulen, 2001) including effects of growth factors and directed cell movement.

One complexity that is central to biomechanical systems is their ability to alter their structure through growth and differentiation. In skeletal tissue differentiation, for example, the differentiation of MSCs is mechanoregulated, producing a complex link between mechanics and tissue adaptation. This complexity led to the explicit inclusion of cell activity in mechanobiology, where cell behaviours such as proliferation, differentiation and migration were modelled with differential equations (Lacroix *et al.*, 2002; Bailon-Plaza and van der Meulen 2003; Lally and Prendergast 2004). The hierarchical structure of biomechanical systems permits modelling at various length scales; from the tissue level, through the cell level to the molecular level. At the level of the cell, we can postulate that mechanics affects the behaviour of cells, i.e. by regulating differentiation, apoptosis, proliferation, etc. One major benefit of this approach is that much of experimental biology is focused on this level (Prendergast *et al.*, 2009; Checa *et al.*, 2010). More recent developments on the modelling approach have incorporated other parameters that may interact with the mechanical stimuli to direct differentiation, most notably alterations in the oxygen

environment and associated angiogenesis (Checa and Prendergast, 2009). This model also incorporates cell migration, proliferation and apoptosis and has been further developed to incorporate physiological variation in cellular parameters to predict animal to animal variation in differentiation reported in vivo within a defined bone chamber model subjected to mechanical loading (Khayyeri *et al.*, 2009).

The lattice-based approach has been used in a wide variety of mechanobiological models. Lattice models are commonly combined with finite element analysis where the calculated stress and strain analysis is mapped on the lattice domain, in which cell activities are modelled. The random walk approach was first introduced in the lattice model by Perez and Prendergast (2007) for cell proliferation and migration in a simulation of tissue differentiation. In their model, the migration and proliferation of MSCs were simulated in a lattice. Finite element analysis was performed at regular intervals to determine the mechanical stimuli of fluid flow and shear stress, which regulated the differentiation of these cells into osteoblasts, chondrocytes or fibroblasts, following the mechanoregulation theory proposed by Prendergast *et al.* (1997). These differentiated cells produced their characteristic tissues, altering the mechanical properties of the tissue, and hence the stimulus. Since then, the lattice model has been applied to various studies, including bone scaffolds (Byrne *et al.*, 2007), fracture healing (Byrne, 2008), tissue differentiation in a bone chamber (Khayyeri *et al.*, 2009), and tissue differentiation with angiogenesis (Checa and Prendergast, 2010).

2.4.3 Corroboration of mechanoregulation theories

The corroboration of mechanoregulation theories would enables simulations to predict the mechanobiological response of an experiment, allowing researchers to test the hypotheses that are interesting on their own and provide better theoretical understanding about the process. The goal of computational mechanobiology, at the currently stage, is to develop a well established computational model for mechanoregulated tissue differentiation that has been robustly corroborated with experiments. In order to achieve this goal, the theories that govern the process of mechanoregulated tissue differentiation must be validated with experiments, such that both qualitative and quantitative predictions, corresponding to experimental observations, can be made with confidence. Towards this direction, many attempts have been made to correlate mechanoregulation theories with experimental observations.

There are certain requirements for the corroboration of mechanoregulation theories. First of all, the theory itself has to have specifically defined boundaries for each tissue differentiation in order to be experimentally validated. Regarding this aspect, some early mechanoregulation theories , for example, Pauwels (1960) and Carter *et al.* (1988), are not corroborable experimentally and therefore cannot be validated due to their pure phenomenological nature (Prendergast, 2001).

Due to the nature of the mechanism of this corroboration process, a partial, or qualitative corroboration is possible as suggested by Isaksson *et al.* (2006) when comparing the experimental observations of fracture healing with simulation results using a mechanoregulation theory (Prendergast *et al.*, 1997). It was also suggested that a partially corroborated mechanoregulation theory could be used to predict certain features of the experimental outcomes.

In the same study (Isksson *et al.*, 2006), the mechanoregulation theories proposed by Carter *et al.* (1988), Claes and Heigele (1999) and Prendergast et al. (1997) were investigated in an identical computer simulation of fracture healing and compared with an in vivo study (Isaksson *et al.*, 2006a). The results revealed that while all three theories were able to predict tissue differentiation during axial loading, only the mechanoregulation model of Prendergast et al. (1997) was able to predict full bridging during torsional rotation as observed in histology. The author believes that while these comparison studies can identify the best performer among a group for a given application, better approaches are needed for comprehensively corroborating mechanoregulation theories.

2.5 Conclusions

Evidence from the above literature suggests that the cell-tissue differentiation potentials of MSCs could be altered b ageing. A predictive computational modelling approach could give an insight into the effects of MSC ageing on tissue differentiation. However, the current modelling approaches, for example, the lattice model, could not capture these age-related changes that occur on cellular components. Moreover, while the current finite element models of single cells could predict various mechanical behaviours observed experimentally, a cell model that is capable of capturing MSC ageing has not been developed. Therefore, there is an emergence in the needs of developing a predictive computational model that could capture the subcellular changes associated with MSC ageing.

It is also evident in the literature that the approaches used for corroborating mechanoregulation theories are not well established and solely based on experimental observations at tissue level. Hence, the author believes there is a necessity of developing a cell-based mechanoregulation model with an increased predicting capacity to sub-cellular level. Such a modelling approach could potentially be used to correlate mechanoregulation theories with basic cell experiments, therefore diminishing the criticisms about the validation of mechanoregulation theories and promoting the development of computational mechanobiology in the future.

Chapter 3

3. Methods

3.1 Overview of methodologies

In this chapter the approaches taken in investigating whether or not donor age affects MSC differentiation under mechanical stimulations are introduced. Computational methodologies are devised to explore four facets of this primary research question: (i) The effects of ageing on mechanical stimuli within cells – for this purpose a computational model of an novel adherent cell that is capable of capturing the age-related changes discovered in our laboratory is created, as described in Section 3.2. It is intended that upon corroboration of the model it will be justifiable to utilise the model to further explore the influence of MSC ageing on cell-tissue differentiation under biophysical stimulation. (ii) Attempting to discover the possibility of performing mechanoregulation simulations using whole cell models – for this purpose a mechanoregulation theory is used and the mechanoregulatory boundaries are converted to a cellular component from a tissue level, so that structural and material changes occur at cellular level can be captured, as described in Section 3.3. It is also intended to demonstrate that the cell-based mechanoregulation modelling approach developed in this thesis increases the predicting capacity to single MSCs where no tissue forma-

tion is necessary, e.g. substrate stretching of MSCs. Interestingly, the proposed modelling approach can potentially be used to corroborate mechanoregulation theories with basic *in vitro* cell experiments. (iii) An investigation of gap tissue formation in the event of post-surgical implant integration for patients with total hip replacement with cementless fixation, in particular the consequences of MSC ageing in cell-tissue differentiation is investigated using the proposed cell-based mechanoregulation modelling approach – this is achieved by simulating the gap tissue between a hip implant and the surrounding bone cavities under stimulation within biophysical ranges, as described in Section 3.4. (iv) An investigation of MSCs differentiation loaded with substrate stretching for the application of tissue engineering, in particular the effects of ageing on MSC differentiation under various uniaxial loading conditions – this is achieved by simulating cells stretched on a substrate, from which a biophysical stimulus is compared with the mechanoregulation index, as described in Section 3.5.

3.2 The effects of MSC ageing on mechanical stimuli within cells

3.2.1 General description of the problem

The mechanisms by which extracellular mechanical stimulation affects the differentiation of cells and ultimately cell fate is not yet well understood, despite its importance for tissue engineering and regenerative medicine (Ingber, 2008; Wang *et al.*, 2009). In particular, the role of MSC ageing on the mechanoregulation of cell-tissue differentiation is a subject that has not yet been given very much consideration. The aim of this study is to create a finite element model of a single cell for the investiga-

tion of the role of MSC ageing in cell-tissue differentiation. The objective is to perform AFM indentation simulations and compare the results with previous published experimental data for validation purposes. It is also the author's intention to find out how age-related changes affect biophysical stimuli inside a cell under AFM indentation loading environments. Specifically, it is hypothesised that changes in both membrane stiffness and CSK density have influence on biophysical stimuli inside a cell.

3.2.2 Cell geometry

The shape of the cell model was determined from experimental observations (Frisch and Thoumine, 2002). The size of the cell model, including the proportion of nucleus, was based on confocal images of MSCs taken in our laboratory (Maguire *et al.*, 2007). The CSK-NSK structure was modelled as follows: MTs modelled as struts, AFs modelled as cables and IFs were combined in the CSK as part of a pre-stressed tensegrity structure. Each tensegrity structure consists of six compression-bearing struts (two in each orthogonal direction) and twenty-four tensional cables representing the aggregate behaviour of MTs and AF bundles, respectively. Twelve common nodes were created at each end of the struts where four cables are connected, representing receptor sites where actin bundles cluster at adhesion complexes in adherent cells. To fit into a spread cell, the tensegrity structures that are derived from rounded configuration used by McGarry and Prendergast (2004) were incorporated. To mimic the complexity of the CSK three tensegrity structures were used (Figure 3.1 (A)). Three tensegrities were also used for the NSK, with struts representing nuclear lamina and chromatin modelled as cables (Figure 3.1 (B)). The nodes, where NSK contacts the nuclear surface, represent nuclear receptors spanning

across the nuclear envelope that can receive mechanical signals from the CSK. Each nuclear receptor is connected to the corresponding cell receptor pointing in the same direction (Figure 3.1 (C)). These direct connections in the model represent the IFs. The cell model was developed using the finite element code ABAQUS/Standard version 6.8-1 (SIMULIA, RI, USA).

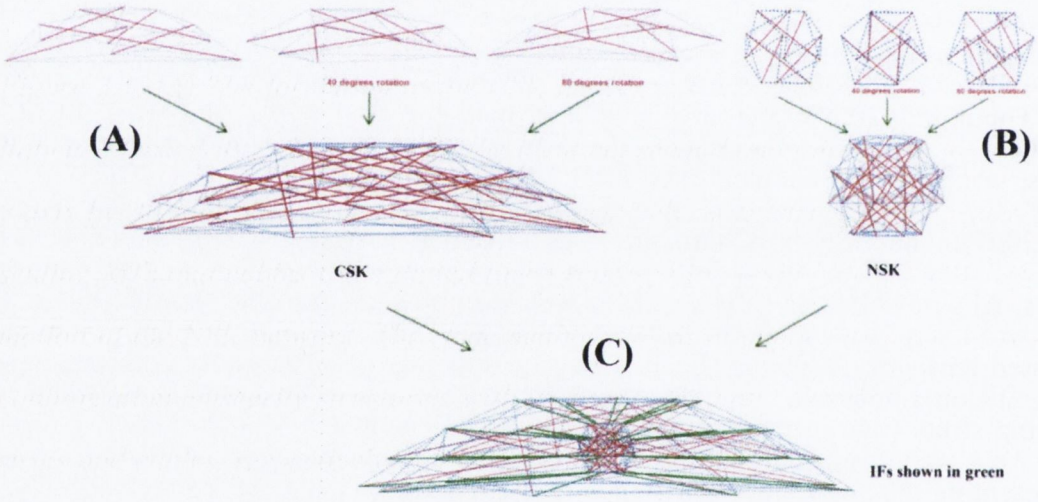


Figure 3.1. (A) The formation of the CSK network. It is formed by 3 sets of 6-strut flattened tensegrity structures, with the identical second and third set rotated along y-axis by 40 and 80 degrees clockwise, respectively, with struts (red lines) representing MTs and cables (blue dotted lines) representing actin bundles. (B) The formation of the NSK network. The same method shown in applies to 3 sets of round-configuration tensegrity structures, with nuclear lamina and chromatin modelled by struts and cables, respectively. (C) NSK is then placed at the centre of the CSK and

the two structures are connected by direct linkages representing IFs (shown in green lines).

Cytoplasm and nucleus were meshed with 4-node tetrahedral elements. Cell membrane and nuclear envelope were meshed with 3-node shell elements. A ''no-slip'' interaction condition was assumed at all nucleus–cytoplasm and cytoplasm–membrane interfaces (by employing the ''tie'' constraint in ABAQUS). Beam elements were used for struts and tension-only connecter elements were assigned to all the cables. A prestress that is equivalent to 2% of prestrain, used by previous studies (McGarry and Prendergast, 2004; De Santis *et al.*, 2011), was assigned to all the cables that constitute tensegrity structures by giving a reference length to each of the connectors. A frictionless hard contact was used between the indenter surface and the cell membrane. Augmented Lagrange method was selected to model the contact by monitoring the gaps between pairs of nodes between the two surfaces.

3.2.3 Material modelling

Material properties for each of the cellular components are not known precisely for MSCs and can only be estimated from various sources. Viscoelastic properties were assigned to the cytoplasm, nucleus and membrane to incorporate time-dependent response to biophysical stimulation. A standard linear solid model, that consists of a spring k_1 paralleled with a series of another spring k_2 and a dashpot η (see Figure 3.2), was used to characterise the viscoelastic behaviour. The time-dependent stress-strain relation was described as:

$$\frac{d\varepsilon(t)}{dt} = (k_1 + k_2)^{-1}[\frac{d\sigma(t)}{dt} + \frac{k_2}{\eta}\sigma(t) - \frac{k_1 k_2}{\eta}\varepsilon(t)] \quad \textit{Equation } 3.1$$

Where k_1 and k_2 are the spring constants, η is the viscosity of the dashpot, and σ(t) and ε(t) are the stress and strain at time t, respectively.

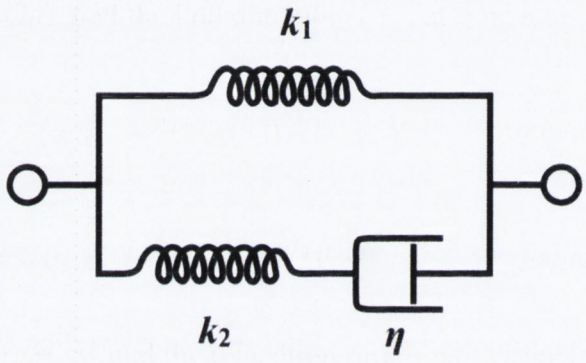


Figure 3.2. Schematic representation of the standard linear solid model taht was used to characterise the viscoelastic behaviours of the cytoplasm and nucleus. It consists of a spring k_1 paralleled with a series of another spring k_2 and a dashpot η.

The shear modulus *G(t)*, and the bulk modulus *K(t)*, at time t, are given as

$$G(t) = G(\infty)(1 - g^P(1 - e^{-\frac{t}{\tau}}))/(1 - g^P) \quad \textit{Equation } 3.1$$

$$K(t) = K(\infty)(1 - k^P(1 - e^{-\frac{t}{\tau}}))/(1 - k^P) \quad \textit{Equation } 3.2$$

where the parameters g^p, k^p and the relaxation time τ, are viscoelastic material constants, and $G(\infty)$ and $K(\infty)$ are the equilibrium shear and bulk moduli, respectively. Table 3.1 and Table 3.2 present the specific material properties for each cellular component from a young donor used in this study.

	k_1 (Pa)	k_2 (Pa)	η (kPa.s)	Piosson's ratio
Cytoplasm[1, 2]	50	100	5	0.37

Nucleus[1, 2]	200	400	10	0.37
Membrane[3, 4]	720	280	25	0.3

[1]Shin and Athanasiou, 2001; [2]Guilak *et al.* 2000;[3]Waugh and Agre 1988; [4]Kamm *et al.* 2000.

Table 3.1. Viscoelastic properties of cellular components.

	Elastic modulus (Pa)	Poisson's ratio	Diameter (nm)
MTs[1]	1.2×10^{9}	0.3	12
AF bundles[2]	0.34×10^{6}	0.3	250
Ifs[3]	7.6×10^{6}	0.3	10
Lamina[4]	1.4×10^{6}	0.3	10
Chromatin[5]	244×10^{6}	0.3	1.2

[1]Gittes *et al.* 1993, [2]Deguchi *et al.* 2005, [3]Bertaud *et al.* 2010, [4]Dahl *et al.* 2004, [5]Smith *et al.* 1996.

Table 3.2. Elastic and geometric properties of CSK-NSK components.

3.2.4 Modelling of age-related changes of MSCs

Age-related changes regarding lipid peroxidation and expression of actin and integrin subunits found by McKayed *et al.* (2010) were interpreted and modelled by the following methods.

(1) In aged cells, both elastic modulus and apparent viscosity of the cell membrane were doubled (×2) relative to young cells to capture the effect of lipid peroxidation, by assuming a proportional relationship between membrane stiffness and the amount of lipid peroxidation products (Hale et al., 2011).

To identify the effects of membrane stiffness, a parametric study with wider range, from 0.1 time (×0.1) to 10 times (×10) of the original young cells, was carried out.

(2) The reduced amount of actin bundles and integrin receptors in aged cells was modelled by structural differences in CSK-NSK formation in the cell models. Specifically, two sets of CSK-NSK tensegrity combinations were used for the aged cells whereas three sets were used for the young cells. This results in a 33.3% decrease in CSK-NSK density and a 33.3% decrease in the number of focal adhesions for the aged cells, as a mechanical modelling interpretation regarding the 35% reduction in the expression of actin and integrin alpha found experimentally by McKayed *et al.* (2010), respectively.

3.2.5 Loading conditions

A rigid conical indenter with a contact angle of 141 degrees was used to indent the cell model. A 3nN indenting force was applied to the indenter during each simulation in a force-control manner and the displacement at the indenter tip was computed with each increment. Simulations were carried out at two indenting positions on the cell membrane: at one of the receptor sites where the CSK contacts with cell membrane, and at the apex of the cell where is most distant from a receptor site (see Figure 3.3). The stiffness of the cell model was calculated using a Hertz formula that relates the indenting force and indentation depth, which is expressed as

$$F = \frac{2E}{\pi \tan\alpha(1-\nu^2)}\delta^2 \qquad \textit{Equation } 3.3$$

where E is the stiffness of the cell, F is the reaction force at the indenter tip, α is a half of opening angle of the indenter tip, ν is Poisson's ratio and δ is indentation depth.

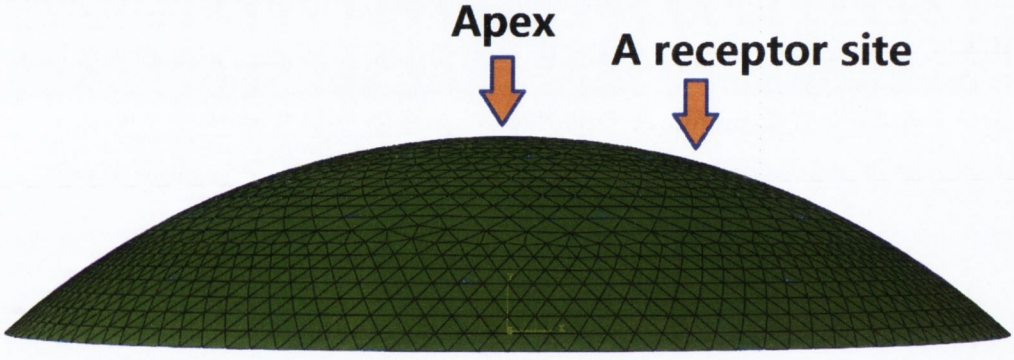


Figure 3.3. AFM indentation simulations were performed at two positions on the cell membrane: the apex and one of the receptor sites.

3.3 Mechanoregulation modelling using whole cell models

3.3.1 General background of the problem

Theoretical models of mechanoregulation has long been established and evolved over the past decades. Despite being able to predict the observed patterns in corresponding time course of tissue differentiation, these models only took account the

biophysical stimuli at tissue level, without considering any sub-cellular stimulus. In reality, cellular activities are believed to initiate the driving force in tissue differentiation as cells synthesise the appropriate ECM leading to tissue formation. To fully investigate the influence of these changes a predictive computational model that is capable of capturing the alterations occur at cellular components is needed. The aim of this study is to demonstrate that mechanoregulation for tissue differentiation can be simulated using finite element models of single cells with mechanoregulation theories implemented. It is also the author's intention to demonstrate that such a modelling approach could potentially be used to corroborate mechanoregulation theories with basic cell experiments.

3.3.2 Finite element model of single cells

A hybrid modelling approach as described in Section 3.2 was adopted to model the cells in this study. The shape of the cell models was idealised as a perfect sphere, with a volume that is identical to the cell models used in previous studies (McGarry and Prendergast, 2004, 2005). The CSK-NSK structure was modelled using multiple sets of regularised tensegrity structures. Each tensegrity structure consists of six compression-bearing struts (two in each orthogonal direction) with the same geometry and twenty-four identical tensional cables representing the aggregate behaviour of MTs and AF bundles, respectively, as shown in Figure 3.4 (A).

3.3.3 Establishment of mechanoregulatory boundaries on cellular components

The governing stimuli for cell-tissue differentiation used in this study was developed based on the algorithm formulated by Prendergast et al. (1997), who described a mechanoregulatory stimulus S as

$$S = \frac{\gamma_{oct}}{a} + \frac{\upsilon}{b} \quad \textit{Equation 3.4}$$

where γ_{oct} is the octahedral shear strain, υ is the fluid velocity. The values of the scaling constants were a = 0.0375 and b = 3μm (Huiskes et al., 1997). This mechanoregulatory stimulus S has a controlling influence on tissue differentiation as follows: high levels of stimuli ($S \geq 3$) promote fibrous tissue formation; low levels of stimuli ($S \leq 1$) favour bone formation; and cartilage is formed for intermediate levels of stimuli ($1 < S < 3$). The intervals for S were established in Huiskes et al. (1997) and later extended to include a bone resorption region where very low level of stimuli ($S < 0.011$) are present (Lacroix and Prendergast, 2002a).

To establish the mechanoregulation boundaries on cellular components the fluid flow was ignored in Equation 3.4 and the octahedral shear strain was converted to an equivalent plain shear strain that applies on the top surface of the block containing a cell at the centre (Figure 3.4 (B)). With fluid flow ignored, the mechanoregulatory stimulus S was reduced to

$$S = \frac{\gamma_{oct}}{a} \quad \textit{Equation 3.5}$$

or,

$$\gamma_{oct} = S \cdot a \quad \textit{Equation 3.6}$$

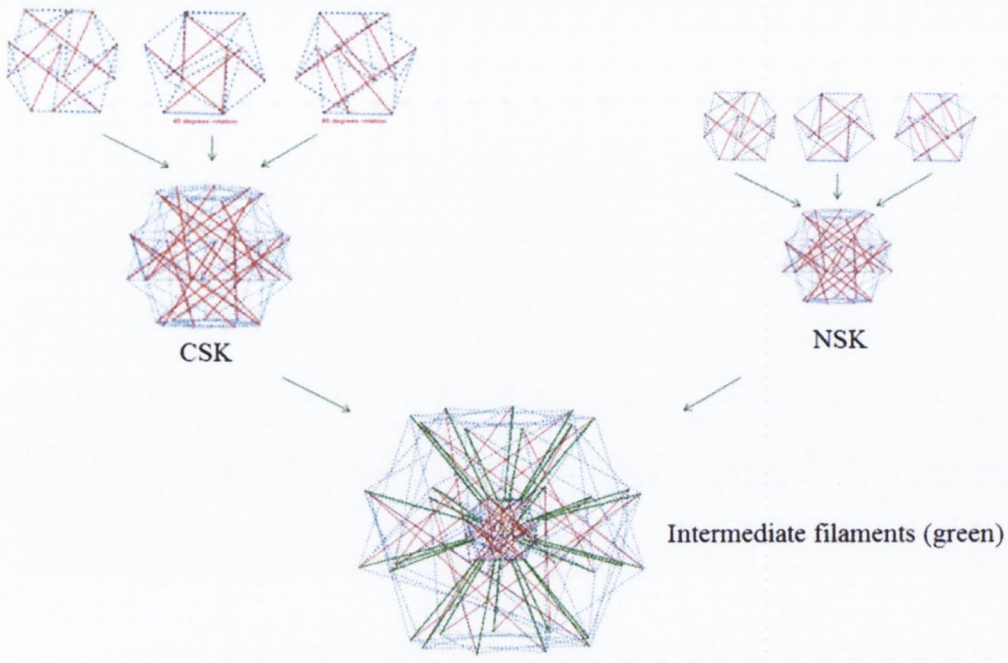
Then the boundaries for tissue differentiation were calculated with each value of S and converted to an equivalent plain shear strain by

$$\gamma_{oct} = \frac{1}{3}[(\varepsilon_x - \varepsilon_y)^2 + (\varepsilon_x - \varepsilon_z)^2 + (\varepsilon_z - \varepsilon_y)^2 + \frac{3}{2}(\gamma_{xy}{}^2 + \gamma_{xz}{}^2 + \gamma_{yz}{}^2)]^{\frac{1}{2}} \quad \textit{Equation 3.7}$$

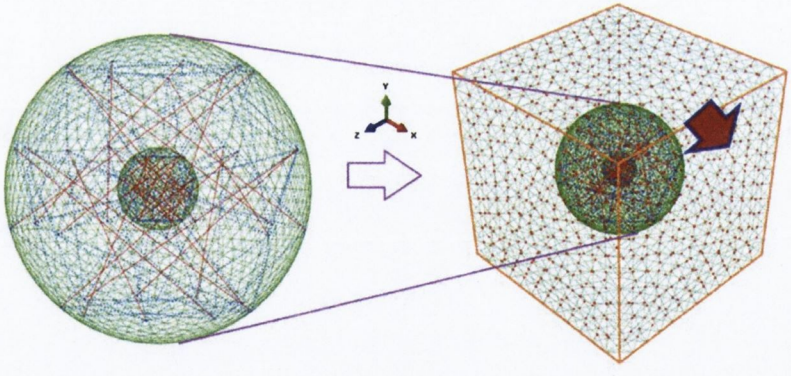
where ε_x, ε_y and ε_z are the normal strain components and γ_{xy}, γ_{xz} and γ_{yz} are the shear strain components. Since the shear strain component γ_{xy} is the only one we apply on top of the tissue block, the rest of the terms in Equation 3.7 were set to zero. Then, the equation was reduced to

$$\gamma_{xy} = \sqrt{6}\gamma_{oct} \quad \textit{Equation 3.8}$$

With the converted shear strains applied to the top of the tissue block (Figure 3.4 (B)), the mechanoregulatory boundaries can then be computed on biophysical stimuli of cellular components, in this case, the equivalent strain in cell membrane. These newly established mechanoregulatory boundaries are listed in Table 3.3 together with the boundaries proposed by Prendergast *et al.* (1997).



(A)



(B)

Figure 3.4. (A) The formation of CSK-NSK network using multiple sets of regularised tensegrity structures. (B) A finite element model of a single cell (left) was placed at the centre of a block of a granulation tissue (right). Shear strains that are equivalent to the boundaries expressed in terms of octahedral shear strain used in mechanoregulation diagram were applied on the top surface of the tissue block.

Mechanoregulatory boundaries (Prendergast et al., 1997)		Computed boundaries on cell membrane strain
$S > 3$	**Fibrous tissue**	$\varepsilon_{mem} > 0.082$
$1 < S \leq 3$	**Cartilage**	$0.027 < \varepsilon_{mem} \leq 0.082$
$0.011 < S \leq 1$	**Bone**	$0.003 < \varepsilon_{mem} \leq 0.027$
$S \leq 0.011$	**Resorption**	$\varepsilon_{mem} \leq 0.003$

Table 3.3. The computed boundaries on cell membrane strain (on the right) as apposed to the mechanoregulatory boundaries (on the left) proposed by Prendergast et al. (1997).

	Granulation tissue[a]	Fibrous tissue[b]	Cartilage[b]	Bone[a]	Implant[c]
Young's modulus (Pa)	0.2×10^6	2×10^6	10^7	10^9	2×10^{11}
Poisson's ratio	0.167	0.167	0.3	0.3	0.28

[a]Lacroix and Prendergast, 2002;

[b]Hori and Lewis, 1982;

[c]Verdonschot and Huiskes, 1997.

Table 3.4. Material properties of different tissue types and the implant.

3.4 Finite element modelling of gap tissue formation

3.4.1 General background of the problem

As one of the most successful orthopaedic procedures performed today, THA improves the quality of life for patients with osteoporosis and osteoarthritis. MSCs are multipotent adult stem cells that are present in practically all tissues as a specialized population of mural cells/pericytes that lie on the abluminal side of blood vessels (Pontikoglou *et al.*, 2011). Not only does this pluripotent nature make MSC differentiation the core focus within tissue engineering research, it also attracts a lot of attention in the field of reconstructive medicine. In the application of THA cementless fixation remains the ideal approach regarding its functional potential in long-term survival rates. However, to achieve this clinical advantage over cemented fixation, the understanding of the ossification process initiated by MSC differentiation at bone/implant interface, allowing bone to grow into or onto the implant as a fixation mechanism, is essential. In pursuit of investigating the role of MSC ageing in tissue differentiation, simulations of a section of gap tissue at the bone/implant interface are performed, with an aim to test the hypothesis that age-related changes of MSCs can affect gap tissue formation.

3.4.2 Finite element model of gap tissue

Eight interconnected tissue blocks (shown in green in Figure 3.5) were used to represent the gap tissue between bone cavity and implant. Each tissue block contains a cell with a round configuration at the centre and connects to the neighbouring blocks. The centre block (shown in grey in Figure 3.5) represent a section of a hip implant and connect to the inner surface of the gap tissue at the corresponding interfaces. The volume of each cell is equivalent to the ones described in Chapter 3.2, which

gives a diameter of 17.90μm for the sphere cell model that is centred at each of the 30μm×30μm×30μm cubical tissue blocks.

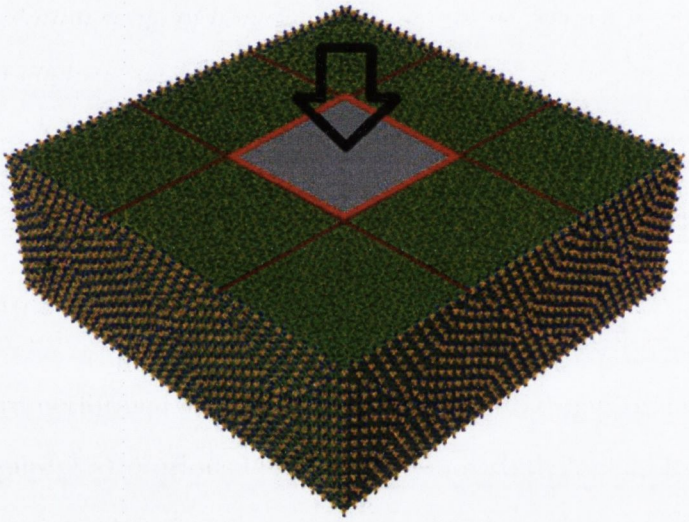


Figure 3.5. Simulation setup of bone/implant gap tissue (shown in green boxes) with a cell placed in each tissue block. The implant is located at the centre (shown in grey).

3.4.3 Loading conditions

Simulations were performed on a three-dimensional (3D) gap tissue between bone and implant (Figure 3.5). Various loading conditions were applied to the top surface of the implant section (shown as the grey centre block in Figure 3.5) with surrounding gap tissue (shown as 8 green blocks in Figure 3.5) securely attached to the inner surface of the bone cavity (not shown in Figure 3.5) at the outer surface of the eight tissue blocks (shown as pink dotted surfaces in Figure 3.5). A vertical load that is within the range used by Perez and Prendergast (2007), either in force-control or

motion-control manner, was applied on the top surface of the implant during each simulation. In case of force-control, vertical forces with magnitudes of 0.12 μN, 0.24 μN , 0.36 μN and 0.48 μN were applied to the implant, whereas vertical displacements of 3 μm, 6 μm, 9 μm and 12 μm were simulated in case of motion-control. The outer surface of the gap tissue where it binds to the bone cavity was restrained in all directions and the implant was only allowed to move vertically during each simulation. Iterative loops were set up in Optimization Module by selecting the cell membrane strain as the design response which was read from ABAQUS data file throughout each simulation. The material properties of each cell-tissue block were updated at the end of each iteration. The interval for each iteration represents the aggregative time taken for the corresponding tissue type change in reality. A stop condition was set to terminate the iterative loops when no further change in tissue type occurred. Each simulation started with MSCs contained within granulation tissue blocks, which differentiated into various cell types (fibroblast, chondrocyte or osteoblast) depending on the cell membrane strain, synthesising different tissue types individually within the surrounding blocks. During each simulation, the material properties of the cytoplasm nucleus, which are the most influential cellular components to the overall cell stiffness (McGarry and Prendergast, 2004), were also updated during each simulation (see Table 3.1 for material properties used for each cell type). The implant material was modelled as linear elastic with the properties of stainless steel, as used by Verdonschot and Huiskes (1997) (see Table 3.4). The material properties for each tissue type were also listed in Table 3.4, as reported by previous studies.

3.4.4 Modelling of debonding

Debonding, of any degree, is clinically undesirable, but somewhat inevitable in practice. To investigate the effects of debonding, when disconnection between the implant surface and bone cavity occurs, four possibilities of dislodging between the bone and the implant were simulated (Figure 3.6). A frictionless condition was assumed at the interface between the implant and the debonded tissue for each debonding case as suggested by Jasty *et al.* (1992), while undebonded interface remains securely attached. Both force-control and motion-control were applied to all debonding cases. All loading conditions were given to both aged and young MSCs, in order to investigate the effect of ageing.

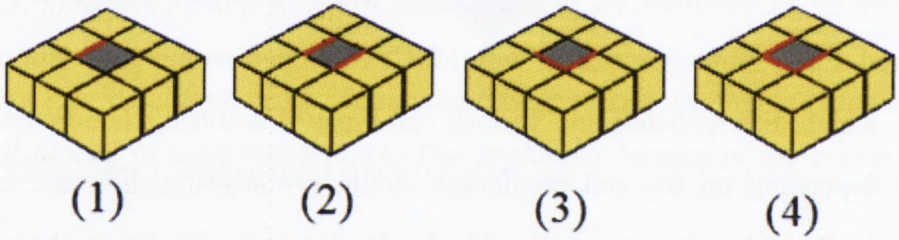


Figure 3.6. There are four possible debonding case in the current simulation setup. The red lines indicate the surface where debonding occurs. Debonding case (1) denotes there is one debonding surface between implant and gap tissue, whereas Debonding case (2), (3) and (4) indicate debonding occurs at two opposite surfaces, two neighbouring surfaces and three surfaces, respectively.

3.5 Finite element modelling of substrate stretching

3.5.1 General description of the problem

Tissue engineering approaches offer the potential of avoiding long-term implantation of reconstructive prostheses by using autologous MSCs harvested from a patient's bone-marrow. It is the process of creating functional tissues using cell-scaffold constructs that facilitate cell proliferation, migration and differentiation in response to mechanical and chemical stimulation. The understanding of bone marrow derived MSCs echoes the field of tissue engineering research as the pluripotent MSCs can provide a promising cell source by differentiating into many tissue-specific lineages, including osteoblasts, chondrocytes and fibroblasts (Jagodzinski *et al.*, 2004; Huang *et al.*, 2004; Sarraf *et al.*, 2011). It is common practice to seed MSCs onto a scaffold and expose the resulting construct to mechanical preconditioning in a bioreactor prior to implantation. Cyclic stretching is among the most commonly used loading methods and has been previously shown to induce osteogenic and chondrogenic differentiation in MSCs (Kearney *et al.* 2010; McMahon *et al.* 2007).

The recent success of tissue engineering has been solely on young patients, particularly those with degenerative disease as a result of sporting injuries (Gudas *et al.*, 2003; Saris *et al.*, 2009). Tissue engineering and regenerative medicine will not realise the true potential without achieving a better scientific understanding of the fundamental issues, chief among which is the influence of age on MSC differentiation under external mechanical stimulation, e.g. uniaxial stretching on a substrate. It has been shown that MSCs from aged donors display typical biomarkers of ageing, such as decreased expression of actin, deceased expression of integrin subunits and increased peroxidation (McKayed *et al*, 2010). It has also been demonstrated that these aged-related changes can be interpreted into alterations in structural and me-

chanical behaviours of cellular components, affecting the mechanics inside a cell under external mechanical stimulation.

The aim of this study is to demonstrate that the mechanoregulation modelling approach established in this thesis can be used to give a scientific explanation on the experimental findings from a mechanoregulatory perspective. Most importantly, it is the author's intention to demonstrate how cell experiments of such a kind can be used to validate mechanoregulation theories. The author would like to investigate whether or not MSC ageing plays a role in cell differentiation subjected to uniaxial stretching. In addition, the influence of seeding density on cell mechanics of MSCs loaded with substrate stretching is also within the author's interests. Specifically, it is hypothesised that the role of MSC ageing on cell differentiation due to uniaxial stretching could be as influential as seeding density and therefore deserves to be considered when designing MSC loading schemes.

3.5.2 Finite element model of substrate stretching

The same model described in Chapter 3.2 was used to investigate the effect of MSC ageing and cell seeding density when subjected to uniaxial substrate stretching. Both a single cell (Figure 3.7) and a group of four and five cells (Figure 3.8) residing on a substrate were simulated. A linear elastic material with Young's modulus of 160 kPa and Poisson's ratio of 0.3 (Stem and Nicolella, 2013) was used for the substrate.

Tissue type	Cell membrane stain
Fibrous tissue	$\varepsilon_{mem} > 0.082$
Cartilage	$0.027 < \varepsilon_{mem} \leq 0.082$
Bone	$0.003 < \varepsilon_{mem} \leq 0.027$
Resorption	$\varepsilon_{mem} \leq 0.003$

Table 3.5. Mechanoregulatory indexes established on cell membrane strain. The calculation and conversion were explained in details in Chapter 3.3.

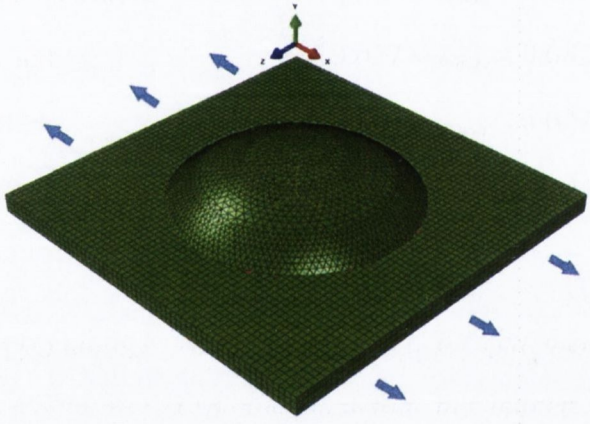


Figure 3.7. A cell model resided on a substrate. The cell-substrate interactions between the cell basal area and the top surface of the substrate are modelled by direct linkers shown in red.

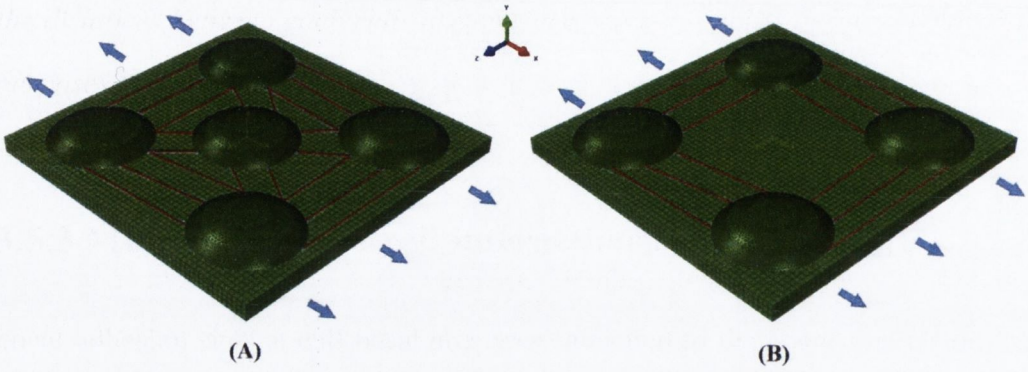


Figure 3.8. Simulation setup for substrate stretching with (A) 5 cells and (B) 4 cells. The interactions between each neighbouring cells are shown in red lines. Note that the distances between each cells are exaggerated for simplification and clarification purposes.

3.5.3 Modelling of cell-cell interactions

Focal adhesion sites at cell basal area were attached to the nearest nodes on the top surface of the substrate (Figure 3.7). These attachments represent the integrin-mediated adherens junctions that mechanically connect the AFs of a cell to the ECM (Wang *et al.*, 2008). Cell-cell interactions were modelled by directly linking the closest corresponding receptors between neighbouring cells (Figure 3.8). Theses linkers can resist both tensile loads generated by anchoring junctions that mechanically bind the IFs and AFs of neighbouring cells and compressive loads initiated by gap junctions that prevent the neighbouring cell from physically contacting each other (Reinhart-king *et al.*, 2008). Both of these linkers were assumed to be rigid in the current study.

3.5.4 Loading conditions

To examine whether ageing affects MSC differentiation when subjected to uniaxial stretching, simulations with a single cell resided on a substrate were performed (Figure 3.7). Four different stretching magnitudes, 2.5%, 5%, 7.5% and 10%, were applied to the substrate with a young cell resided on (Figure 3.7). To investigate the influence of seeding density and the role of cell-cell interactions in uniaxial loading conditions, a 10% stretching was applied to the substrate with a monolayer of four and five young cells seeded on, respectively (Figure 3.8). Comparative studies were performed to capture the effects of MSC ageing and seeding density.

Chapter 4

4. Results

4.1 Finite element modelling of a single adherent cell

4.1.1 Cell stiffness

Using Equation 3.3 the elastic moduli of the cell models were calculated and averaged at 4.08 kPa at the apex and 5.87 kPa at the receptor site, indicating that indentation location has a great influence on the predicted cell stiffness. In comparison, age-related changes proposed in this study are not predicted to impact greatly on the stiffness of cells. A mere 5% increase in predicted stiffness is seen with the addition of age-related changes, from 4.85 kPa for young cells to 5.09 kPa for aged cells. These predicted cell stiffness values are within the range of experimentally measured cell stiffness using AFM indentation (Table 4.1).

Cell type	Measured stiffness (kPa)
mESC[1]	1.49±0.09
Fibroblast[2]	6.00±2.30
Myoblast[3]	11.50±1.30
Osteoblast[4]	5.20±0.60 (S phase) 2.30±3.30 (G1 phase)

[1]Pillarisetti *et al.* 2011; [2]Azeloglu *et al.* 2008; [3]Collinsworth *et al.* 2002; [4]Kelly *et al.* 2011.

Table 4.1. Experimentally measured cell stiffness using AFM from previous studies.

4.1.2 Force-displacement curves

A non-linear force-displacement behaviour was predicted for all AFM indentation simulations, with the degrees of non-linearity differing depending on indentation site. The indenting position, at a receptor site vs. at the apex distant from the receptor site, is the most influential to the cells response to indenting force. An approximately 30% stiffer response is predicted when indenting at the receptor site, compared to the case when indentation occurs at the apex of the cell. Though slight, age-related changes do affect the cells behaviour under AFM indentation, indicating that cell stiffness changes with ageing (solid green curve vs. dashed brown curve; solid lime curve vs. dashed orange curve in Figure 4.1). An increase in the membrane stiffness stiffens cells response to indenting force at both indentation locations, whereas a decrease in the complexity of CSK-NSK network increases the predicted cell stiffness at both indenting locations. The difference in cell stiffness caused by ageing is most apparent when indentation takes place at the apex of the cell (Figure 4.1). In the case of indenting at a receptor site where the CSK is in contact with cell membrane, a direct load transfer from indenter and CSK diminishes the impact of CSK complexity and membrane stiffness. In all cases, the indentation depth ranges from 13.7% to 23.4% of the original cell height, indicating that simulations are reliable and would return realistic results in a real experimental environment (Moeendarbary *et al.*, 2013).

4.1.3 Biophysical stimuli inside cells

There is a striking difference in the pattern of stress inside a cell depending on indentation at the apex compared to receptor site, compare Fig 3.4A with Fig 3.4C, and compare Fig 3.4B with Fig 3.4D. However, the difference due to ageing is not so visually obvious, compare Fig 3.4A with Fig 3.4B, and compare Fig 3.4C with Fig 3.4D. Apart from a stress concentration at the indenting location, the stress in the nucleus is higher than any other location in the cytoplasm: This is due to the IFs that transmit indenting force from cell membrane directly to the nucleus.

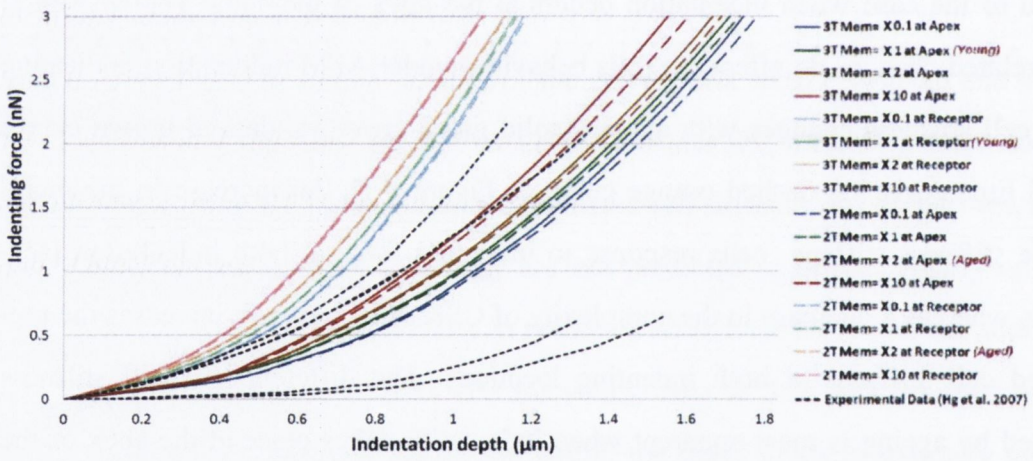
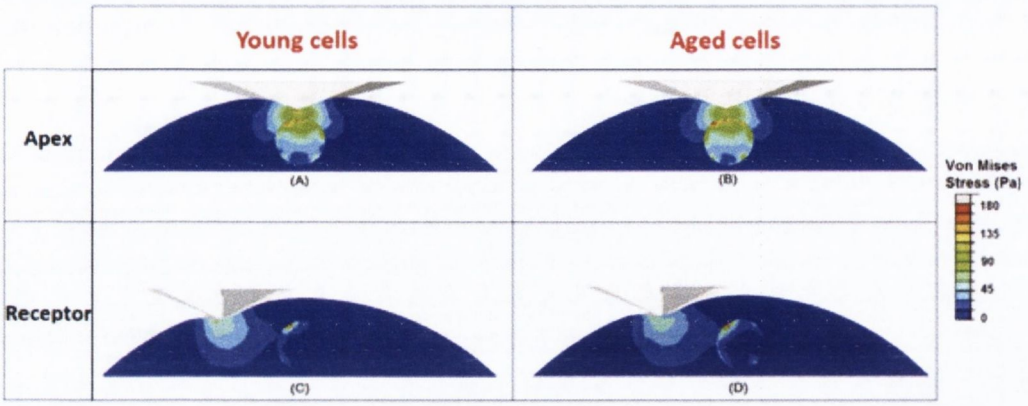
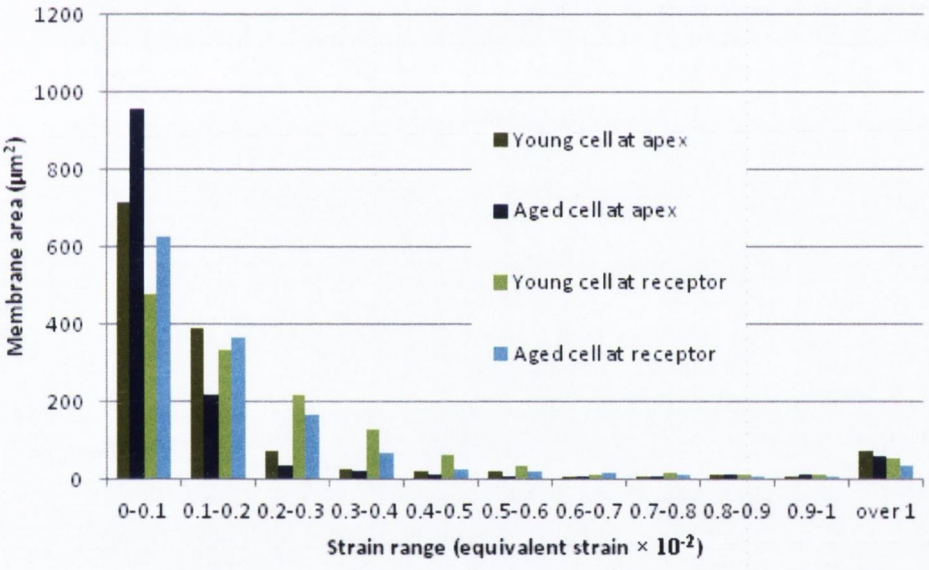


Figure 4.1. Force-displacement curves from indentation at two different indenting locations (apex and a receptor site), with the stiffness of cell membrane varying from 0.1 time (x0.1) to 10 times (x10) of the original value for a normal (young) cell. The experimental data are taken from a study measuring the stiffness of bovine chondrocytes using AFM indentation (Ng et al. 2007) and shown in the figure as dotted black curves.



(A)



(B)

Figure 4.2. (A) Contour plots of Von Mises stress during indentation simulation with different indenting locations, at apex (A, B) and a receptor site (C, D) of young cells (A, C) and aged cells (B, D). Cut-views are shown for visual comparison of Von Mises stress inside the cells. (B) Area of membrane within a given strain range. Aged cells have smaller membrane area under high strain and correspondingly have greater membrane area under low strain, than young cells subjected to indentation.

To quantify the strain difference in cell membrane when subjected to an indenting force, equivalent strain was compared across all scenarios (Figure 4.2). Despite the difference made by cell age and indentation location, the total strained surface area decreases as strain range increases (Figure 4.2 (B)). While almost no difference can be seen at mid-range, the differences are quite evident at low strain ranges. At high strain range, possibly at the interface between the cell and indenter, small differences in strained area can also be found.

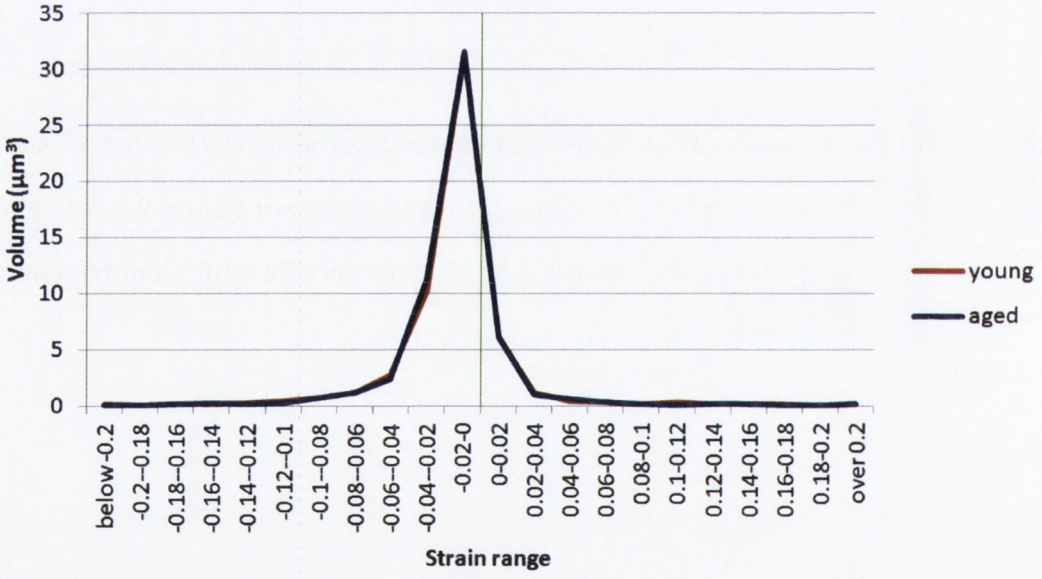


Figure 4.3 (A). Volume of nucleus within a given strain range (hydrostatic strain) when the cell model was indented at the apex. The slim green line indicates zero strain location. Little difference can be seen between the aged and young cells.

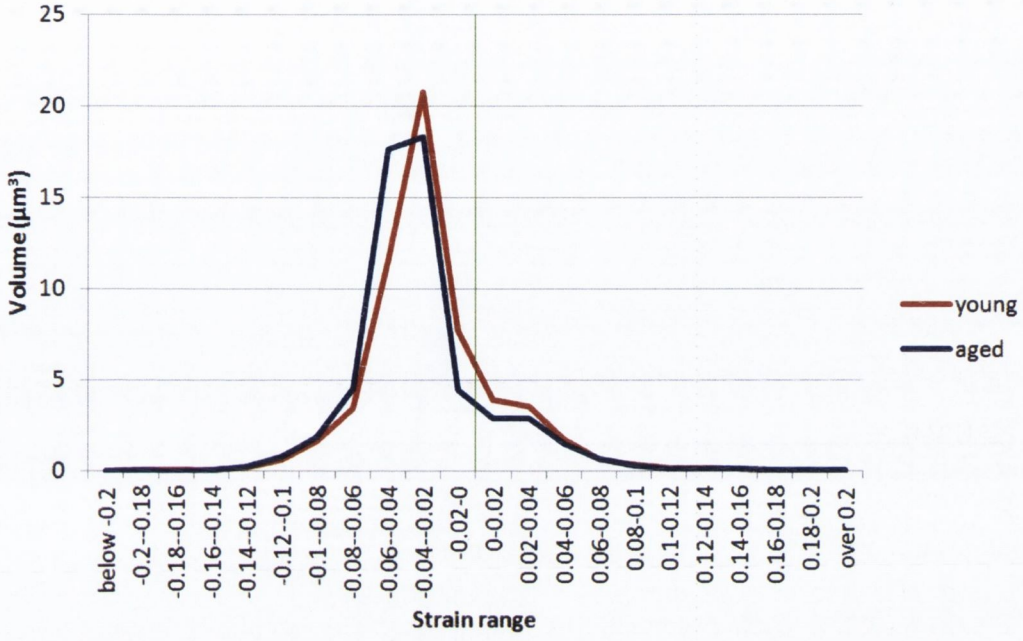


Figure 4.3 (B). Volume of nucleus within a given strain range (deviatoric strain) when the cell model was indented at the apex. The slim green line indicates zero strain location. Differences are seen between aged and young cells at mid-low strain ranges, particularly in the negative region.

A comparative study was carried out on the hydrostatic and deviatoric strain in the cell nucleus when undergoing indentation simulation at the cell apex (Figure 4.3). While the young and aged cells exhibit no difference in terms of hydrostatic strain, deviatoric strain does show a slight difference, especially at low strain ranges. This suggests that the nuclei of the cells may be strained differently depending on the degree of ageing, with particular emphasis on the change in shape rather than volume.

4.2 Finite element modelling of gap tissue formation

4.2.1 Tissue differentiation under force control

Under force control, the stimulation on the gap tissue that is created by the displacement between the bone and the implant decreased over time, as a result of cell-tissue stiffening over the course of simulation, as shown in Figure 4.4. Depending on the debonding scenarios, the displacement of the implant varied upon the initial application of the force, ranging from 21.89 μm, for the most serious debonded case, to 10.85 μm when no debonding occurred. It is also predicted that different behaviours of tissue stiffening occur as a result of gap tissue differentiation in response to different loading magnitudes on the implant (Figure 4.6 – 4.9). When a large force was applied in loading case 1 (0.48 μN), the membrane of MSCs that were imbedded in the granulation tissue blocks experienced a large strain and differentiated into fibroblasts, which in turn secreted and formed fibrous tissue to fill in the surrounding blocks representing the ECM. As the cell-tissue blocks stiffened from granulation tissue to fibrous tissue, the displacement of the implant decreased and, as a result, the strain that the cell membrane received decreased to a level that fits into the cartilage region of the mechanoregulation chart as shown in Table 3.3. As a consequence, it was assumed that fibroblast apoptosis occurs due to the change in mechanical stimuli (Perez and Prendergast, 2007) and fresh MSCs invade into the space and differentiate into chondrocytes, producing cartilage under such a mechanical environment. This differentiation process carried on, through the formation and apoptosis of chondrocytes and cartilage, and eventually reached the region of ossification before an equilibrium condition was achieved in which no further change in cell-tissue types occurs. In cases when smaller forces are applied, the ini-

tial displacements of the implant were not large enough to strain the cell membrane to fibrous tissue region (loading case 2) and cartilage region (loading case 3) in the mechanoregulation chart. As a consequence, the process of differentiating into such tissue types did not occur and skipped to the next corresponding phenotype.

Though it is evident that different tissue types can appear simultaneously at a specific given time point of a simulation, ossification is predicted under force-control for the majority of the scenarios investigated in this study (Figure 4.14-4.17), with an exception of the formation of a mixture of cartilage and bone when a serious debonding occurred (Figure 4.18). A full set of simulation results under force-control with different loading magnitudes are provided in Appendix A – E.

4.2.2 Tissue differentiation under motion control

Under motion control, the resultant reaction force on the implant jumped upon the initial application of vertical downward displacements, to a level ranging from 0.42 μN, in debonding case 4, to 0.89 μN for the fully bonded case (Figure 4.5). As a result, the original granulation tissue differentiated into different tissue types, depending on the level of membrane strain the cells felt, just like the situation under force-control. However, little change in membrane strain was found in subsequent iterations as the displacement of the implant remained constant during each simulation. Consequently, no further tissue differentiation occurrence was predicted. Therefore, loading magnitude is predicted to be the dominant factor in deciding MSCs fate. If a large displacement is applied to the implant, the cell membrane receives a large enough strain and differentiates into fibroblasts and fibrous tissue is formed as a result (Figure 4.10 – 4.11). If a smaller displacement is applied to the implant, a gap

tissue differentiation towards osteochondral direction is predicted under motion-control (Figure 4.12 – 4.13). A full set of simulation results under motion-control with different loading magnitudes are provided in Appendix F – J.

4.2.3 The effects of debonding

Debonding has a substantial influence to the mechanical behaviours of the gap tissue loaded with both force-control and motion-control manners. The mechanical response from the gap tissue was weakened by all debonding cases and tended to deteriorate as debonding propagated (from debonding case 1 to case 4) as illustrated in Figure 4.4 and Figure 4.5, for force-control and motion-control, respectively.

Debonding is also predicted to have a great impact on the differentiation process of gap tissue. Without debonding, ossification occurred with all loading conditions under force-control. However, any debonding scenario promoted bone resorption, leaving a mixture of bone with different proportions of resorped regions (Figure 4.14 – 4.17). In the most extreme scenario, when a force was applied to the implant with serious debonding (debonding case 4), the gap tissue contained a mixture of bone, cartilage and resorption (Figure 4.18). Different results were also predicted under motion-control with debonding taken into account. The debonded cell-tissue block was under-stimulated compared to fully bonded scenario in the same loading condition, and differentiated into different tissue types as a result (Figure 4.19 – 4.23).

4.2.4 The effects of age-related changes

Age-related changes were also predicted to affect tissue differentiation. Despite the small changes in gap tissue differentiation patterns found between young and aged cells under both force-control (Figure 4.6 – 4.9) and motion-control (Figure 4.10 – 4.13), varying the membrane stiffness to an extensive range does induce greater differences in tissue differentiation (Figure 4.14 – 4.23). Specifically, an earlier bone formation can be seen as a result of an increased membrane stiffness under force-control (Figure 4.14 – 4.18), indicating a stiffer membrane promotes quicker ossification under such loading conditions.

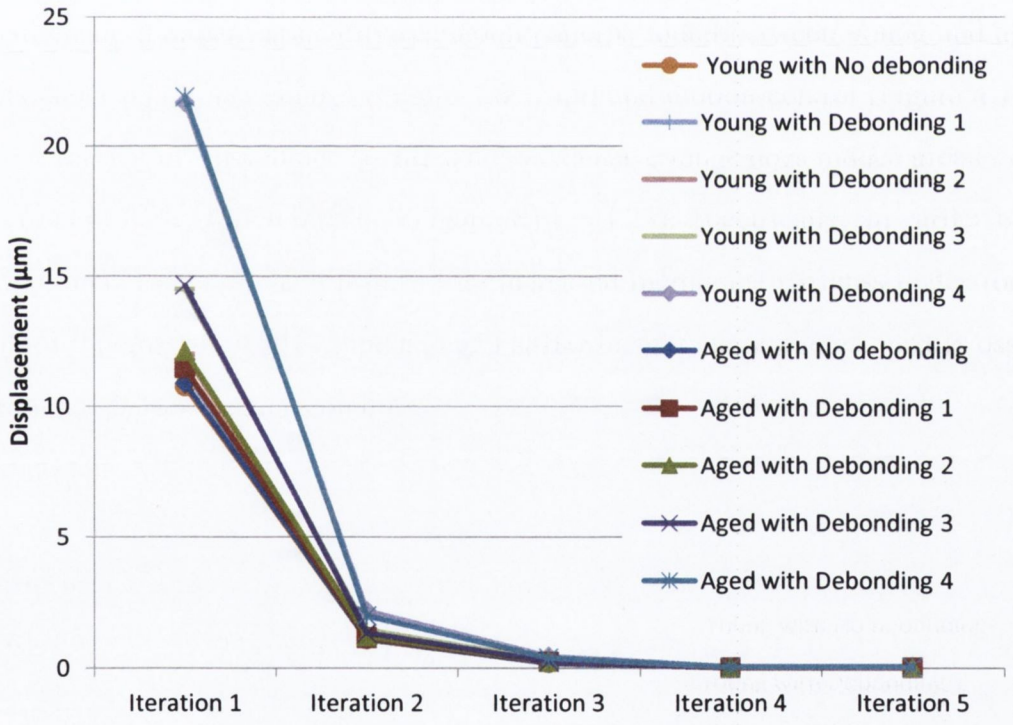


Figure 4.4. Displacements of the implant when loaded with a vertical downward force of 0.48 µN. Debonding greatly alters the implants' behaviour. However, little change can be seen between young and aged cells. Debonding 1 – 4 denotes different debonding cases shown in Figure 4.3.

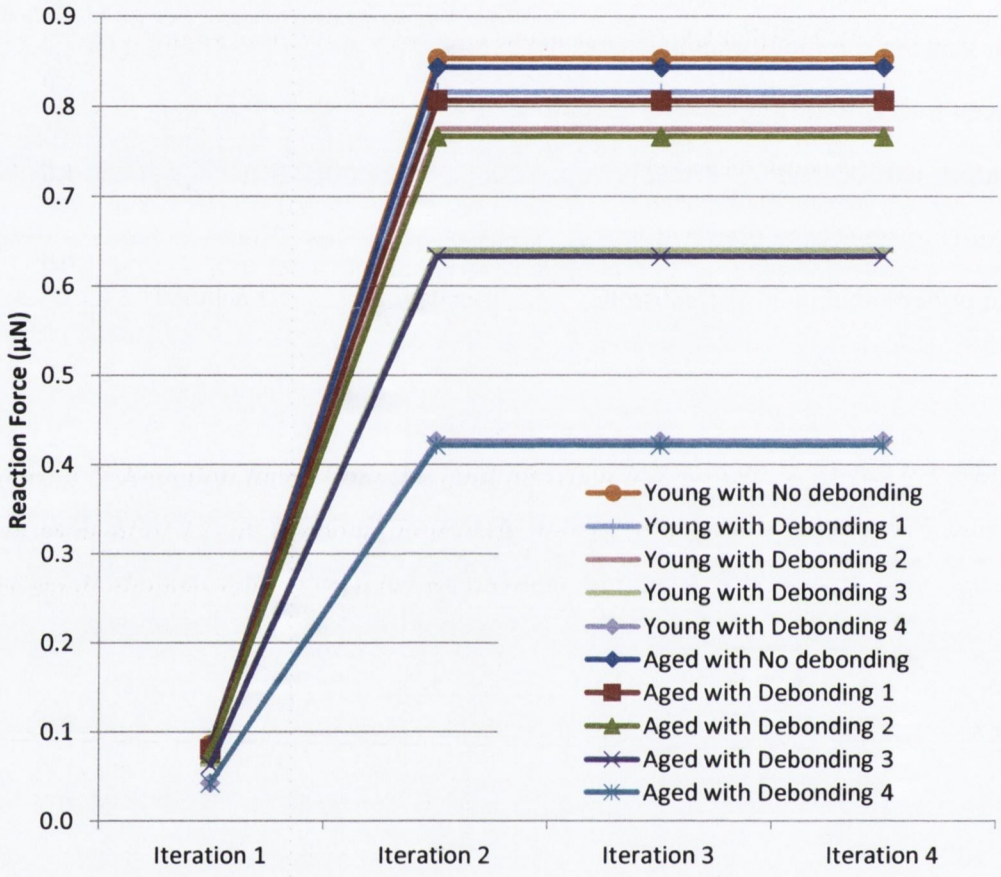


Figure 4.5. Reaction force from the implant when loaded with a vertical downward displacement of 12 μm. Debonding greatly alters the implants' behaviour. However, very small changes can be seen between young and aged cells.

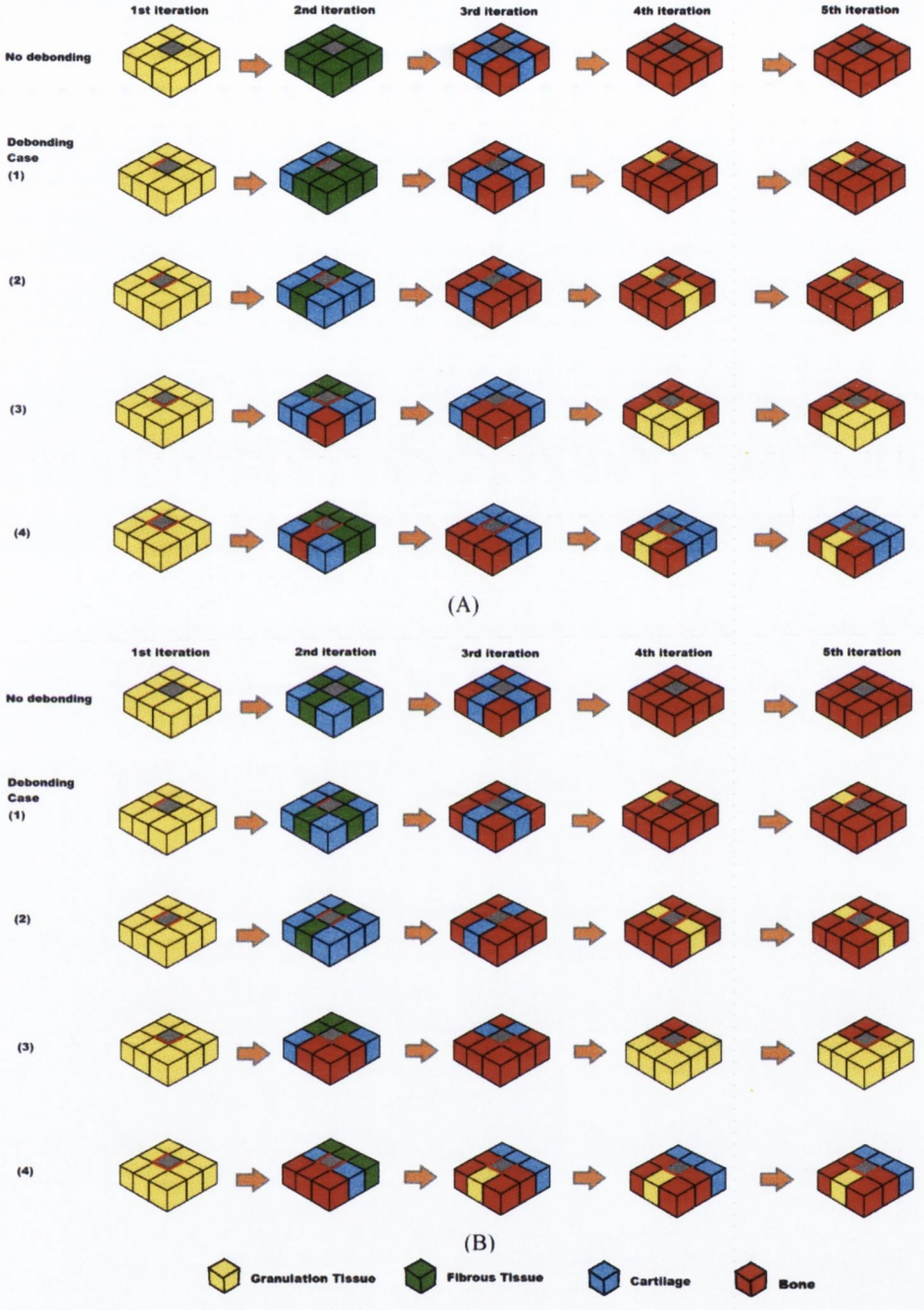


Figure 4.6. Tissue differentiation patterns of young (A) and aged (B) cells under force-control with a loading magnitude of 0.48 μN. Four different debonding scenarios were simulated and compared with un-debonded case.

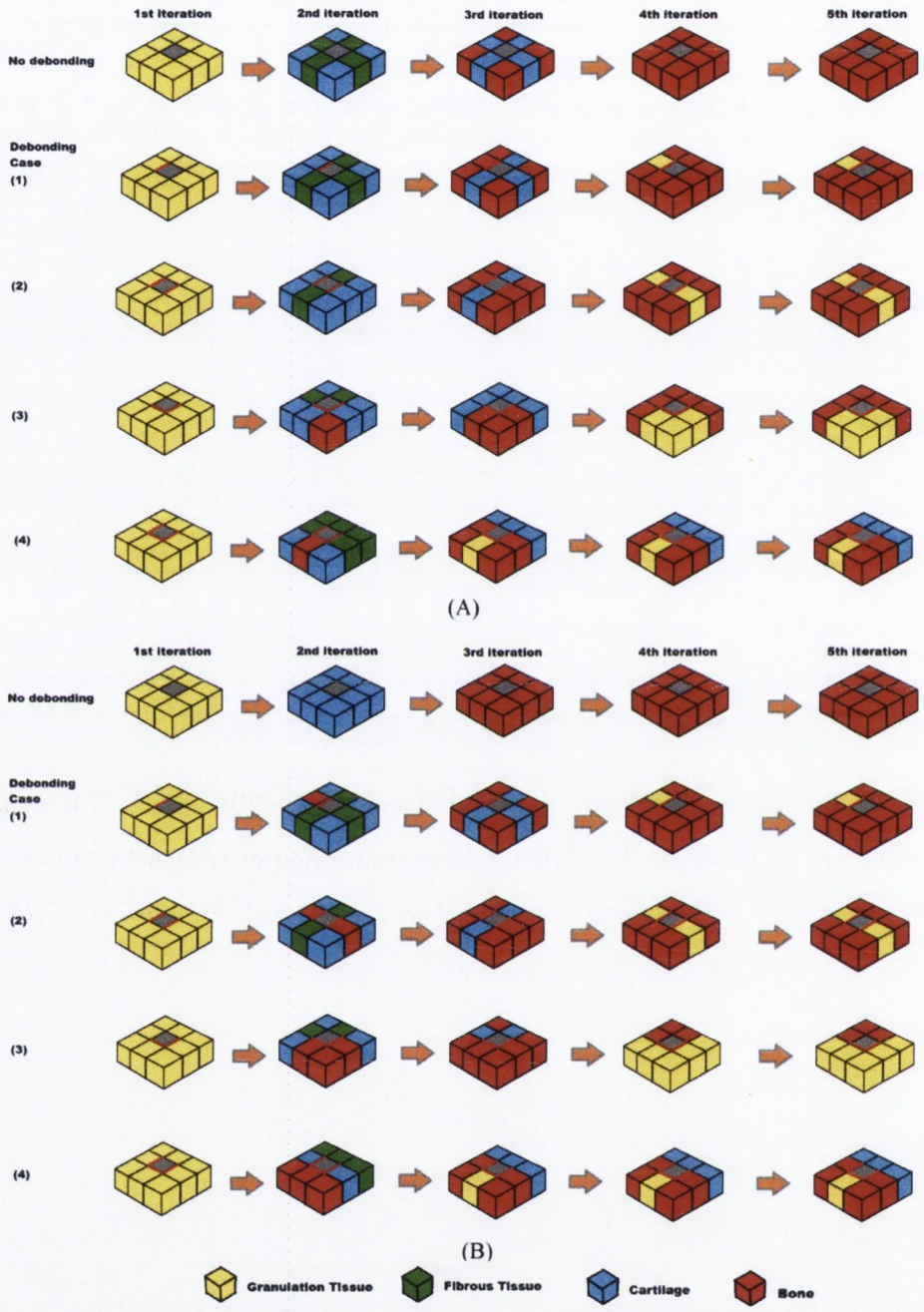


Figure 4.7. Tissue differentiation patterns of young (A) and aged (B) cells under force-control with a loading magnitude of 0.36 μN. Four different debonding scenarios were simulated and compared with un-debonded case.

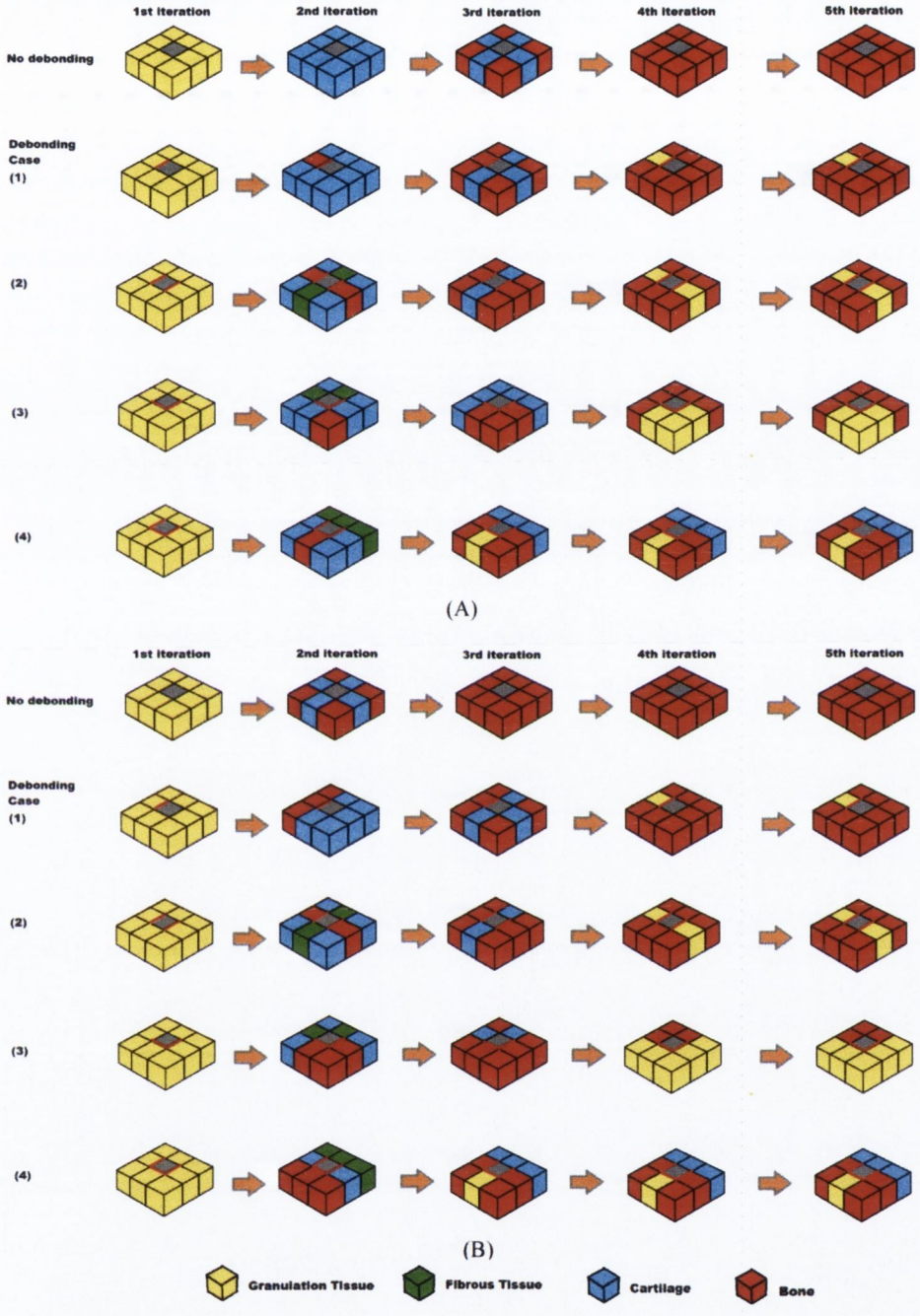


Figure 4.8. Tissue differentiation patterns of young (A) and aged (B) cells under force-control with a loading magnitude of 0.24 μN. Four different debonding scenarios were simulated and compared with un-debonded case.

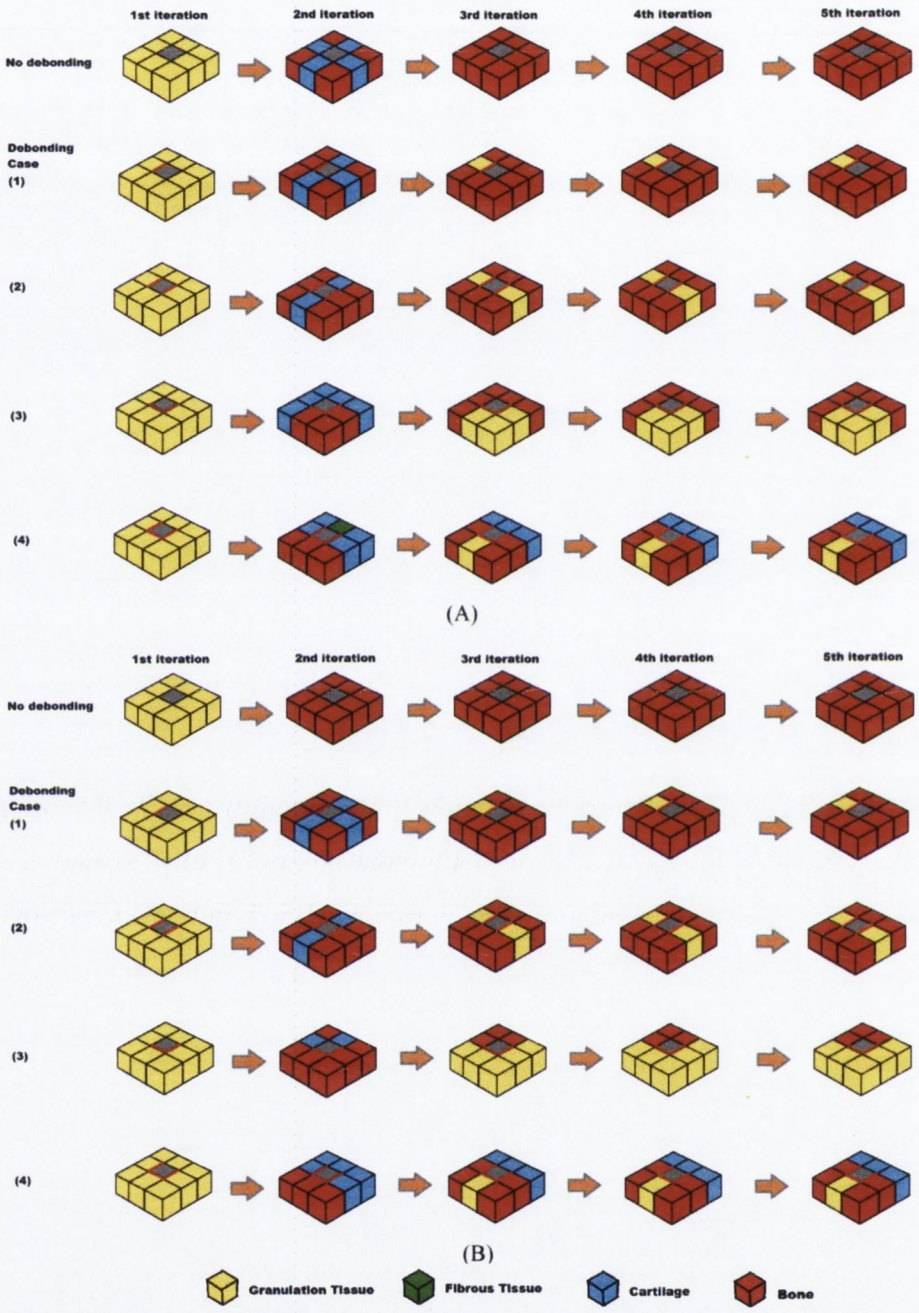


Figure 4.9. Tissue differentiation patterns of young (A) and aged (B) cells under force-control with a loading magnitude of 0.12 μN. Four different debonding scenarios were simulated and compared with un-debonded case.

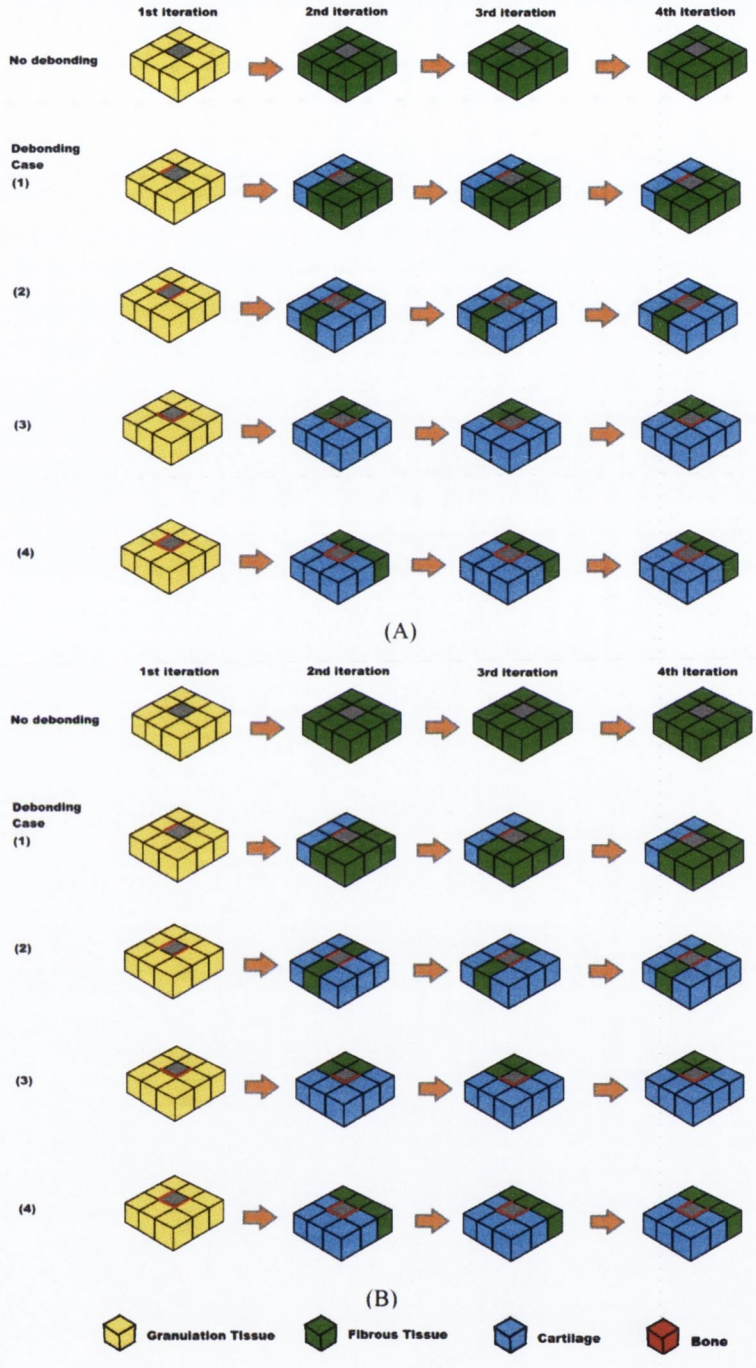


Figure 4.10. Tissue differentiation patterns of young (A) and aged (B) cells under motion-control with a loading magnitude of 12 μm. Four different debonding scenarios were simulated and compared with un-debonded case.

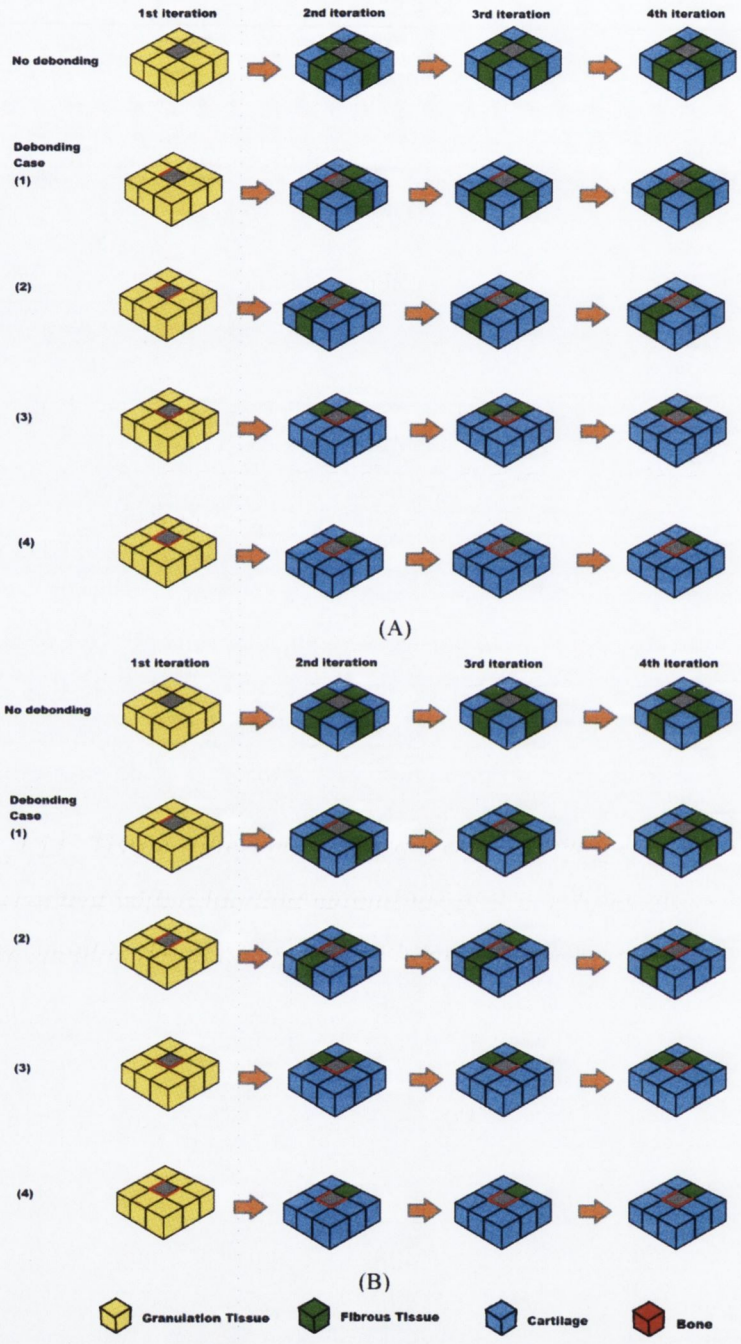


Figure 4.11. Tissue differentiation patterns of young (A) and aged (B) cells under motion-control with a loading magnitude of 9 μm. Four different debonding scenarios were simulated and compared with un-debonded case.

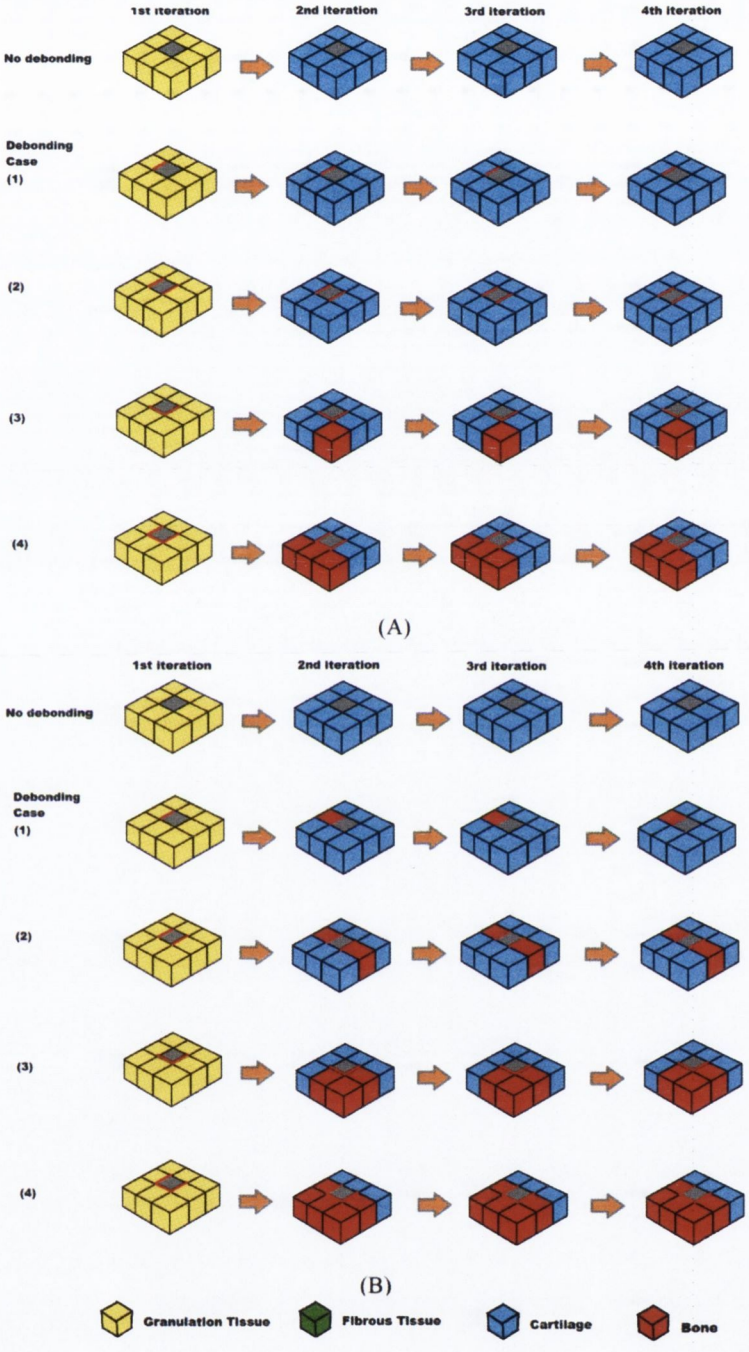


Figure 4.12. Tissue differentiation patterns of young (A) and aged (B) cells under motion-control with a loading magnitude of 6 μm. Four different debonding scenarios were simulated and compared with un-debonded case.

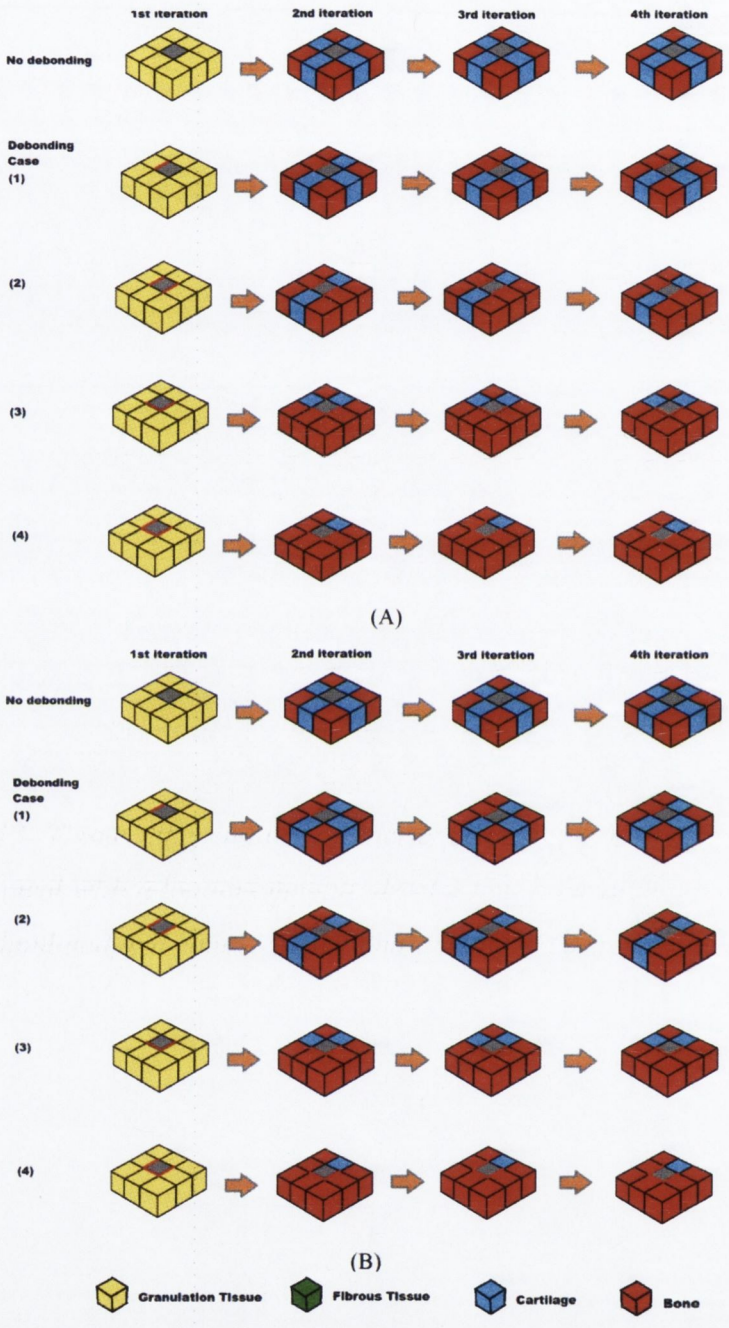


Figure 4.13. Tissue differentiation patterns of young (A) and aged (B) cells under motion-control with a loading magnitude of 3 μm. Four different debonding scenarios were simulated and compared with un-debonded case.

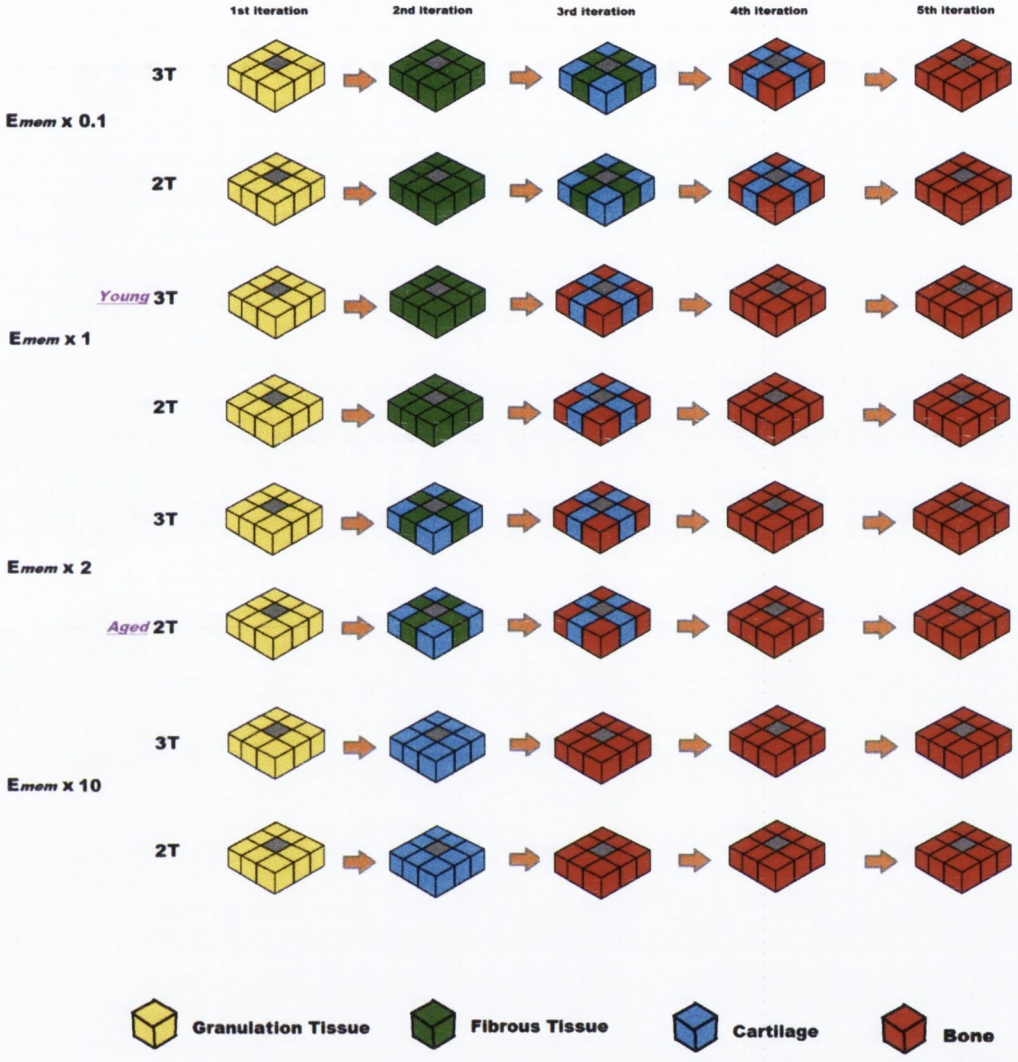


Figure 4.14. Tissue differentiation patterns under force-control with a loading magnitude of 0.48 μN without debonding. The stiffness of cell membrane was altered from 10% (x0.1) to 10 times (x10) of the original young cell. The highlighted two lines, i.e. Emem x1 (3T) and Emem x2 (2T) are the young and aged cells, respectively, according to the descriptions in the Methods in this study.

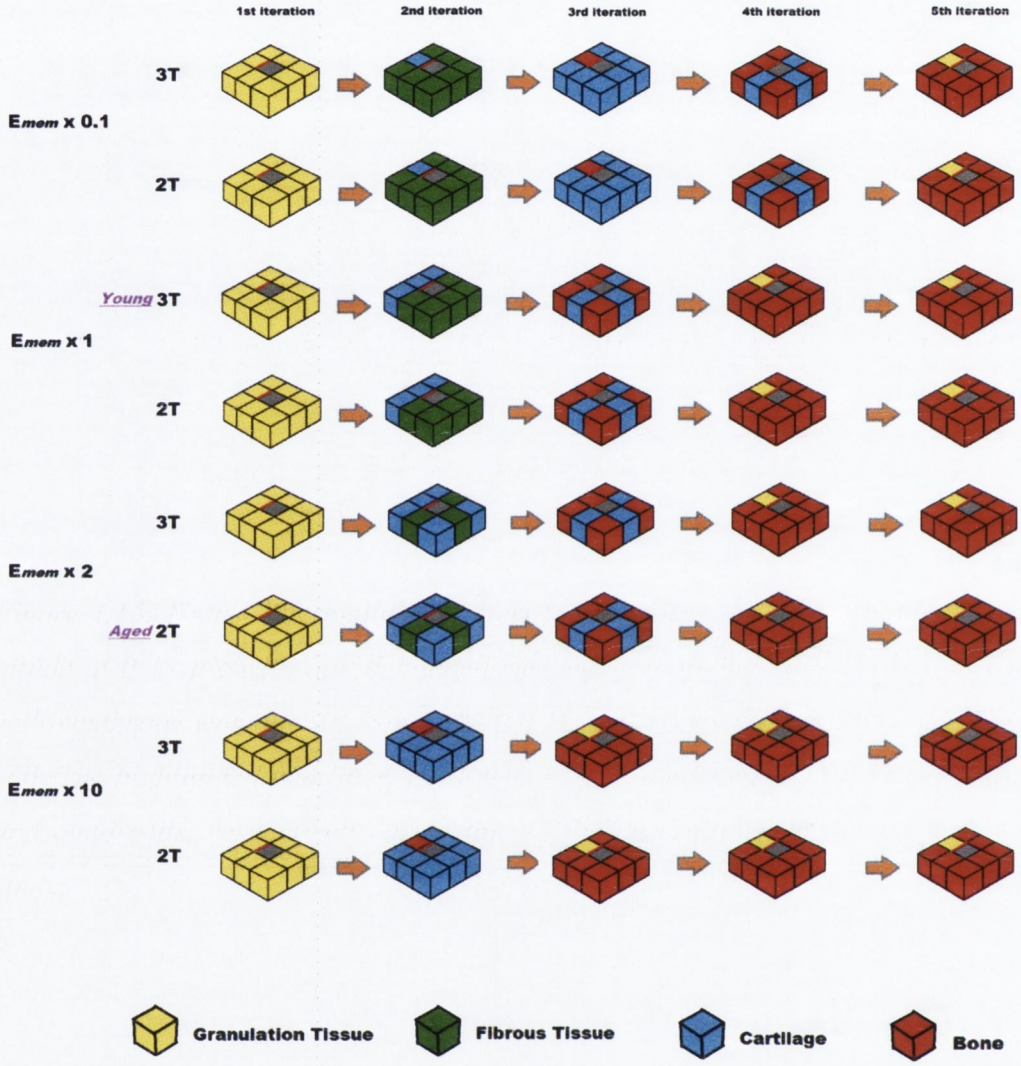


Figure 4.15. Tissue differentiation patterns under force-control with a loading magnitude of 0.48 μN with one debonded surface (Debonding case 1). The stiffness of cell membrane was altered from 10% (x0.1) to 10 times (x10) of the original young cell. The highlighted two lines, i.e. Emem x1 (3T) and Emem x2 (2T) are the young and aged cells, respectively, according to the descriptions in the Methods in this study.

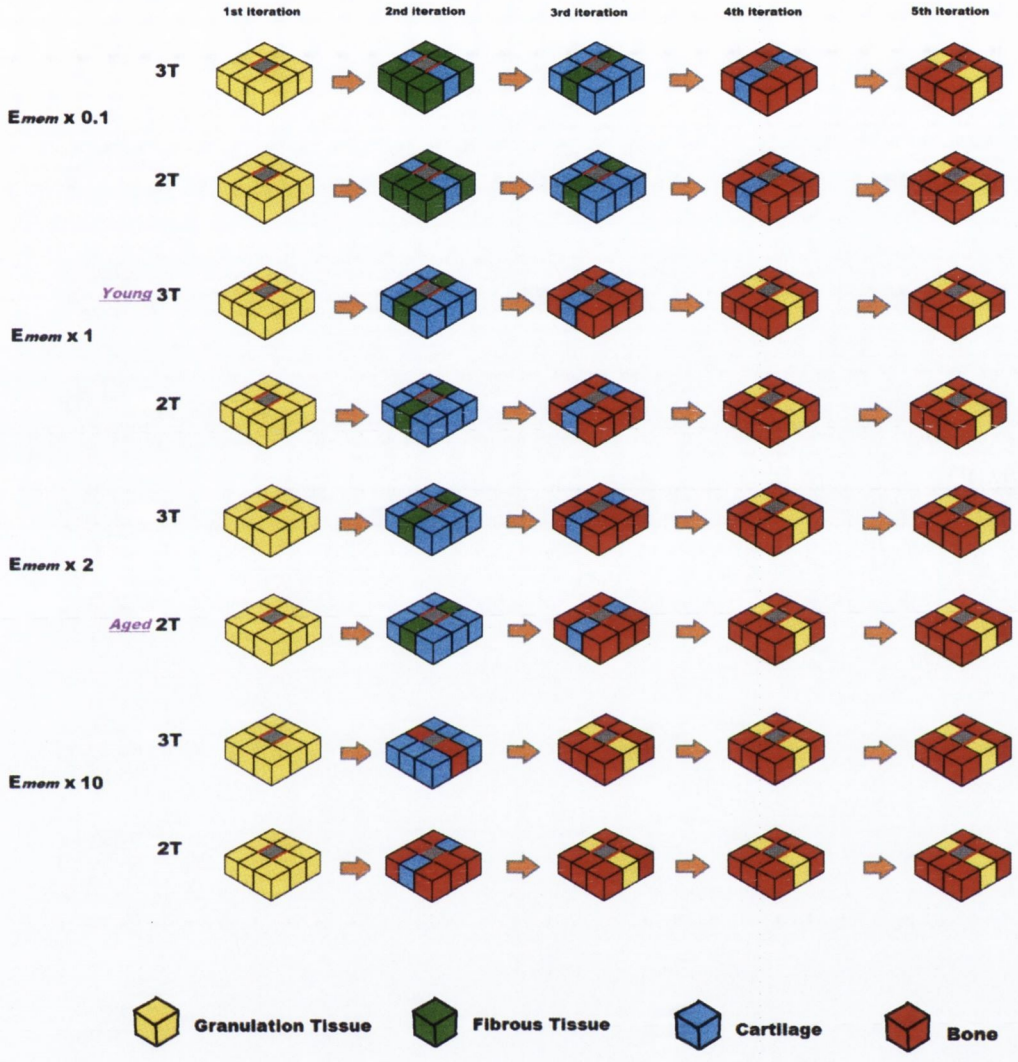


Figure 4.16. Tissue differentiation patterns under force-control with a loading magnitude of 0.48 μN with two opposite debonded surfaces (Debonding case 2). The stiffness of cell membrane was altered from 10% (x0.1) to 10 times (x10) of the original young cell. The highlighted two lines, i.e. Emem x1 (3T) and Emem x2 (2T) are the young and aged cells, respectively, according to the descriptions in the Methods in this study.

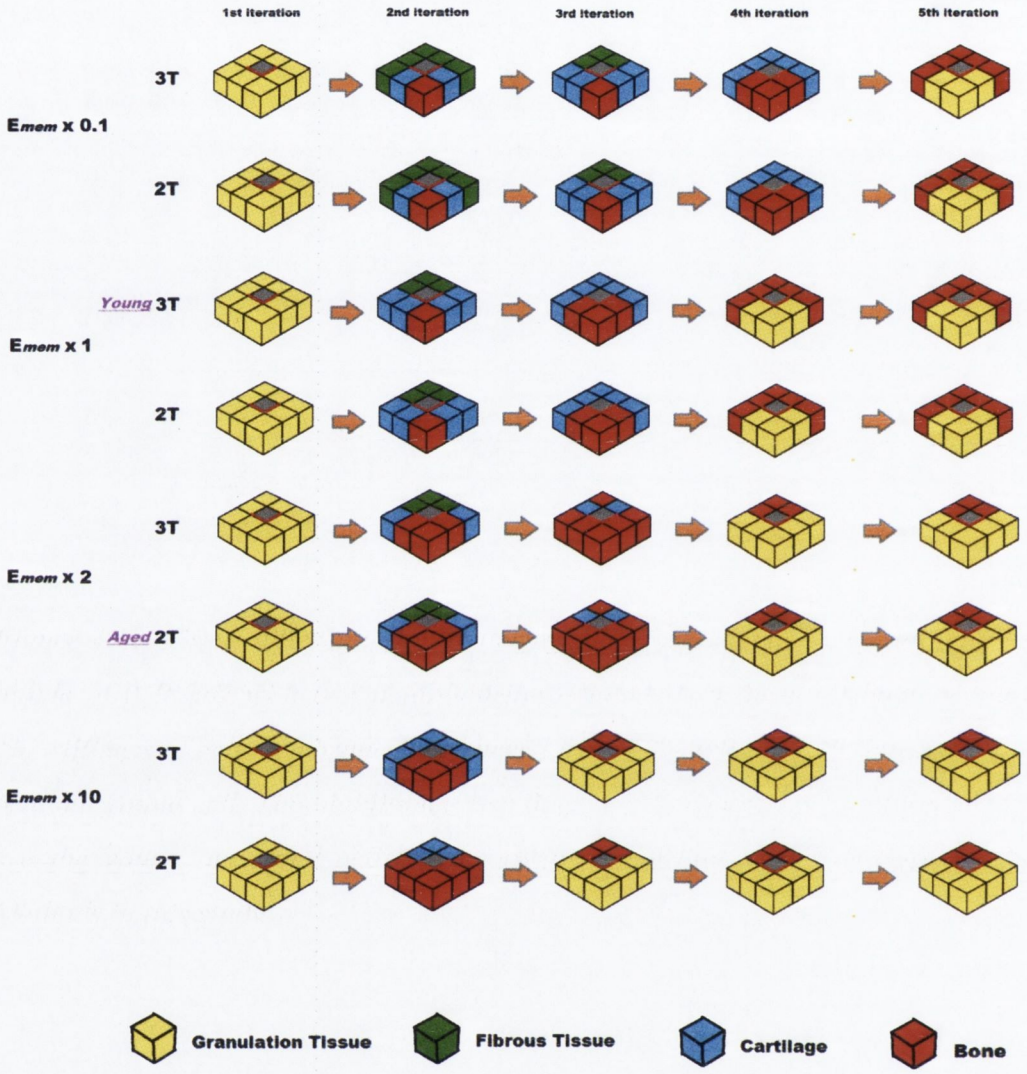


Figure 4.17. Tissue differentiation patterns under force-control with a loading magnitude of 0.48 μN with two neighbouring debonded surfaces (Debonding case 3). The stiffness of cell membrane was altered from 10% (x0.1) to 10 times (x10) of the original young cell. The highlighted two lines, i.e. Emem x1 (3T) and Emem x2 (2T) are the young and aged cells, respectively, according to the descriptions in the Methods in this study.

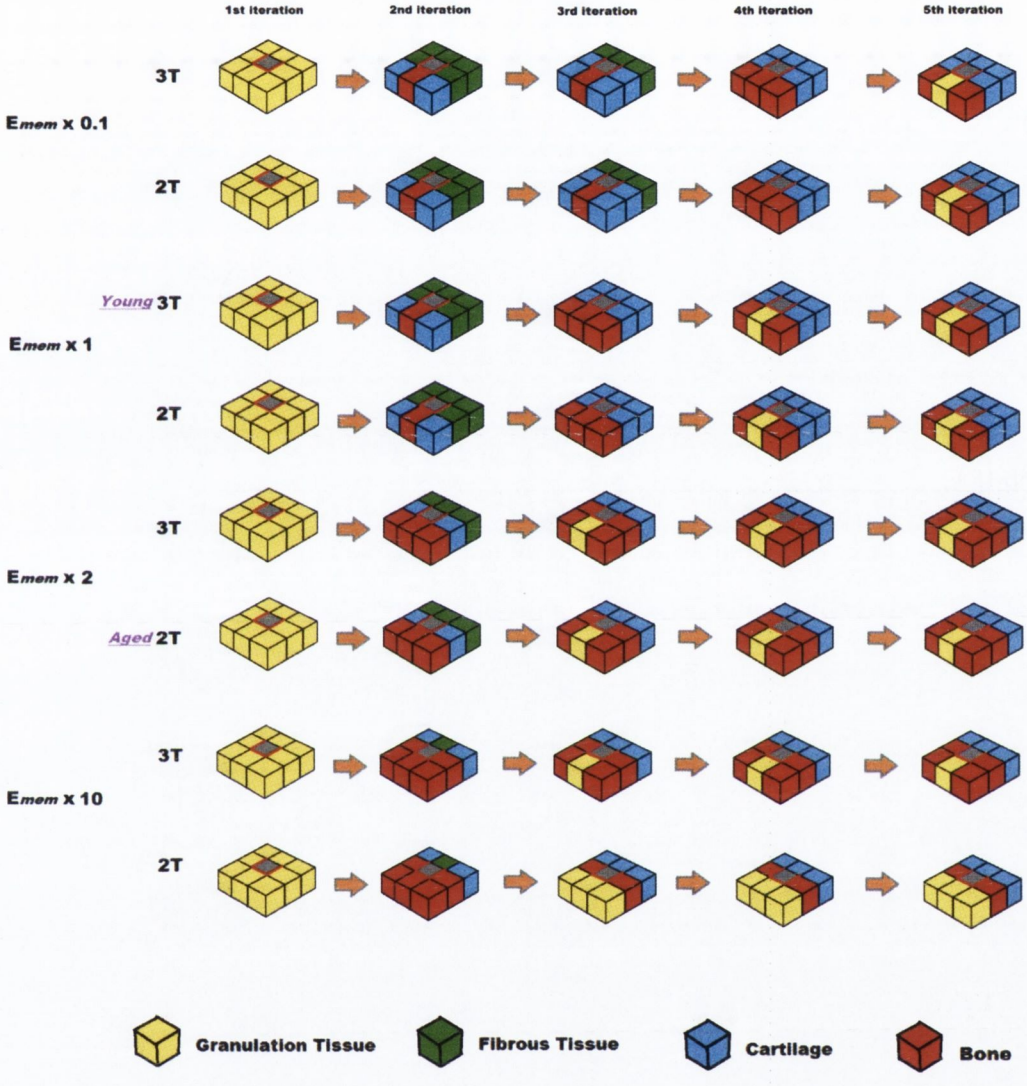


Figure 4.18. Tissue differentiation patterns under force-control with a loading magnitude of 0.48 μN with three debonded surfaces (Debonding case 4). The stiffness of cell membrane was altered from 10% (x0.1) to 10 times (x10) of the original young cell. The highlighted two lines, i.e. Emem x1 (3T) and Emem x2 (2T) are the young and aged cells, respectively, according to the descriptions in the Methods in this study.

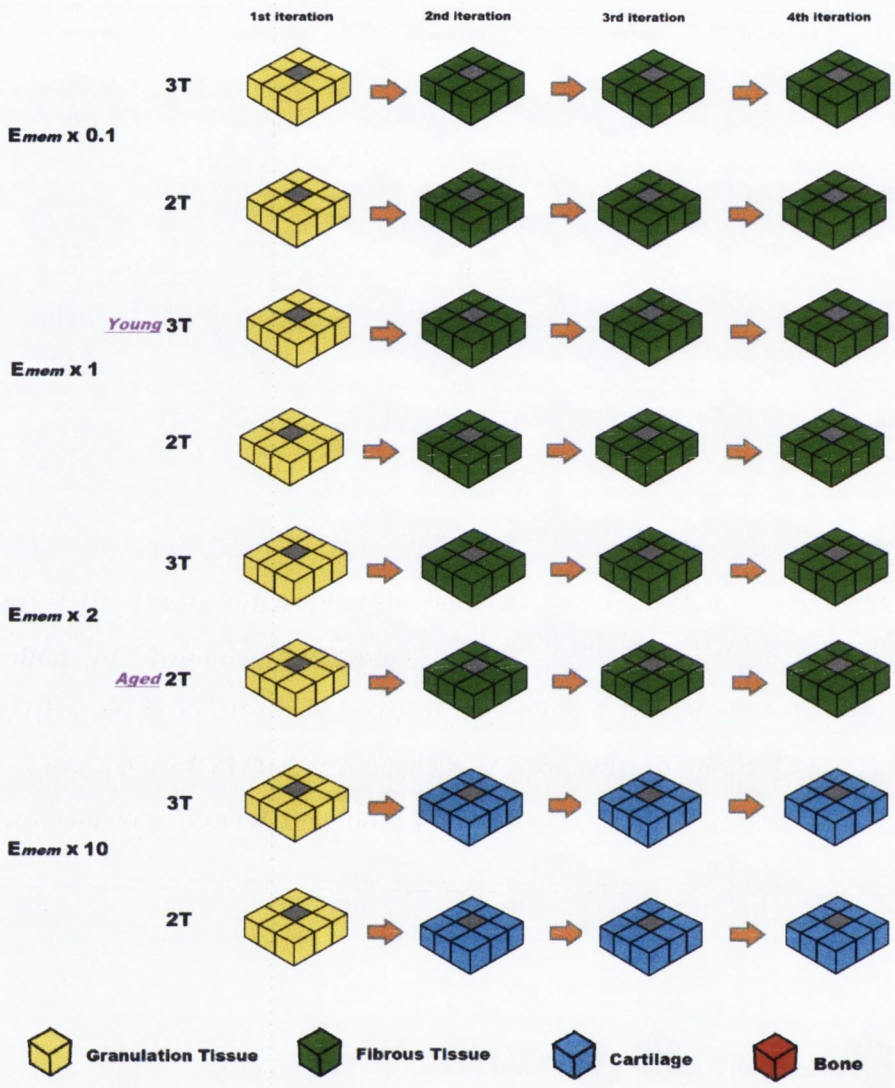


Figure 4.19. Tissue differentiation patterns under motion-control with a loading magnitude of 12 μm without debonding. The stiffness of cell membrane was altered from 10% (x0.1) to 10 times (x10) of the original young cell. The highlighted two lines, i.e. Emem x1 (3T) and Emem x2 (2T) are the young and aged cells, respectively, according to the descriptions in the Methods in this study.

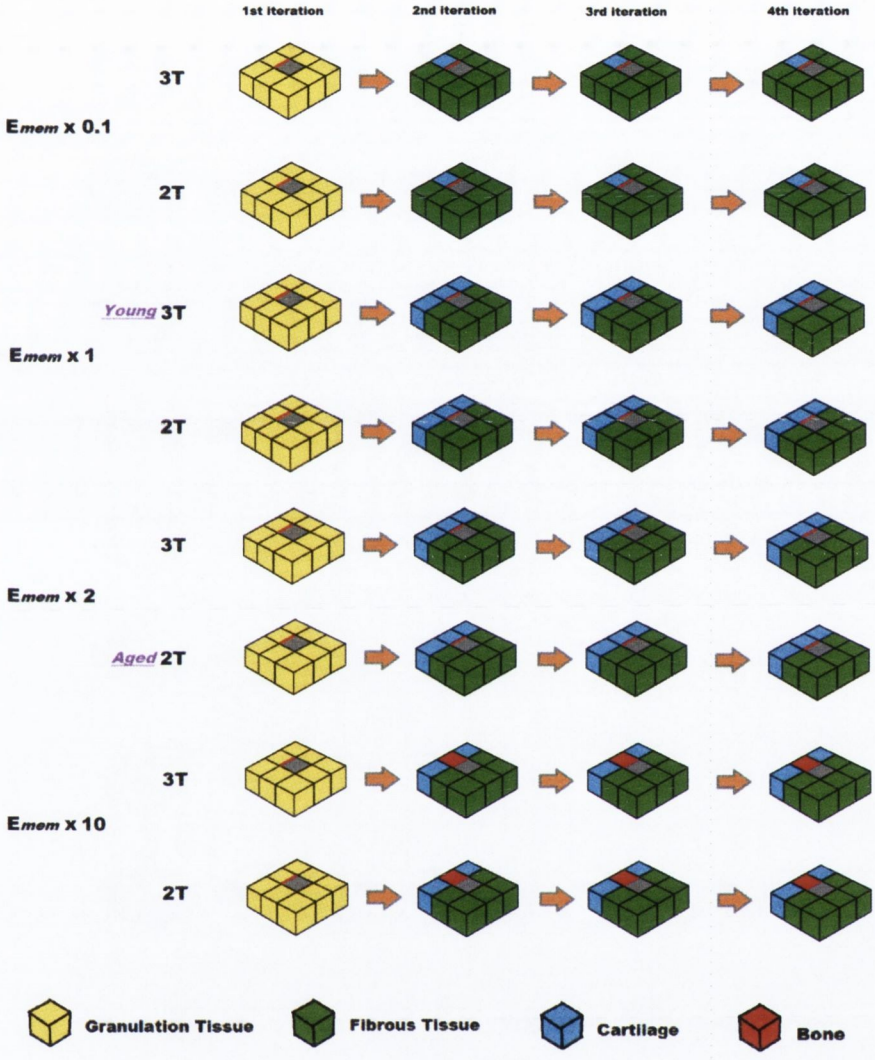


Figure 4.20. Tissue differentiation patterns under motion-control with a loading magnitude of 12 μm with one debonded surface (Debonding case 1). The debond stiffness of cell membrane was altered from 10% (x0.1) to 10 times (x10) of the original young cell. The highlighted two lines, i.e. Emem x1 (3T) and Emem x2 (2T) are the young and aged cells, respectively, according to the descriptions in the Methods in this study.

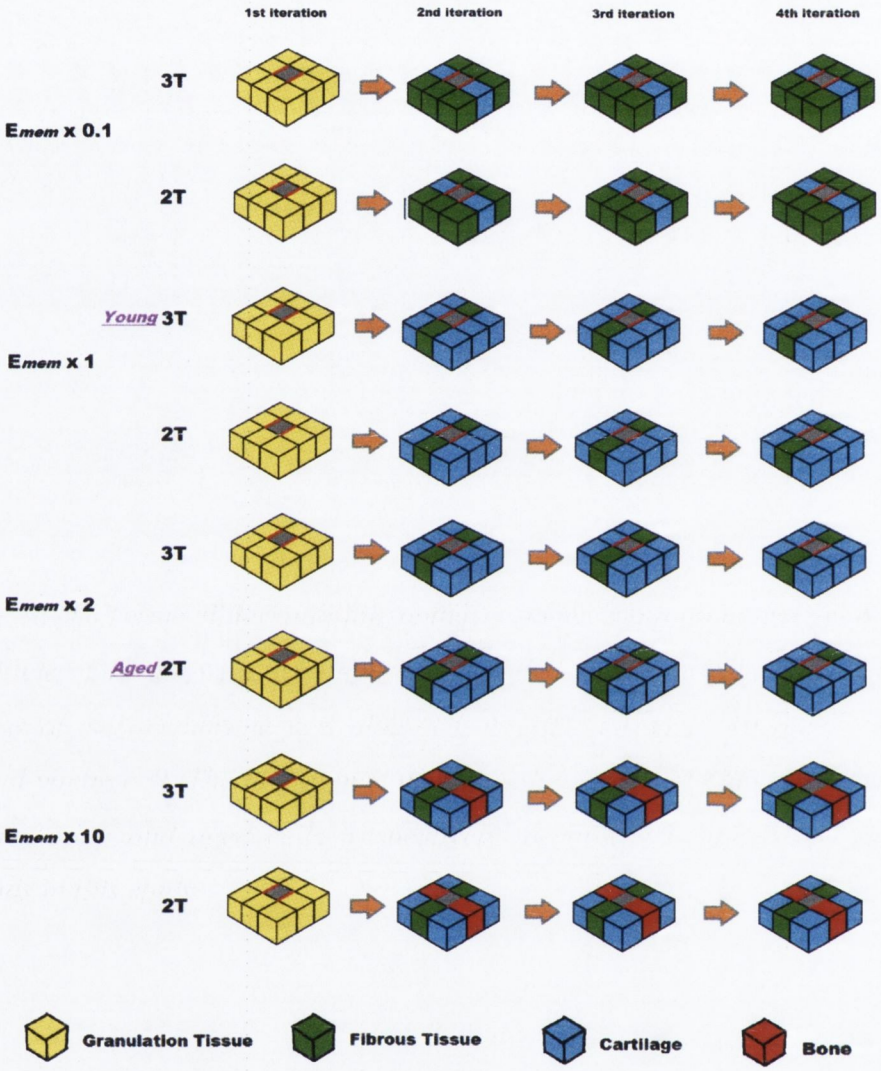


Figure 4.21. Tissue differentiation patterns under motion-control with a loading magnitude of 12 μm with two opposite debonded surfaces (Debonding case 2). The stiffness of cell membrane was altered from 10% (x0.1) to 10 times (x10) of the original young cell. The highlighted two lines, i.e. Emem x1 (3T) and Emem x2 (2T) are the young and aged cells, respectively, according to the descriptions in the Methods in this study.

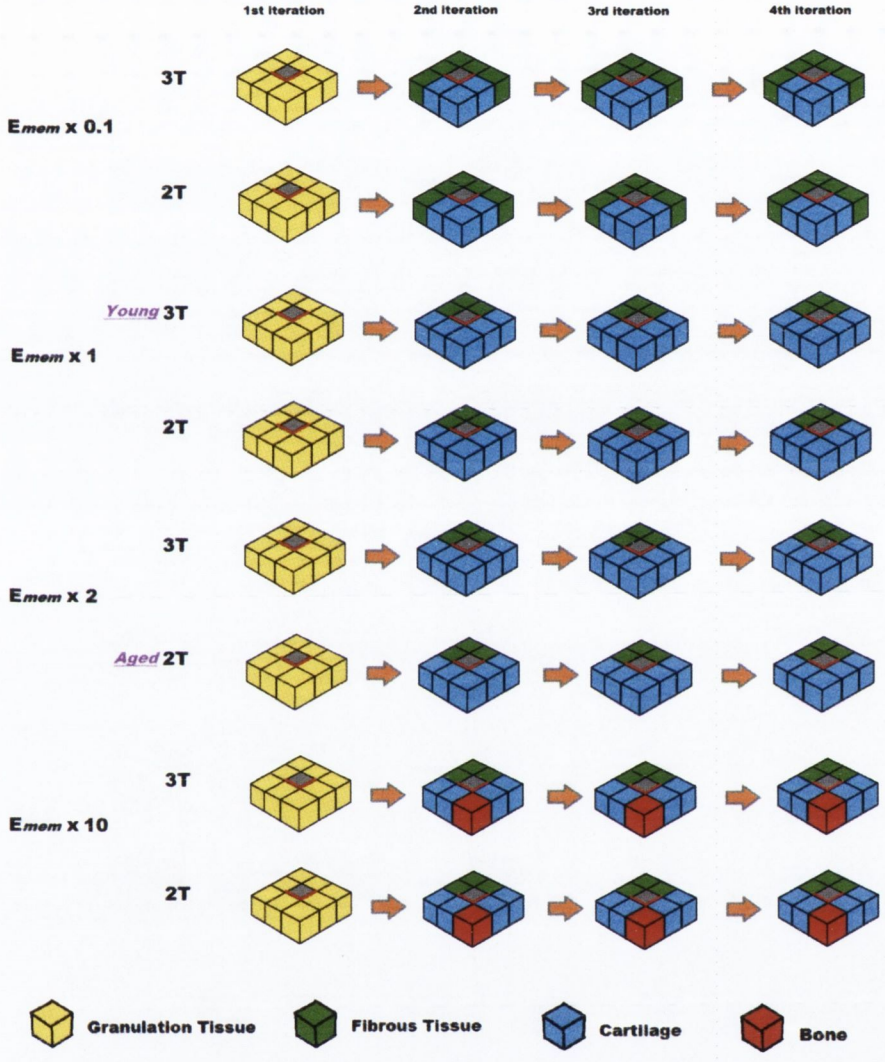


Figure 4.22. Tissue differentiation patterns under motion-control with a loading magnitude of 12 μm with two neighbouring debonded surfaces (Debonding case 3). The stiffness of cell membrane was altered from 10% (x0.1) to 10 times (x10) of the original young cell. The highlighted two lines, i.e. Emem x1 (3T) and Emem x2 (2T) are the young and aged cells, respectively, according to the descriptions in the Methods in this study.

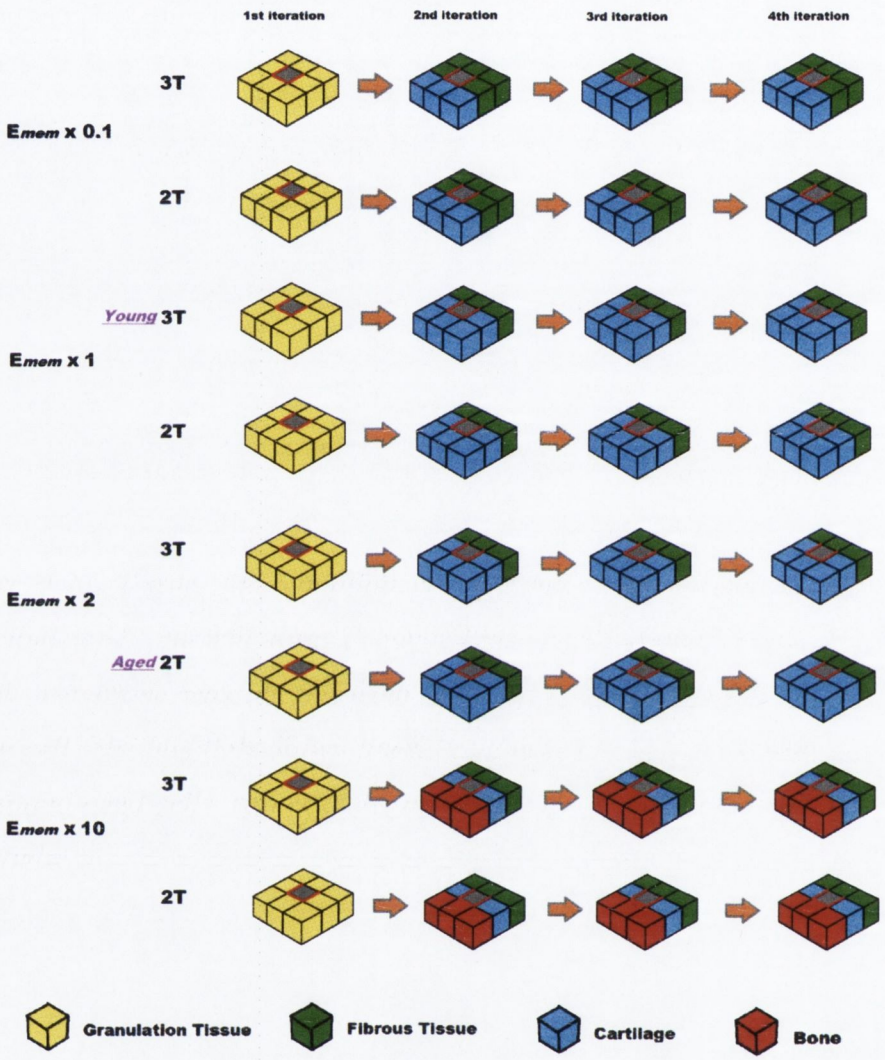
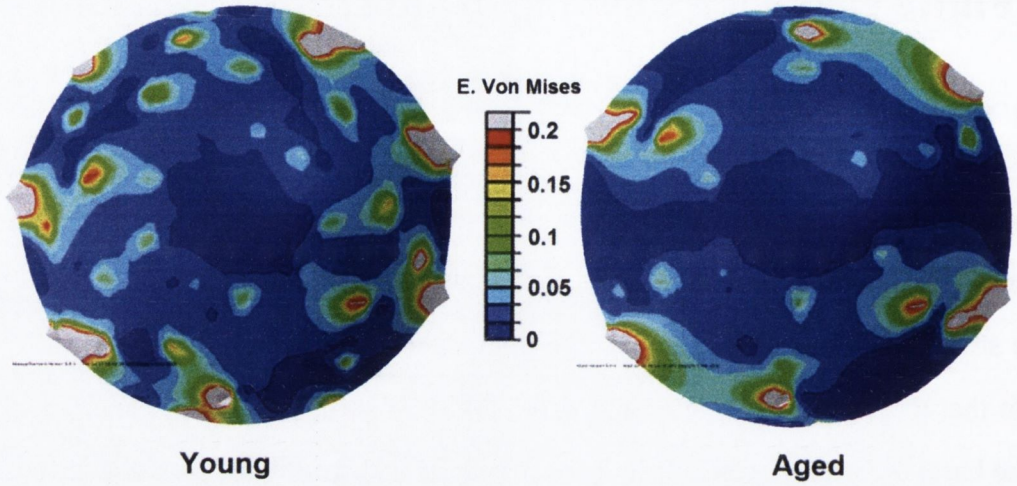


Figure 4.23. Tissue differentiation patterns under motion-control with a loading magnitude of 12 μm with three debonded surfaces (Debonding case 4). The stiffness of cell membrane was altered from 10% (x0.1) to 10 times (x10) of the original young cell. The highlighted two lines, i.e. Emem x1 (3T) and Emem x2 (2T) are the young and aged cells, respectively, according to the descriptions in the Methods in this study.

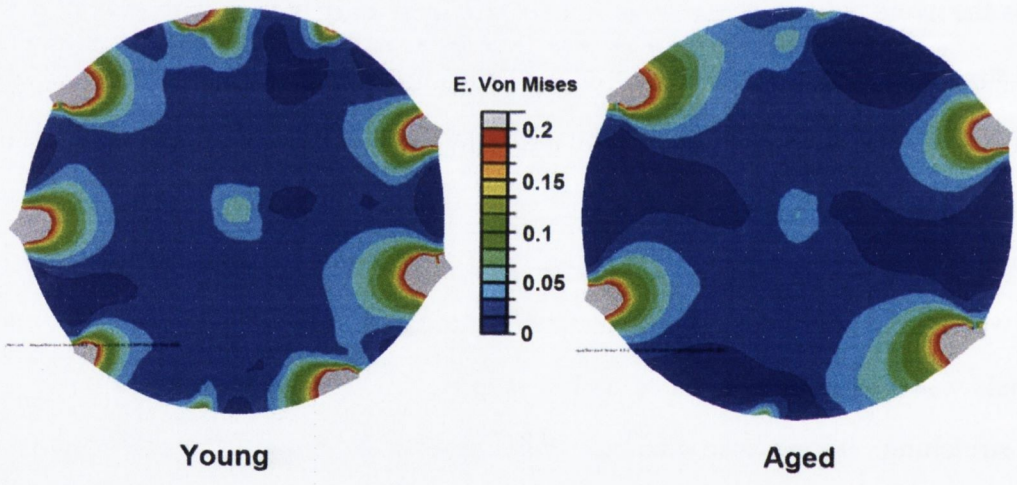
4.3 Finite element modelling of substrate stretching

4.3.1 Effects of MSC ageing

Though non-uniform strain distribution were shown in the membrane for both young and aged MSCs under uniaxial stretching stimulation, there is a striking difference in the strain pattern between the two age groups. The contour plots in Figure 4.24 exhibit that there are strain concentrators on both top surface of the cell membrane and the basal area where cells made contact with the substrate, for both age groups. What differentiate the two age groups are the number of strain peaks and locations where the peak strains appear. To quantify the difference between the two age groups the averaged equivalent membrane strain were computed under uniaxial substrate stretching with various loading magnitudes. It is shown in Figure 4.25 that the membrane strain reduces with ageing at each stretching magnitude, by approximately 25%. To investigate the effects of MSC differentiation under peak strain, a criterion was adopted to identify the number of peak strains. A peak strain was defined when the probabilities of the opening of mechanosensitive, strain-activated ion channels was one, as demonstrated by Lunze et al. (2009), with the application of a 10% stretching. It was also assumed that these peak strain locations remained counted when stretched with smaller magnitudes. Similar to the average membrane strain, a 25% decrease in the peak strain was also evident with ageing in all stretching magnitudes (Figure 4.26). Furthermore, 26 peak strain locations were identified for the young cell, as apposed to 18, the number of peak strains found in aged cell membrane.



(A)



(B)

Figure 4.24. Contour plots of cell membrane strain of young and aged cells from top view (A) and bottom view (B) when loaded with 10% uniaxial substrate stretching.

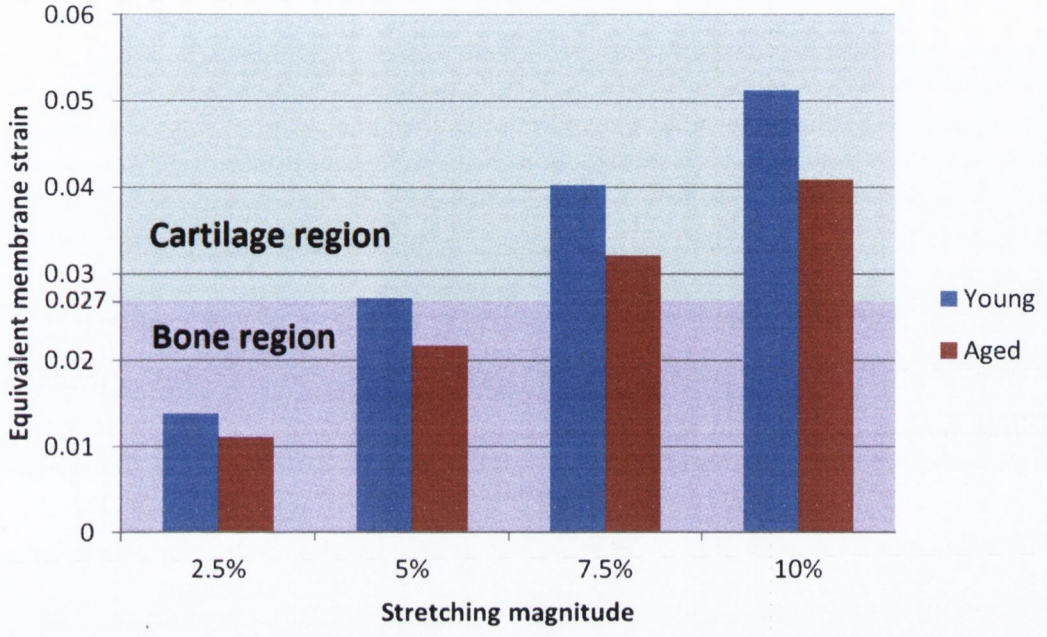


Figure 4.25. The membrane stain of young and aged cells subjected to uniaxial stretching with different magnitudes. The value 0.027 shown on the Y-axis is the index for cell-tissue differentiation between bone and cartilage regions as shown in Table 3.5.

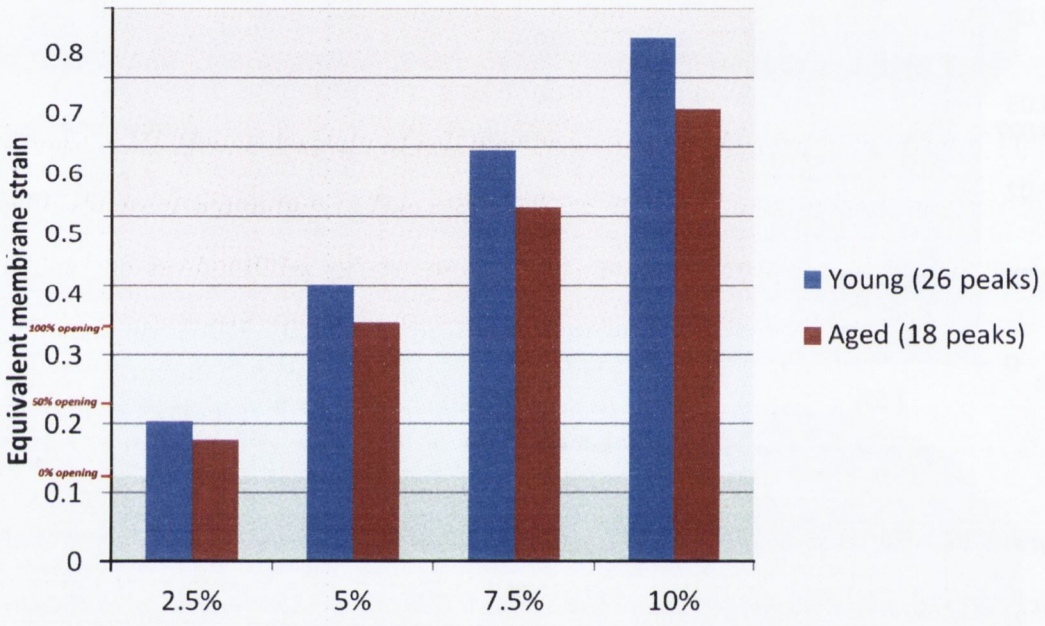


Figure 4.26. The peak strain of cell membrane when subjected to uniaxial stretching with different magnitudes. The red markers on the Y-axis indicate the strains at which the probabilities of the opening of mechanosensitive, strain-activated ion channels are 100%, 50% and 0%, as demonstrated by Lunze et al. (2009).

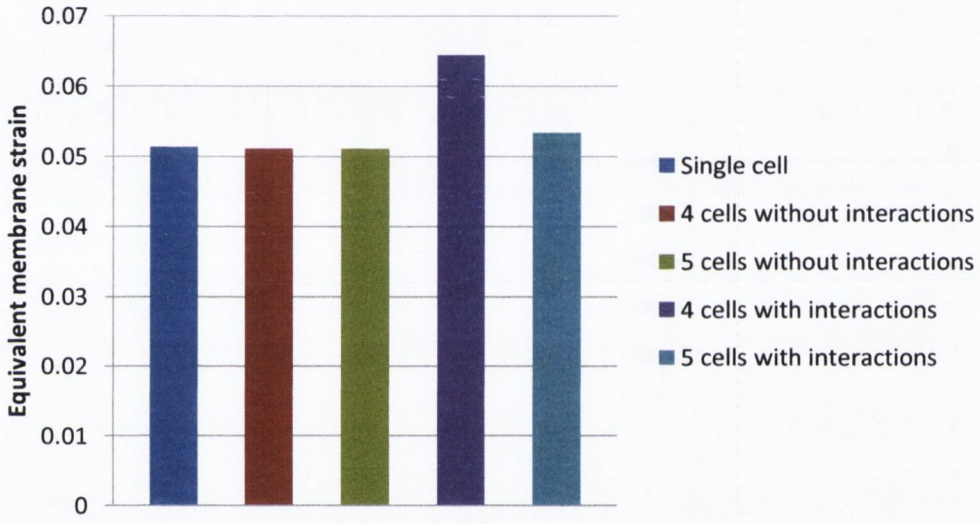


Figure 4.27. The equivalent membrane strain of a single cell, four cells and five cells, with or without cell-cell interactions when loaded with 10% uniaxial stretching.

4.3.2 Effects of seeding density

To investigate the effect of seeding density the equivalent membrane strain was computed on all cells that form the monolayer on the stretched substrate and averaged as an indicator to compare with the results from single cell simulations. No visible difference was found in the cell membrane strain between a single cell and a monolayer of cells stretched on a substrate when physical interactions between cells were not present. However, an increase of 26% in membrane strain was gained with cell-cell interactions were enabled when five cells were stretched on a substrate. In the case of a monolayer of four cells, the membrane strain increased by 5% as a result of cell-cell interactions. It was also evident that increasing the seeding density by a quarter, from 4 cells to 5 cells, induced a 20% gain in membrane strain (Figure 4.27).

Chapter 5

5. Discussion

5.1 Introduction

In this work, a 3D computational model was developed using finite element models of single cells implemented with the mechanoregulation theory proposed by Prendergast *et al.* (1997), with an aim to demonstrate that mechanoregulation simulations can be performed using whole cell models. One of the key strengths of this modelling approach is the capability of corroborating mechanoregulation theories with basic *in vitro* experiments. To illustrate this potential capability two events in the applications of mechanoregulation, the gap tissue formation in reconstructive medicine and the MSC differentiation upon substrate stretching in tissue engineering, were simulated to test the hypothesis that sub-cellular changes associated with MSC ageing affect cell-tissue differentiation. The results have supported the author's thesis and it is believed that the work presented in this thesis will have an impact on the development of computational mechanobiology.

5.2 Limitations

Combining the continuum and tensegrity structures into one model enables biomechanical investigation of several features of cell behaviour, such as the interaction of the CSK with ECM and cellular organelles under uniaxial substrate stretching. In particular, the unique configuration of CSK-NSK modelled by multiple sets of tensegrity structures enabled a direct force transfer from the ECM to the nucleus. Nevertheless, even this relatively complex tensegrity representation of the CSK-NSK does not capture the true complexity and dynamic behaviour observed in real cells and should therefore be considered a tool to understand the aggregate behaviour of cytoskeletal mechanics at instants of time rather than an accurate representation of CSK-NSK structure and mechanics under all circumstances. Furthermore, due to the nature of a passive model, this approach does not capture any active behaviour that a cell would exhibit under mechanical loading, including changes in cell morphology, stiffness and CSK reorganisation.

The mechanoregulation boundaries for tissue differentiation used in this study have not been experimentally established, though it has been successfully used to predict mechanoregulated tissue differentiation for various applications. The author believes this could be done by the proposed cell-based mechanoregulation approach presented in this thesis. Implications were also made to the conversion of the mechanoregulatory boundaries from the mechanoregulation theory (Prendergast *et al.*, 1997), by only considering the effects of shear strain, with those of fluid flow neglected. This simplification allowed us to investigate on situations where shear strain, but not fluid flow, is the focus of interest. It fitted in the purpose of this thesis as the two biomechanical contexts simulated were purely strain-mediated applications (Meneghini and Hanssen, 2008; Lai *et al.*, 2010). However, it would be necessary to

study the influence of fluid flow, in order to fully corroborate the mechanoregulation theory from cell experiments.

The sub-cellular changes associated with MSC ageing were based on experimental observations, not direct measurements, between MSCs from young and aged mice donors. These observations were then interpreted into a mechanical context with the recommendations from the literature. Therefore, the age-related changes applied to the model only included the effects of membrane stiffness, cytoskeletal density and the number of focal adhesion site across the cell membrane.

Regarding gap tissue simulations, the most extreme scenario of simplifications were assumed on the implant stem and gap tissue setup, where only a single layer of eight tissue blocks were included. While this setup allowed us to study the interactions of cells and tissue at the same horizontal plane, it did not permit any investigation on the vertical direction. Furthermore, only one round cell was implanted in each of the tissue blocks for simplification and as a result, this model did not capture any change induced by the orientation of irregularly shaped cells in the gap tissue. When simulating substrate stretching, the mechanical linkages for cell-cell and cell-substrate interactions were assumed to be rigid, in both tensile and compressive motion, in the simulation of substrate stretching. In reality, the mechanics of these interactions are far more complex. This simplification could have magnified the effect of cell-cell interactions.

Homogeneous isotropic material properties were assumed on all cellular components and tissues. The viscoelastic properties of cellular components were neglected when performing mechanoregulation simulations throughout this thesis due to computational expenses. While using less simplified material properties could be seen as

an improvement on the model, this complexity would require a further understanding of cell and tissue mechanics. Furthermore, the material properties of cytoplasm used in mechanoregulation for each of the specific cell types were estimated based on previous computational studies. While it is arguable that the liquid-like cytosol contributes little to the overall cell stiffness and therefore should not be taken into consideration when updating material properties at the end of each iteration when performing mechanoregulation simulations, the author believes that it is the aggregative change contributed by all cellular components that alters the overall cells response. Changes in cytosol could change the interactions between other cellular components that are more influential to the cells behaviour. The Poisson's ratio of granulation tissue was set to be 0.167 as suggested by previous studies (Lacroix and Prendergast, 2002a, Lacroix *et al.*, 2002), where poroelastic properties were used. However, a higher value is suggested when modelling the liquid-like granulation tissue using linear elastic properties. While under-estimating the Poisson's ratio would definitely impact on the biomechanics of cell-tissue interaction, little change would be expected to the pattern of tissue differentiation since cell membrane strain was used as the mediator for cell-tissue differentiation in this particular study.

5.3 Finite element modelling of a single adherent cell

We tested the hypothesis that there is a change in the biophysical stimuli inside a cell as a consequence of the changes in membrane stiffness and cytoskeletal element density that occur with age. This hypothesis has been corroborated because the analysis predicted that strains, both in cell membrane and nucleus, differ with age-related changes known to occur in cellular components.

5.3.1 Cell modelling approach

This study exemplifies the potential utility of a hybrid continuum-tensegrity representation of a cell. A particular strength of this approach is the ability to separate the potential load transfer mechanisms within a cell due to externally applied stimuli. Nevertheless, even this relatively complex tensegrity representation of the CSK-NSK does not capture the true complexity and dynamic behaviour observed in real cells and should therefore be considered a tool to understand the aggregate behaviour of cytoskeletal mechanics at instants of time rather than an accurate representation of CSK-NSK structure and mechanics under all circumstances. Furthermore, due to the nature of a passive model, this approach does not capture any active behaviour that a cell would exhibit under mechanical loading.

Cellular finite element modelling provides insights into the cell biomechanics which could not be achieved experimentally. The tensegrity approach utilising prestressed tensegrity structures with internal molecular struts and cables has gained much circumstantial evidence. Biophysical studies have revealed that the linear shaped AFs and tangled IFs are responsible for resisting externally applied tension, whereas the curved hollow MTs are much more effective at withstanding compression due to higher second moment of inertia in living cells (Mizushima-Sugano *et al.*, 1983). This is consistent with the structural behaviour of the components of tensegrity structures and could explain many cell activity, including cell spreading and stiffening (Maniotis *et al.*, 1997; Brown *et al.*, 2001). The experimental validation of cellular tensegrity model, including the cytoskeleton behaviour, cytoskeletal prestress and the establishment of a tensegrity force balance between MTs and AFs

with ECM, has been comprehensively demonstrated in a review paper written by Ingber (2003). However, scepticism still remained regarding the tensegrity cell modelling approach on the basis that, if cells used tensegrity, the disruption of one molecular support element, a actin bundle for instance, would result a total cellular collapse, as in a single prestressed tensegrity structure (Forgacs, 1995). This view has been backed up with experimental observations that cells still exhibit functional behaviours after individual fragmentation of cytoskeletal elements (Albrecht-Buehler, 1980). Not only does the idea of using multiple units of tensegrity structures presented in this paper enable us to investigate the influence of ageing on cell behaviour by capturing aged-related structural changes in the CSK, It also provides us a closer-to-reality view on cell modelling, compared to the single tensegrity approach (Ingber, 1993). By integrating the CSK and NSK networks in a cell model, the presentation of direct mechanical linkages from cell membrane to nucleus through AFs and IFs (Wang and Stamenovic, 2000, 2002), then reaching deep into the nucleus via LINC-complex (Linker of NSK and CSK) that were discovered recently (Wang *et al.*, 2009; Dahl *et al.*, 2010) allows us to explore the possibilities of how external mechanical signal affects nuclear biophysical stimuli. The difference found in CSK complexity with regard to donor age alters force transfer pattern within the cells and ultimately differentiate the biophysical stimuli received by the nuclei (see Figure 4.3).

5.3.2 AFM indentation simulation

AFM is frequently used to investigate mechanical properties of biological cells (Radmacher *et al.*, 1994). For example, Ng *et al.*, (2007) measured non linear strain

hardening in bovine chondrocytes using AFM indentation. During AFM indentation simulation, common mechanical nonlinear responses are present in all force displacement curves. These strain-hardening behaviours are consistent with previous experimental data in the literature (Figure 4.1). There are several sources contributing to this typical strain-hardening behaviour. First of all, it is most obvious that this nonlinearity is due to the viscoelastic nature of the cytoplasm, nucleus and membrane. Secondly, tensegrity structures contribute to this nonlinear behaviour; It has been demonstrated by Stamenovic *et al.* (1996) that 6-strut tensegrity structures of such a type used in this study have strain-hardening, non-linear characteristics. This contribution can be further confirmed by a computational study done by McGarry and Prendergast (2004), in which a nonlinear behaviour was predicted, even without viscoelastic properties used in any cellular component. Also, during the indentation process, the area of contact surface between the indenter and the cell membrane increases as the indenter travels deeper into the cell. An increasing resistance to the indenter induced by this enlarging contact area decelerates the indenter and nonlinearity is achieved as a result.

Simulation results suggest that indentation location greatly affects the measured cell stiffness using AFM (Figure 4.1, 4.2). While this is in agreement with experimental investigations in the literature (Ohashi *et al.*, 2002), a much stiffened behaviour is predicted in the case of indenting at a receptor site, compared to experimental observations. In theory, this is due to the fact that the indenting force is directly transferred to the CSK, which is a much stiffer structure. In practice, such a difference will not be evident due to slippage between the indenter tip and cell membrane, with an exception that coatings are applied to the indenter tip to specifically target receptors on the membrane by chemical binding.

5.3.3 MSC ageing

It is found that age-related changes assigned to the cell model influence the predicted cell stiffness. Specifically, the aged cell is slightly stiffer than the young cell at both indenting locations. This is consistent with experimental observations obtained across various cell types in previous studies. A comparison study using AFM indentation (Lieber et al., 2003) revealed that ageing increases the stiffness of cardiac myocytes sampled from rats. A higher stiffness was also reported for aged human umbilical vein endothelial cells measured by AFM indentation (Chouinard et al., 2008). Using the same technique, Qiu *et al.* (2010) discovered that the stiffness of smooth muscle cells of monkeys increase with ageing. The difference in predicted stiffness of the cells in this computational study is largely due to the higher stiffness used for membrane of aged cells, which is assumed to be caused by products of increased lipid peroxidation in aged cells. In this study, the membrane stiffness was doubled for the aged cells by assuming a proportional relationship between the amount of lipid peroxidation product and membrane stiffness (Hale *et al.*, 2011). However, as much as 450% increase in membrane stiffness is suggested when doubling the amount of lipid peroxidation products according to Ajmani *et al.* (2000). This would further increase the difference in predicted cell stiffness at both indentation locations (Figure 4.1). Differences caused by ageing can also be seen deep in the nucleus. Despite the almost identical hydrostatic strains found in the nuclei of both young and aged cells the deviatoric strain in the nucleus differs between young and aged cells, which is due to the difference in the density of cytoskeletal filament and the number of focal adhesion sites which transmit extracellular mechanical stimuli into the cell. This could be important as it has been demonstrated that these

direct linkages transmit mechanical signals many times faster than biochemical responses (Wang *et al.*, 2009).

The predicted results on cell membrane strain during AFM indentation simulations suggest that young cells tend to have a greater membrane area under high strain (Figure 4.2 (B)). If this is true, it would lead to more mechanosensitive stretch-activated ion channels opening (Charras and Horton, 2002a, 2002b). It has been shown that mechanosensitive channel openings could give rise to whole cell cytosolic calcium responses, thereby reinforcing the putative role of mechanosensitive channels as the first step in the transduction of external physiological mechanical stimuli into whole cell responses (Charras *et al.*, 2004). The differences in the number of receptor sites and the complexity of the CSK-NSK network that mechanically connect the ECM to the nucleus, between the young and the aged cells, could result in a difference in stimulation patterning in the nucleus, as shown in Figure 4.3. This is significant since nuclear strain has been suggested to influence higher-order chromatin organization, thereby restricting or promoting the accessibility of transcription factors or other regulatory factors to specific gene sequences, which could similarly influence gene transcription (Stein *et al.*, 2007).

5.3.4 Main conclusions

A 3D finite element model of a single cell with a complex CSK-NSK network was developed. AFM indentation tests were simulated on the cell model with age-related changes applied. The AFM simulation results were comparable with experimental data, in term of force/displacement curves. Simulation results also showed that while indenting location dominates cell's response age-related changes were also influen-

tial to the cell's behaviour under indentation loading environment. Based on the simulation results, the cell model performed well comparing against experimental data and was able to translate MSC ageing into alterations in biophysical stimuli, and therefore can be used for the development of mechanoregulation simulation in the following chapters.

5.4 Finite element modelling of gap tissue formation

The computational model presented in this chapter is a development of the idea that mechanoregulation simulations can be performed using whole cell models. Finite element models of single cells presented in Chapter 3.2 were adapted, and implemented with the mechanoregulation theory proposed by Prendergast et al. (1997). Though it has been used in many occasions for various applications the boundaries indicated on the mechanoregulation diagram have yet to be established experimentally. Furthermore, a frictionless condition was assumed to all debonded surfaces between bone and implant and as a result the debonded cell-tissue blocks were only stimulated by means of force transfer from neighbouring blocks, rather than directly from the implant during the course of simulation. Moreover, when converting the mechanoregulatory boundaries,

Despite these simplifications, the model was capable of performing mechanoregulation simulations to investigate the influence of MSC ageing on tissue differentiation. Simulation results revealed that age-related changes on cellular components can influence gap tissue differentiation, indicating that such changes should be taken into consideration when designing mechanoregulation algorithms.

In this section, the mechanoregulation theory proposed by Prendergast *et al.* (1997) was extended to capture the sub-cellular changes associated with MSC ageing. Following the extensions made to the existing mechanoregulatory algorithm , such as the previous improvements with additions of cell dispersal (Lacroix and Prendergast, 2002a; Perez and Prendergast, 2007), angiogenesis (Checa and Prendergast, 2010) and collagen fibre orientation (Nagel and Kelly, 2010), the current modelling approach could provide further improvements in several aspects. First of all, by incorporating finite element models of single cells, more variables, particularly those discrete variables at sub-cellular level, can be considered when constructing mechanoregulation algorithm. Recent evidence suggests that the morphology of the nucleus (Mazumder and Shivashankar, 2010) and cell stiffness (Pilarisetti et al., 2011) that are cell-type dependent throughout the developmental stages of MSC differentiation process can potentially be used as markers for MSC differentiation. The presented model is capable of capturing such changes, offering more possibilities of further developments of mechanoregulation algorithm, and potentially increasing the prediction accuracy. Secondly, by establishing mechanoregulation boundaries to cellular components it extended the range of applications that mechanoregulation predictions can be performed, particularly in situations when no tissue formation occurs, for example, substrate stretching of MSCs for applications in tissue engineering, which will be further discussed in Chapter 5.5. Most interestingly, it could diminish the immense criticisms about computational mechanobiology as a whole, by providing a possible means of validation with basic in vitro experiments. Inversely, cell experiments could also be served to calibrate well established mechanoregulation algorithms to fit for specific targets. Evidence indicates that mechanoregulatory boundaries are highly likely to be species-specific and possibly individual-dependent since high variabilities between individual specimen have been encoun-

tered in several *in vivo* investigations of mechanoregulated tissue differentiation (Tajil and Aspenberg, 1999; De Rooij *et al.*, 2001). Ultimately, computational mechanobiology would realise its true clinical potential if mechanoregulation boundaries could be established on a patient-specific basis.

5.4.1 The effects of debonding

Total joint replacement, although considered an excellent surgical procedure, can be complicated by aseptic loosening of the implant that is initiated by debonding between the implant and bone surface (Harris, 1992), has been identified as the main failure mechanics of total hip arthroplasty (Malchau *et al.*, 1993) and total knee arthroplasty (Bozic *et al.*, 2013). With an interest in discovering the effects of debonding on gap tissue differentiation, a comparison study was carried out for both force-control and motion-control. In case of force-control, bone is predicted to fill the interfacial gap, through different intermediate tissue types (fibrous and cartilage tissue), with all loading magnitudes in fully bonded cases, indicating such mechanical environments promote ossification if debonding could be avoided. This is the most desired scenario in reality when bone is forming and fill up the space between the implant stem and bone cavity. In reality, since debonding with some degree will always occur, which will naturally initiate resorption, proactive solutions, for instance using ossification promoting materials or coatings (Abramovitch-Gottlib et al., 2006; Lu *et al.*, 2012), are required to prevent such an outcome. In addition, the order of the appearance of intermediate tissue types at developmental stages was consistent with previous computational investigations (Lacroix and Prendergast, 2002a; Perez and Prendergast, 2007). However, bone resorption was predicted to occur at the

debonded interface for all debonding cases under force-control, leaving a mixture of bone and resorption, or cartilage and resorption in the most seriously debonded scenarios, with different proportionalities. This indicates a partial occurrence of ossification at interfacial surface between the bone and the implant, suggesting that a stable fixation of the implant will not be achieved. Therefore, debonding is not desirable under force-control loading conditions and should be avoided for cementless fixation during the implantation process. In practice, it would require a extremely high level of surgical precision to minimise the area of debonding, in order to achieve the real potentials of cementless fixation (Dorr *et al*, 2009).

In case of motion-control, a completely different relationship between mechanical environments and tissue differentiation patterns was predicted. It was also revealed that the phenotype was decided at early stages and stays on until the end of each simulation for both fully bonded and debonded cases. This indicates that the initial displacement applied to the implant is the only factor that influence the gap tissue differentiation. As expected, debonding was predicted to alter the tissue differentiation pattern for all loading conditions under motion-control loading conditions. However, no resorption was predicted with debonding under such a loading scheme. The sharp contrast in predicted tissue differentiation between force-control and motion-control agrees with previous computational investigations (Prendergast, 2004) and a mechanistic explanation can be provided. If the biological context could be interpreted into a mechanical situation such that a certain motion is maintained (motion-control) at a high level then the local cell membrane strain stays high due to the high global stimulation and no bone will form as a result, instead softer tissues will be maintained, whereas if the synthesis of ECM permits a reduction in motion (force-control) then the cell membrane strain will reduce and a mechanical environ-

ment favouring ossification formation will be achieved, possibly through intermediate tissue types during ossification process.

5.4.2 The effects of age-related changes

Though slightly, MSC ageing is predicted to affect tissue differentiation pattern in both force-control (Figure 4.6 – 4.9) and motion-control (Figure 4.10 – 4.13) loading scenarios where debonding occurs. However, little change in the implant's behaviour was found between the two age groups, by plotting the displacements under force-control (Figure 4.14) and the reaction force under motion-control (Figure 4.15) conditions. This phenomenon could be explained using mechanoregulatory terms. Specifically, doubling the membrane stiffness reduces the local membrane strain, to a level that could induce the cell to differentiate into a different phenotype. However, such an increase in local cell-tissue stiffness does not contribute much to the behaviour of the implant globally as a result of the disconnection at the debonded bone/implant interface. In such a situation, the current mechanoregulation algorithm would have given a different prediction by only looking at the stimuli at tissue level, without being able to capture any sub-cellular alteration. Varying the cell membrane stiffness to an extended range magnifies the change in tissue differentiation pattern at developmental stages throughout the differentiation process for both force-control (Figure 4.14 – 4.18) and motion-control (Figure 4.19 – 4.23), indicating such a change alters the biophysical inside the cells, while the global mechanical environment remains the same.

This exemplifies the improvements in prediction accuracy this modelling approach could contribute to the current mechanoregulation algorithm, elucidating the

necessity of capturing changes at sub-cellular level when performing mechanoregulation predictions. In contrast, change in the configuration of CSK-NSK structure is not as influential on the tissue differentiation pattern, with exceptions when cells with high membrane stiffness ($E_{mem} \times 10$) stimulated under force-control and coupled with the occurrence of debonding (Figure 4.18). In these cases, Altering the CSK-NSK structure, from three to two sets of tensegrity structures, changes the pathways that external mechanical stimuli transfer into the cells and therefore varying the mechanical behaviour of cells that are imbedded into the tissue blocks. Though the change in membrane strain induced by such an alteration is minimal at low membrane stiffness range, it escalates as membrane stiffens, changing the mechanics inside the cell. As a result, the difference in membrane strain induced by the change in CSK-NSK configuration is amplified when coupled with a stiffer membrane at focal adhesion sites where the CSK connects the membrane and transfers external mechanical stimuli deep into the cell.

5.4.3 Main conclusions

In summary, the goal of this study was to demonstrate that mechanoregulation simulations for tissue differentiation can be performed using finite element models of single cells. A model was created using whole cell models implemented with mechanoregulation boundaries that were established on the cell membrane. The model was fully capable of capturing the changes occur at sub-cellular level, allowing a thorough computational investigation of how tissue differentiation can be influenced by MSC ageing. Most impotently, this modelling approach could provide a possible means to corroborate mechanoregulation theories with experiments, so that reliable

predictions can be performed. This would potentially help to axe the amount of animal experiments and promote the development of computational mechanobiology.

Simulation results showed that while the differentiation of gap tissue under motion-control solely depends on the loading magnitudes, force-control promotes ossification if debonding could be avoided, since it is also predicted that debonding of any configuration at the bone/implant interface causes bone resorption. It was also evident that changes occur at sub-cellular level associated with MSC ageing can influence the predicted patterns of gap tissue formation, indicating that such changes should be considered when constructing mechanoregulation algorithms for predicting the outcomes in the field of reconstructive medicine. Based on the simulation results regarding the influence of MSC ageing, it is further recommended that different design parameters, surgical procedures and loading schemes should be adopted for aged patients, in order to achieve the true clinical potentials of cementless fixation by compensating the mechanobiological impacts MSC ageing could make.

5.5 Finite element modelling of substrate stretching

We tested the hypothesis that MSC differentiation could be altered as a consequence of the changes in membrane stiffness and cytoskeletal element density that occur with age when subjected with uniaxial stretching. This hypothesis has been corroborated because simulation predicted that the change in membrane strain, as a measure in cell differentiation, in response to MSC ageing is as significant as that induced by a 25% increase in seeding density.

5.5.1 MSC differentiation

Seen as the ideal cell source in tissue engineering applications due to their pluripotent differentiation potentials and *in vitro* manipulability, MSCs interrogate numerous microenvironmental cues, including soluble factors, adhesive contexts, and mechanical signals, in order to mount physiologically relevant differentiation responses. While much is known about how soluble factors and adhesion receptors regulate differential gene expression, the molecular basis for how mechanical signalling controls gene transcription and differentiation programs has recently gained the position in focus. In order to understand the mechanistic basis for mechanically-induced differentiation, it is crucial to explore how mechanical forces are transduced into biochemical signals, that can in turn regulate and synergize with signalling cascades induced by other stimuli. While fluid flow can influence MSC differentiation, for instance, the interstitial fluid flow governs the physiological responses to mechanical loading (Burger and Klein-Nulend, 1999), it is mechanical strain that plays pivotal roles in osteochondral differentiation of MSCs (Kelly and Jacobs, 2010). Therefore, it is considered to be a valid approach to investigate MCS differentiation by emphasising the shear stain part of the mechanoregulatory theory as a exploratory study of cellular mechanoregulation. However, the author is aware of the differential influences of fluid flow on cell membrane strain, as apposed to that of shear strain. It should also be noted that the mechanoregulation boundaries on cell membrane were converted by simulating a 3D loading environment with a cell surrounded by ECM and tissue. It might be biased when used to predict cells response subjected to uniaxial stretching that is, in essence, a two-dimensional stimulating environment. The author believes this should not be an issue since the cellular mechanoregulator was set on the average membrane strain across the whole cell surface and as a result any

local or partial plateau in membrane strain would be averaged out and not dominate the prediction in cell phenotype.

When stretched on a substrate, MSCs experience cyclic mechanical strain transferred from substrate through physical interactions and differentiate into specific cell types depending on the level of stimulation received from the substrate. Simulation results indicate that stretching magnitudes, ranging from 2.5% to 10%, induce MSCs differentiation towards osteochondral lineages (see Figure 4.25), according to the mechanoregulation index that was derived in Chapter 3.4 from mechanoregulatory boundaries (see Table 3.5). This is consistent with previous experimental investigations in the literature (McMahon *et al.*, 2008; Kearney *et al.*, 2010). A study carried out by Kearney *et al.* (2010) on MSCs derived from rat bone marrow revealed that a 2.5% uniaxial substrate stretching induces osteogenic differentiation in the absence of osteogenic factors. The simulation results were in full agreement with this experimental finding in supporting that low level of stimuli promotes osteogenesis (Prendergast *et al.*, 1997). When a 2.5% uniaxial tensile stretching was applied, the membrane of the MSCs seeded on the substrate was only stimulated to a level that was significantly lower than the mechanoregulatory boundary for chondrogenesis indexed as the membrane strain, and therefore osteogenesis was predicted (Figure 4.25). In order to study The effect of cyclic tensile strain on the chondrogenic differentiation of MSCs McMahon *et al.* (2008) applied a 10% stretching to rat MSCs and discovered that the rate of glycosaminoglycan synthesis was increased following the application of cyclic stretching for seven days, suggesting this magnitude of strain was sufficient to mechanoregulate the chondrogenic differentiation process (McMahon *et al.,* 2008). Again, our results correlated well with this observation as when the stretching magnitude increased to 10%, the computed membrane strain of MSCs

fully reached into the "cartilage" region and chondrogenesis was predicted as a result (Figure 4.25). Cells adapt to their mechanical environment by a mechanotransduction process, involving a cascade of signalling pathways. The difference in stretching magnitude would provoke a series of biological events that could possibly affect gene expression (Chen *et al.*, 2004).

5.5.2 MSC apoptosis

This modelling approach could also be used to provide a possible mechanistic explanation of strain-mediated apoptosis upon uniaxial stretching. The effects of cyclic substrate stretching on MSC viability was recently examined. It was found that strains lower that 5% elicit differentiation whilst higher strains, particularly with magnitudes greater than 7.5%, promote apoptosis of MSCs loaded with cyclic stretching (Kearney *et al.*, 2008, 2010). Biologically, what happened was the L-type voltage-activated calcium channels coupled the applied mechanical stress to calpain and JNK activation, leading to apoptosis through DNA fragmentation (Kearney *et al.* 2008). While it is important to understand the biological fundaments regarding the communication between biochemical signal transduction in response to mechanical stimuli and the activation of pro-apoptotic pathways in order to gain a full understanding of apoptosis, computational models can contribute to achieving this goal from cellular mechanics point of view. Simulation results indicate that the membrane strain fits closely between the regions of osteogenesis and chondrogenesis with 5% stretch and slightly above the threshold with a stretching magnitude of 7.5%. In such a situation, due to the nature of cyclic stretching, MSCs tend to differentiate into chondrocytes at full stretch, while having a osteogenic differentiation tendency when the substrate

is in the process of reaching to or releasing from a full stretch. This periodic alteration in differentiation commands created by cyclic loading schemes could confuse the MSCs and cause apoptosis as suggested by Perez and Prendergast (2007). If this is the case, then stretching schemes for MSC chondrogenic differentiation should be designed such that the range of stretching magnitudes only cover the cartilage region in the mechanoregulation index, without overlapping to the bone and other phenotype regions, in order to promote chondrogenesis.

5.5.3 Linkage between basic cell experiments to mechanoregulation theories

Interestingly, this cell based mechanoregulation modelling approach has brought us the prospect that basic *in vitro* cell experiments, like substrate stretching, can be used to validate mechanoregulation models by establishing accurate boundaries for MSC differentiation for each specific phenotype on the stretching magnitudes. Each stretching magnitude could be converted to biophysical stimuli on cellular components with the help of computational models, such as the one presented in this chapter. Then, these boundary values could be converted back to parameters that fit into the mechanoregulation algorithms using the approach described in Chapter 3.3. This process is illustrated in Figure 1.1. The author believes this exciting outcome is promising and is ready to be achieved with the current advancing of experimental techniques, coupled with the excellence of computational models and the power of statistical methods.

5.5.4 MSC ageing

As expected, ageing is predicted to influence MSC differentiation when loaded with uniaxial tensile strain. Similar to other finite element studies in the literature, non-uniform strain distribution were present when imposed within stretching environments (Pfeiler *et al.*, 2008; Stops *et al.*, 2008). However, it was evident that local maxima in membrane strain occurred at focal adhesion sites in response to substrate stretching for both young and aged cells, whereas in reality, these strains may dissipate due to cytoskeletal rearrangements under loading environments. The difference in strain pattern between young and aged cells is caused by the alterations in the arrangement of the CSK-NSK structures as seen in the confocal images (McKayed *et al.*, 2010). In quantifying the difference in peak membrane strain between the two age groups, a 25% reduction was found in aged MSCs and it was accompanied with a decrease in the number of peak strains. This indicates that MSC ageing is influential to MSC differentiation. To visualise this change in an experimental context a parametric study on the influence of seeding density were performed. It was found that in order to gain a 20% membrane strain the seeding density had to be increased by 25%, which would be unacceptable in reality within any laboratory. Hence, based on our results, if seeding density is a parameter that well taken care of when performing cell experiments, MSC ageing definitely should be considered when designing loading schemes for aged patients for MSC-based applications in tissue engineering and regenerative medicine.

5.5.5 Main conclusions

In this study, it was demonstrated that the mechanoregulatory boundaries established in Chapter 3.3 can be used to give a scientific explanation on some experimental

findings of MSC differentiation subjected to uniaxial tensile strain from a mechanoregulatory perspective. More importantly, cell experiments of such a kind could potentially be used to validate mechanoregulation theories.

Simulations with a single cell, or a monolayer of cells, seeded on a substrate were performed, with tensile strains ranging from 2.5% to 10% applied to the substrate. Simulation results showed that the influence of ageing on MSC differentiation was as great as, if not greater than, the influence induced by a 25% increase in seeding density. This suggests that MSC ageing deserves to be considered when designing loading scheme for tissue engineering applications.

5.6 Corroboration of mechanoregulation theories

The corroboration of mechanoregulation theories enables simulations to predict the mechanobiological response of an experiment, allowing researchers to test the hypotheses that are interesting on their own and provide better theoretical knowledge about the process. To achieve this goal, the theories that govern the mechanoregulated tissue differentiation process must be validated by comparing to experimental data due to their phenomenological nature. Currently, the efforts of the validation of mechanoregulation theories predominantly focus on the data attained from the same type of experiments that the computational models are meant to be used in the first place, as criticised by Jacobs and Kelly (2011), who stated "The paradox is that the experimental data collected to validate the model may actually obviate the need for the model". In response to this immense criticism about the necessity of the use of computational models in the field of mechanobiology, the author would like to argue

that the role of computational models in mechanobiology is as important as that of experiments and the collaboration of the two will pace up the development of mechanobiology.

While Khayyeri *et al.* (2013) have defended the needs of computer models from the perspectives of computational power and how to interpret from the simulation results, the author intends to tackle the criticism explicitly by demonstrating that the proposed cell-based mechanoregulation approach provides a possible way to validate mechanoregulation theories from basic *in vitro* cell experiments as shown in Figure 1.1, allowing us to perform accurate predictions within a more complex biological context, which is possibly without the reach of *in vitro* experiments. The proposed validation process consists of a series of events and would not proceed without the collaborations between experimental observations and computer simulations. Once validated, the predictive power of mechanoregulation algorithms could then be materialised in the applications in tissue engineering, regenerative medicine and reconstructive therapies. In the future stages, when mechanoregulation algorithms are well established, the proposed approach would still be required for the calibration of the mechanoregulation algorithms to perform accurate individual-base simulations to target specific populations, and ultimately, computational mechanobiology would realise its true clinical potentials if reliable patient-specific predictions can be given before surgeries at a clinical stage.

Chapter 6

6. Conclusions

6.1 Summary of key events

6.1.1 Cell modelling

In this work, a 3D finite element cell model was developed based on the hybrid approach used by McGarry and Prendergast (2004) with a number of improvements. It consists of various cellular components, providing numerous possibilities that could look into for the future development of cell-based mechanoregulation theories. A unique feature of the model is the CSK-NSK structure that allows us to explore the possibilities of how external mechanical signal affects nuclear biophysical stimuli through a direct mechanical linkage that was discovered experimentally (Wang *et al.*, 2009). Inspired by the use of tensegrity structures in cell mechanics (Ingber, 1993, 2003) multiple sets of tensegrity structures were used for both the CSK and NSK to capture the changes in CSK density associated with MSC ageing, whereas the previous cell modelling approach (McGarry and Prendergast, 2004) could not capture such a change. With all three major cytoskeletal components incorporated, this model is also a perfect candidate for the modelling of cell-cell and cell-ECM interactions at the receptor sites where the CSK connect with cell membrane. The previous

cell model (McGarry and Prendergast, 2004), however, could not handle such a task, since IFs, the major player in cell-cell interaction (Braga, 2002), were not included in their model.

The force/displacement curves obtained by simulating AFM indentation on the cell model were in good agreement with experimental data, indicating that the cell model was capable of displaying mechanical behaviours within the bounds of experimental observations. Furthermore, a parametric study revealed that the cell model was able to capture the effects of MSC ageing by depicting the differences in biophysical stimuli within a cell, both qualitatively and quantitatively, under AFM indentation environments. All these pieces of evidence suggest that the cell model was sufficient enough for the investigation of cell-based mechanoregulation for tissue differentiation.

6.1.2 Role of MSC ageing in gap tissue differentiation

In this thesis, the age-related changes discovered on MSCs (Mckayed et al., 2010), including cytoskeletal density and membrane stiffness, were explicitly included in the simulation of gap tissue differentiation. Due to the fact that though undesirable, debonding of various degrees is practically inevitable with cementless fixation (McMinn, 2003), four different debonding cases were also simulated for a thorough investigation. Simulation Results revealed that while debonding was the most influential factor to gap tissue differentiation, age-related changes also affect the patterns of gap tissue formation. However, the alteration in tissue differentiation caused by MSC ageing was mainly contributed by membrane stiffness changes, whereas cytoskeletal density played little role in gap tissue formation, except for extreme cases

when cells with high membrane stiffness ($E_{mem} \times 10$) loaded under force-control, together with the occurrence of debonding. Nonetheless, evidence suggests that MSC ageing should be considered when constructing mechanoregulation algorithms for predicting the outcomes of gap tissue formation. Furthermore, it is recommended that different design parameters, surgical procedures and loading schemes should be adopted for aged patients, in order to achieve the true clinical potentials of cementless fixation.

6.1.3 Role of ageing in MSC differentiation subjected to uniaxial loading

To investigate the influence of ageing to MSC differentiation, simulations with a single cell, or a monolayer of cells, resided on a substrate were performed. Tensile strains ranging from 2.5% to 10% were applied to the substrate to create the same mechanical environments as previous experimental investigations. Using the mechanoregulatory boundaries as an index, several experimental observations, including cell differentiation and apoptosis, were explained from a mechanobiological perspective. Simulation results showed that young MSCs had a higher averaged peak membrane strain and a greater number of peak membrane strains, compared with aged cells, indicating higher probabilities of the opening of mechanosensitive, strain-activated ion channels in young MSCs in response to substrate stretching, which would suggest that ageing can affect MSC differentiation. It was also revealed that, according to the computed equivalent membrane strain, the influence of ageing on MSC differentiation was as great as, if not greater than, the influence induced by a 25% increase in seeding density. This suggests that MSC ageing de-

serves to be considered when designing loading scheme for tissue engineering applications.

6.2 Main findings of this work

This work has corroborated the hypothesis that the sub-cellular changes associated with MSC ageing could affect cell-tissue differentiation in both gap tissue formation and MSC differentiation subjected to uniaxial stretching. A predictive cell based computational model was developed using 3D finite element models of single cells implemented with the mechanoregulation theory developed by Prendergast *et al.* (1997). A particular strength of this modelling approach is the capability of capturing the changes on cellular components. This modelling approach could potentially be used to correlate mechanoregulation theories with basic *in vitro* cell experiments, enabling an information interchange between computational models and experimental observations. Parametric studies were performed using the computational model on two biomechanical procedures and results revealed that MSC ageing can alter cell-tissue differentiation in both events. The main conclusions of this work are:

- The simulation results regarding AFM indentation on a single cell were in good agreement with experimental data, indicating that the cell model was capable of displaying mechanical behaviours that are within the bounds of experimental observations. Results from a parametric study also revealed that differences in the internal biophysical stimuli between young and aged cells were evident. This could trigger a differing biochemical response between the two age groups in response to mechanical stimulation.

- A predictive cell-based mechanoregulation model was created using finite element model of single cells implemented with a mechanoregulation theory. Simulation results showed that while gap tissue differentiation at bone/implant interface was solely dependent on the loading magnitudes under motion-control conditions, force-control was predicted to promote ossification while no debonding occurs. However, simulation also predicted that debonding of any scale would initiate bone resorption, which is undesirable and should be avoided for cementless fixation.
- Age-related changes were predicted to affect gap tissue differentiation patterns. Despite the small changes found between young and aged cells, altering the membrane stiffness to an extended range amplified the differences in gap tissue differentiation between the two age groups. Hence, the hypothesis that MSC ageing could affect gap tissue differentiation was corroborated.
- With the mechanoregulatory boundaries established on cell membrane, the presented modelling approach could be applied to an extensive range of biomechanical events, particularly in those without the occurrence of tissue differentiation. Simulation results indicate the role of ageing on MSC differentiation subjected to substrate stretching could be as important as, if not more important than, that of seeding density, which is well taken control of, indicating the necessity of considering MSC ageing in tissue engineering and regenerative medicine applications. This also corroborated the hypothesis that ageing could affect MSC differentiation subjected to uniaxial loading conditions.
- By testing the hypotheses using the computational model developed in this work, a possible means of correlating mechanoregulation theories with experimental observations, for potential validation and calibration purposes,

has been outlined. The author believes it is achievable and ready to be explored to the next stage.

6.3 Future work

This work represents an early step in the development of computational techniques for the study of mechanoregulation modelling using whole cell models, and for the potential platforms for corroborating mechanoregulation theories with basic *in vitro* cell experiments. In order to proceed to the next phase, the recommendations are:

- The mechanoregulatory boundaries were converted from the mechanoregulation theory (Prendergast *et al.*, 1997) by only considering the effects of shear strain, with those of fluid flow neglected. This simplification allowed us to investigate on situations where shear strain, but not fluid flow, is the focus of interested. It would be necessary to study the influence of fluid flow, for other situations. It would also be required in order to fully corroborate the mechanoregulation theory.
- Regarding the cell model used in this study, though it has a relatively complex structure and is capable of capturing various changes that occur at subcellular level, it could not predict any active behaviour of a cell, e.g. CSK remodelling, under mechanical stimulation. This general cell model platform could be further developed in this direction.
- When converting the stimulus from mechanoregulation theories, the mechanoregulatory boundaries could be established on more cellular components, especially those can be easily accessed in cell experiments, e.g. the shape of

the nucleus. This would potentially be useful when corroborating mechanoregulation theories from experiments.

- Regarding gap tissue simulation setup, a monolayer of eight cell-tissue blocks was incorporated in the model due to computational expenses. A simulation setup with multiple layers of cell-tissue combinations, with time-dependent material properties, would be able to gain a better understanding on the effects of MSC ageing and debonding in gap tissue differentiation.
- Regarding cell-cell and cell-substrate interactions in the simulation of substrate stretching, the linkers that mechanically connect cells were modelled as rigid in both tensile and compressive directions. In reality, the mechanics of these interactions are far more complex. A further look in this direction is recommended.

Bibliography

Abdulkarim, R., Berkman, B.E., Wendler, D., Rid, A., Khan, J., Badgett, T., Hull, S.C., 2013. Disclosure of incidental findings from next-generation sequencing in pediatric genomic research. Pediatrics 131(3): 564-571.

Abramovitch-Gottlib, L., Geresh, S., Vago, R., 2006. Biofabricated marine hydrozoan: a bioactive crystalline material promoting ossification of mesenchymal stem cells. Tissue Engineering 12(4): 729-739.

Ajmani, R.S., Meter, E.J., Jaykumar, R., Ingram, D.K., Spangler, E.L., Abugo, O.O., Rifkind, J.M., 2000. Hemodynamic changes during ageing associated with cerebral blood flow and impaired cognitive function. Neurobiology of Ageing 21(2): 257-269.

Albrecht-Buehler, G., 1980. Autonomous movements of cytoplasmic fragments. Proceedings of the National Academy of Sciences 77: 6639-6643.

Amstutz, H.C., Yao, J., Dorey, F.J., Nugent, J.P., 1988. Survival analysis of T-28 hip arthroplasty with clinical implications. The Orthopaedic Clinics of North America 19(3): 491-503.

Ashhurst, D.E., 1986. The influence of mechanical conditions on the healing of experimental fractures in the rabbit: a microscopical study. Philosophical Transactions of the Royal Society B: Biological Science 313: 271-302.

Azeloglu, U., Bhattacharya, J., Costa, K.D., 2008. Atomic force microscope elastography reveals phenotypic differences in alveolar cell stiffness. Journal of Applied Physiology 105(2): 652- 661.

Banes, A. J., Link, G. W., Jr., Gilbert, J. W., Tran Son Tay, R., Monbureau, O., 1990. Culturing cells in a mechanically active environment. American Biotechnology Laboratory 8: 12-22.

Bartling, B., Tostlebe, H., Darmer, D., Holtz, J., Silber, R. E., Morawietz, H., 2000. Shear stress-dependent expression of apoptosis-regulating genes in endothelial cells. Biochem. Biochemical and Biophysical Research Communications 278: 740-746.

Bertaud, J., Qin, Z., Buehler, M.J., 2010. Intermediate filament-deficient cells are mechanically softer at large deformation: a multi-scale simulation study. Acta Biomaterialia 6(7): 2457-2466.

Bozic, K.J., Lau, E., Ong, K., Chan, V., Kurtz, S., Vail, T.P., Rubash, H.E., Berry, D.J., 2013. Risk Factors for Early Revision After Primary TKA in Medicare Patients. Clinical Orthopaedics and Related Research 285: 67-72.

Braga, V.M., 2002. Cell-cell adhesion and signalling. Current Opinion in Cell Biology 14(5): 546-556.

Brangwynne, C. P., MacKintosh, F. C., Kumar, S., Geisse, N. A., Talbot, J., Mahadevan, L., Parker, K. K., Ingber, D. E., & Weitz, D. A., 2006. Microtubules can bear enhanced compressive loads in living cells because of lateral reinforcement. Journal of Cell Biology 173: 733-741.

Brown, M. J., Hallam, J. A., Colucci-Guyon, E., Shaw, S., 2001. Rigidity of circulating lymphocytes is primarily conferred by vimentin intermediate filaments. Journal of Immunology 166: 6640-6646.

Burger, E.H., Klein-Nulend, J. 1999., Mechanotransduction in bone–role of the lacuno-canalicular network. The FASEB Journal 13: 101-112.

Burridge, K., Chrzanowska-Wodnicka, M., 1996. Focal adhesions, contractility, and signaling. Annual Review of Cell and Developmental Biology 12: 463-518.

Byrne, D.P., Lacroix, D., Planell, J.A., Kelly, D.J., Prendergast, P.J., 2007. Simulation of tissue differentiation in a scaffold as a function of porosity, Young's modulus and dissolution rate: application of mechanobiological models in tissue engineering. Biomaterials 28(36): 5544-5554.

Caplan, A.I., Bruder, S.P., 2001. Mesenchymal stem cells: building blocks for molecular medicine in the 21st century. Trends in Molecular Medicine 7: 259-264.

Carter, D.R., Blenman, P.R., Beauprce, G.S., 1988. Correlations between mechanical stress history and tissue differentiation in initial fracture healing. Journal of Orthopaedic Research 6(5): 736-748.

Carter, D.R., Beauprce, G.S., Giori, N.J., Helms, J.A., 1998. Mechanobiology of skeletal regeneration. Clinical Orthopaedics and Related Research 355: 41-55.

Charras, G.T., Horton, M.A., 2002a. Single cell mechanotransduction and its modulation analyzed by atomic force microscope indentation. Biophysical Journal 82(6): 2970-2981.

Charras, G.T., Horton, M.A., 2002b. Determination of cellular strains by combined atomic force microscopy and finite element modelling. Biophysical Journal 83(2): 858-879.

Charras, G.T., Williams, B.A., Sims, S.M., Horton, M.A., 2004. Estimating the Sensitivity of Mechanosensitive Ion Channels to Membrane Strain and Tension. Biophysical Journal 87(4): 2870-2884.

Chicurel, M.E., Chen, C.S., Ingber, D.E., 1998. Cellular control lies in the balance of forces. Current Opinion in Cell Biology 10(2): 232-239

Chien, S., Li, S., Shiu, Y. T., Li, Y. S., 2005. Molecular basis of mechanical modulation of endothelial cell migration. Frontiers in Bioscience 10: 1985-2000.

Checa, S., Prendergast, P.J. 2009. A mechanobiological model for tissue differentiation that includes angiogenesis: A lattice-based modeling approach. Annals of Biomedical Engineering 37: 129-145.

Checa, S., Prendergast, P. J., 2010. Effect of cell seeding and mechanical loading on vascularisation and tissue formation inside a scaffold: a mechanobiological model using a lattice approach to simulate cell activity. Journal of Biomechanics 43(5): 961-968.

Chouinard, J.A., Grenier, G., Khalil, A., Vermette, P., 2008. Oxidised-LDL induce morphological changes and increase stiffness of endothelial cells. Experimental Cell Research 314: 3007-3016.

Collinsworth, A.M., Zhang, S., Kraus, W.E., Truskey, G.A., 2002. Apparent elastic modulus and hysteresis of skeletal muscle cells throughout differentiation. The American Journal of Physiology - Cell Physiology 283(4): 1219-1227.

Coughlin. M. F., Stamenovic, D., 1998. A tensegrity model of the cytoskeleton in spread and round cells. Journal of Biomechanical Engineering 120(6): 770-777.

Dahl, K.N., Booth-Gauthier, E.A., Ladoux, B., 2010. In the middle of it all: mutual mechanical regulation between the nucleus and the cytoskeleton. Journal of Biomechanics 43(1): 2-8.

Dahl, K.N., Kahn, S.M., Wilson, K.L., Discher, D.E., 2004. The nuclear envelope lamina network has elasticity and a compressibility limit suggestive of a molecular shock absorber. Journal of Cell Science 117(20): 4779-4786.

Dalby, M.J., 2005. Topographically induced direct cell mechanotransduction. Medical Engineering & Physics 27(9): 730-742.

Davies, P. F., Barbee, K. A., Lal, R., Robotewskyj, A., Griem, M. L., 1995. Hemodynamics and atherogenesis. Endothelial surface dynamics in flow signal transduction. Annals of the New York Academy of Sciences 748: 86-102; discussion 102-103.

Deguchi, S., Ohashi, T., Sato, M., 2005. Evaluation of tension in actin bundle of endothelial cells based on preexisting strain and tensile properties measurements. Molecular & Cellular Biomechanics 2(3): 125-133.

De Rooij, P. P., Siebrecht, M. A., Tagil, M., Aspenberg, P., 2001. The fate of mechanically induced cartilage in an unloaded environment. Journal of Biomechanics 34 (7): 961-966.

De Santis, G., Lennon, A.B., Boschetti, F., Verhegghe, B., Verdonck, P., Prendergast, P.J., 2011. How can cells sense the elasticity of a substrate? An analysis using a cell tensegrity model. Journal of European Cells and Materials 22: 202-213.

Dong, C., Skalak, R., Sung, K. L., Schmid-Schonbein, G. W., Chien, S., 1991. Cytoplasmic rheology of passive neutrophils. Journal of Biomechanical Engineering 28: 557-567.

Dorr, L.D., Wan, Z., Malik, A., Zhu, J., Dastane, M., Deshmane, P., 2009. A comparison of surgeon estimation and computed tomographic measurement of femoral component anteversion in cementless total hip arthroplasty. Journal of Bone Joint Surgery 91(11): 2598-2604.

Evans, E., Yeung, A., 1989. Apparent viscosity and cortical tension of blood granulocytes determined by micropipet aspiration. Biophysical Journal 56(1): 151-160.

Engh, C.A., Bobyn, J.D., Glassman, A.H., 1987. Theory and practice of cementless revision total hip arthroplasty. The Hip 271-317.

Firth, A.L., Yuan, J.X., 2012. Identification of functional progenitor cells in the pulmonary vasculature. Pulmonary Circulation 2(1): 84-100.

Frangos, J. A. (Ed.), 1993. Physical Forces and Mammalian Cell. Academic Press, San Diego, CA, 400 pp.

Friedenstein, A.J., Piatetzyky-Shapiro, I., Petrovka, K.V., 1966. Osteogenesis in transplants of bone marrow cells. Journal of Embryology and. Experimental Morphology 16: 381-90.

Frisch, T., Thoumine, O., 2002. Predicting the kinetics of cell spreading. Journal of Biomechanics 35(8): 1137-1141.

Firth, A.L., Yuan, J.X., 2012. Identification of functional progenitor cells in the pulmonary vasculature. Pulmonary Circulation 2(1): 84-100.

Harris, W.H., 1992. Is it advantageous to strengthen the cement-metal interface and use a collar for cemented femoral components of total hip replacements? Clinical Orthopaedics and Related Research 285: 67-72.

Geiger, B., Bershadsky, A., 2002. Exploring the neighborhood: Adhesion-coupled cell mechanosensors. Cell 110: 139-142.

Gerstenfeld, L.C., Cullinane, D.M., Barnes, G.L., Graves, D.T., Einhorn, T.A., 2003b. Fracture healing as a post-natal developmental process: molecular, spatial, and temporal aspects of its regulation. Journal of Cellular Biochemistry 88: 873-884.

Gittes, F., Mickey, B., Nettleton, J., Howard, J., 1993. Flexural rigidity of microtubules and actin filaments measured from thermal fluctuations in shapeThe Journal of Cell Biology 120(4): 923-934.

Golding, J.S.R., 1993 Causes and Mechanisms of Linear Growth Retardation, in Waterlow, J.C. & Schürch (eds), The mechanical factors which influence bone growth, International Dietary Energy Consultancy Group, London, 15-18 January 1993.

Grinnell, F., 2003. Fibroblast biology in three-dimensional collagen matrices. Trends in Cell Biology 13: 264-269.

Grodzinsky, A. J., Levenston, M. E., Jin, M., Frank, E. H., 2000. Cartilage tissue remodeling in response to mechanical forces. Annual Review of Biomedical Engineering 2: 691-713.

Gudas, R., Kalesinskas, R.J., Monastyreckiene, E., Valanciūte, A., Trumpickas, V., 2003. Medicina Osteochondral transplantation (mosaicplasty) in the treatment of knee joint cartilage defects. Medicina 39(5): 469-475.

.Guilak, F., Tedrow, J.R., Burgkart, R., 2000. Viscoelastic properties of the cell nucleus. Biochemical and Biophysical Research Communications 269(3): 781-786.

Hale, J.P., Winlove, C.P., Petrov, P.G., 2011. Effect of hydroperoxides on red blood cell membrane mechanical properties. Biophysical Journal 11(8): 1921-1929.

Hammerick, K.E., Huang, Z., Sun, N., Lam, M.T., Prinz, F.B., Wu, J.C., Commons, G.W., Longaker, M.T., 2011. Elastic properties of induced pluripotent stem cells. Tissue Engineering 17(3-4): 495-502.

Horwitz, E.M., Gordon, P.L., Koo, W.K., Marx, J.C., Neel, M.D., McNall, R.Y., Muul, L., Hofmann, T., 2002. Isolated allogeneic bone marrow-derived mesenchymal cells engraft and stimulate growth in children with osteogenesis imperfecta: Implications for cell therapy of bone, Proceedings of the National Academy of Sciences of United States of America 99: 8932-8937.

Hozack, W.J., Rothman, R.H., Booth, R.E., Balderston, R.A., Cohn, J.C., Pickens, G.T., 1990. Survivorship analysis of 1,041 Charnley total hip arthroplasties. The Journal of Arthroplasty 5(1): 41-7.

Hsieh, M. H., Nguyen, H. T., 2005. Molecular mechanism of apoptosis induced by mechanical forces. International Review of Cytology 245, 45-90.

Huang, C.Y., Hagar, K.L., Frost, L.E., Sun, Y., Cheung, H.S., 2004. Effects of cyclic compressive loading on chondrogenesis of rabbit bone-marrow derived mesenchymal stem cells. Stem Cells 22(3): 313-323.

Huiskes, R., Van Driel, W. D., Prendergast, P. J., Soballe, K., 1997. A biomechanical regulatory model for periprosthetic brous-tissue differentiation. Journal of Materials Science: Materials in Medicine 8(12): 785-788.

Hu, S., Chen, J., Fabry, B., Numaguchi, Y., Gouldstone, A., Ingber, D. E., Fredberg, J. J., Butler, J. P., & Wang, N., 2003. Intracellular stress tomography reveals stress focusing and structural anisotropy in cytoskeleton of living cells. American Journal of Physiology - Cell Physiology 285: 1082-1090.

Ingber, D., 1991. Integrins as mechanochemical transducers. Curr. Opin. Cell Biology 3: 841-848.

Ingber, D.E., 1993. Cellular tensegrity: defining new rules of biological design that govern the cytoskeleton. Journal of Cell Science 104(3): 613 -627.

Ingber, D.E., 1997. Tensegrity: the architectural basis of cellular mechanotransduction. Annual Review of Physiology 59: 575-599.

Ingber, D.E., 2003. Mechanobiology and diseases of mechanotransduction. Annals of Internal Medicine 35(8): 564-577.

Ingber, D.E., 2008. Tensegrity-based mechanosensing from macro to micro. Progress in Biophysics and Molecular Biology 97(2-3): 163-179.

Isaksson, H., 2007. Mechanical and mechanobiological influences on bone fracture repair identifying important cellular characteristics, Ph.D. Dissertation, Eindhoven University of Technology, Netherlands.

Isaksson H, Wilson W, van Donkelaar, C.C., Huiskes, R., Ito, K., 2006b. Comparison of biophysical stimuli for mechano-regulation of tissue differentiation during fracture healing Journal of Biomechanics 39(8):1507-1516

Isaksson, H., Comas, O., van Donkelaar, C.C., Mediavilla, J., Wilson, W., Huiskes, R., Ito, K., 2007. Bone regeneration during distraction osteogenesis: mechano-

regulation by shear strain and fluid velocity. Journal of Biomechanics 40(9): 2002-2011.

Iwaki, A., Jingushi, S., Oda, Y., Izumi, T., Shida, J.I., Tsuneyoshi, M., Sugioka,Y., 1997. Localization and quantification of proliferating cells during rat fracture repair: detection of proliferating cell nuclear antigen by immunohistochemistry Journal of Bone and Mineral Research 12: 96-102.

Jacobs, C.R., Kelly, D.J., 2011. Cell mechanics: the role of simulation. In: Fernandes PR, Ba´rtolo PJ, editors. Advances on modeling in tissue engineering. Springer Netherlands. p. 1-14.

Jagodzinski, M., Drescher, M., Zeichen, J., Hankemeier, S., Krettek, C., Bosch, U., van Griensven, M., 2004. Effects of cyclic longitudinal mechanical strain and dexamethasone on osteogenic differentiation of human bone marrow stromal cells. Journal of European Cells and Materials 16(7): 35-41.

Jasty, M., Burke, D., Harris, W.H., 1992. Biomechanics of cemented and cementless prostheses. La Chirurgia degli Organi di Movimento 77(4): 349-358.

Kamm, R.D., McVittie, A.K., Bathe, M., 2000. On the Roleof Continuum Models in Mechanobiology. ASME International Congress - Mechanics in Biology. 242: 1-9.

Kakisis, J. D., Liapis, C. D., Sumpio, B. E., 2004. Effects of cyclic strain on vascular cells. Endothelium 11: 17-28.

Karcher, H., Lammerding, J., Huang, H., Lee, R.T., Kamm, R.D., Kaazempur-Mofrad, M.R.,2003. A three-dimensional viscoelastic model for cell deformation with experimental verification. Biophysical Journal 85(5): 3336-3349.

Kearney, E. M., Prendergast, P. J., Campbell, V. A., 2008. Mechanisms of strain-mediated mesenchymal stem cell apoptosis. Journal of Biomechanical Engineering 130(6): 061004.

Kearney, E. M., Farrell, E., Prendergast, P. J., Campbell, V. A., 2010. Tensile train as a regulator of mesenchymal stem cell osteogenesis. Annals of Biomedical Engineering 38: 1767-1779.

Kelly, D. J., Jacobs, C. R., 2010. The role of mechanical signals in regulating chondro-genesis and osteogenesis of mesenchymal stem cells. Birth Defects Research, Part C: Embryo Today 90(1): 75-85.

Kelly, D.J., Prendergast, P.J., 2005. Mechano-regulation of stem cell differentiation and tissue regeneration in osteochondral defects. Journal of Biomechanics 38(7): 1413-1422.

Kelly, D.J., Prendergast, P.J., 2006. Prediction of the optimal mechanical properties for a scaffold used in osteochondral defect repair. Tissue Engineering 12(9): 2509-2519.

Kelly, G.M., Kilpatrick, J.I., van Es, M.H., Weafer, P.P., Prendergast, P.J., Jarvis, S.P., 2011. Bone cell elasticity and morphology changes during the cell cycle. Journal of Biomechanics 44(8): 1484-1490.

Khayyeri, H., Checa, S., Tagil, M., Prendergast, P.J., 2009. Corroboration of mechanobiological simulations of tissue differentiation in an in vivo bone chamber using a lattice-modeling approach. Journal of Orthopaedic Research 27: 1659-1666.

Koc, O.N., Gerson, S.L., Cooper, B.W., Dyhouse, S.M., Haynesworth, S.E., Caplan, A.I., Lazarus, H.M., 2000. Rapid hematopoietic recovery after coinfusion of autologousblood stem cells and culture-expanded marrow mesenchymal stem cells

in advanced breast cancer patients receiving high-dose chemotherapy, Journal of Clinical Oncology 18: 307-316.

Lacroix, D., Prendergast, P.J., Li, G., Marsh, D., 2002. Biomechanical model to simulate tissue differentiation and bone regeneration: application to fracture healing. Medical & Biological Engineering & Computing 40: 14-21.

Lacroix, D., Prendergast, P. J., 2002a. A mechano-regulation model for tissue differentiation during fracture healing: analysis of gap size and loading. Journal of Biomechanics 35(9): 1163-1171.

Lacroix, D., Prendergast, P. J., 2002b. Three-dimensional simulation of fracture repair in the human tibia. Computer Methods in Biomechanics and Biomedical Engineering 5(5): 369-376.

Lacroix, D., Prendergast, P. J., Li, G., Marsh, D., 2002. Biomechanical model to simulate tissue differentiation and bone regeneration: application to fracture healing. Medical and Biological Engineering and Computing 40(1): 14-21.

Lai, Y., Sun, Y., Skinner, C.M., Son, E.L., Lu, Z., Tuan, R.S., Jilka, R.L., Ling, J., Chen, X., 2008. Reconstitution of Marrow-Derived Extracellular Matrix Ex Vivo: A Robust Culture System for Expanding Large-Scale Highly Functional Human Mesenchymal Stem Cells. Stem Cells and Development 19(7): 1095-1107.

Lammerding, J., Kamm, R.D., Lee, R.T., 2004. Mechanotransduction in cardiac myocytes. Annals of the New York Academy of Sciences 1015: 53-70.

Lehoux, S., Castier, Y., Tedgui, A., 2006. Molecular mechanisms of the vascular responses to haemodynamic forces. Journal of Internal Medicine 259: 381-392.

Lieber, S.C., Aubry, N.. Pain, J., Diaz, G., kim, S., Vatner, S.F., 2004. Ageing increases stiffness of cardiac myocytes measured by atomic force microscopy nanoindentation. American Journal of Physiology Heart Circulatory Physiology 287: 645-651.

Lu, Y., Lee, J.S., Nemke, B., Graf, B.K., Royalty, K., Illgen III, R., Vanderby Jr, R., Markel, M.D., Murphy, W.L., 2012. Coating with a Modular Bone Morphogenetic Peptide Promotes Healing of a Bone-Implant Gap in an Ovine Model. PLoS ONE 7(11): e50378.

Lunze, K., Stalhand, J., Leonhardt, S., 2010. Modeling of Stretch-Activated Sarcolemmal Channels in Smooth Muscle Cells. FMBE Proceedings 25(4): 740-743.

Maguire, P., Kilpatrick, J.I., Kelly, G.M., Prendergast, P.J., Campbell, V.A., O'Connell, B.C., Jarvis, S.P., 2007. Direct mechanical measurement of geodesic structures in rat mesenchymal stem cells. Human Frontier Science Program Journal 1(3): 181-191.

Maniotis, A. J., Chen, C. S., & Ingber, D. E., 1997. Demonstration of mechanical connections between integrins, cytoskeletal laments, and nucleoplasm that stabilize nuclear structure. Proceedings of the National Academy of Sciences 94: 849-854.

Matthews, B.D., Overby, D.R., Mannix, R., Ingber, D.E., 2006. Cellular adaptation to mechanical stress: role of integrins, Rho, cytoskeletal tension and mechanosensitive ion channels. Journal of Cell Science 119(3): 508-518.

Mazumder, A., Shivashankar, G.V., 2010. Emergence of a prestressed eukaryotic nucleus during cellular differentiation and development. Journal of the Royal Society Interface 7(3): 321-330.

McGarry, J.G., Prendergast, P.J., 2004. A three-dimensional finite element model of an adherent eukaryotic cell, European Cells and Materials Journal 7: 27-33.

McGarry, J.G., Klein-Nulend, J., Prendergast, P.J., 2005a. The effect of cytoskeletal disruption on pulsatile fluid flow-induced nitric oxide and prostaglandin E2 release in osteocytes and osteoblasts. Biochemical and Biophysical Research Communications 330(1): 341-8.

McGarry, J.G., Klein-Nulend, J., Mullender, M.G., Prendergast, P.J., 2005b. A comparison of strain and fluid shear stress in stimulating bone cell responses--a computational and experimental study. The FASEB Journal 19(3): 482-484.

McKayed, K.K., Campbell, V.A., Prendergast, P.J., 2010. The influence of age on mesenchymal stem cell mechanoresponsiveness to tensile strain. Paper presented at: ESB 2010. Proceedings of the 17th Congress of European Society of Biomechanics, July 5-8, University of Edinburgh, UK.

McMahon, L.A., Reid, A.J., Campbell, V.A., Prendergast, P.J., 2008. Regulatory effects of mechanical strain on the chondrogenic differentiation of MSCs in a collagen-GAG scaffold: experimental and computational analysis. Annals of Biomedical Engineering 36(2): 185-194.

Meneghini, R.M., Hanssen, A.D., 2008. Cementless fixation in total knee arthroplasty: past, present, and future. Journal of Knee Surgery 2008 21(4): 307-314.

Mizushima-Sugano, J., Maeda, T., Miki-Noumura, T., 1983. Flexural rigidity of singlet microtubules estimated from statistical analysis of their contour lengths and end-to-end distances. Biochimica et Biophysica Acta 755: 257-262.

Moeendarbary, E., Valon, L., Fritzsche, M., Harris, A.R., Moulding, D.A., Thrasher, A.J., Stride, E., Mahadevan, L., Charras, G.T., 2013. The cytoplasm of living cells behaves as a poroelastic material. Nature Materials 12: 253-261.

Morris, R., Cox, H., Mombelli, E., Quinn, P.J., 2004. Rafts, little caves and large potholes: how lipid structure interacts with membrane proteins to create functionally diverse membrane environments Subcellular Biochemistry 37: 335-118.

Mueller, S.M., Glowacki, J., 2001. Age-related decline in the osteogenic potential of human bone marrow cells cultured in three-dimensional collagen sponges. Journal of Cellular Biochemistry 82(4): 583-590..

Nagel, T., Kelly, D. J., 2010. Mechano-regulation of mesenchymal stem cell differentiation and collagen organisation during skeletal tissue repair. Biomechanics and Modeling in Mechanobiology. 9(3): 359-372.

Ng, L., Hung, H., Sprunt, A., Chubinskya, S., Ortiz, C., Grodzinsky, A., 2007. Nanomechanical properties of individual chondrocytes and their developing growth factor-stimulated pericellular matrix. Journal of Biomechanics 40: 1011-1023.

Ohashi, T., Ishii, Y., Ishikawa, Y., Matsumoto, T., Sato, M., 2002. Experimental and numerical analyses of local mechanical properties measured by atomic force microscopy for sheared endothelial cells. Bio-Medical Materials and Engineering 12(3): 319-327.

Pauwels, F., 1960. A new theory of the influence of mechanical stimuli on the differentiation of supporting tissue. the tenth contribution to the functional anatomy and causal morphology of the supporting structure. Zeitschrift fur Anatomie und Entwicklungsgeschichte 121: 478-515.

Perez, M. A., Prendergast, P. J., 2007. Random-walk models of cell dispersal included in mechanobiological simulations of tissue differentiation. Journal of Biomechanics 40(10): 2244-2253.

Petite, H., Viateau, V., Bensaid, W., Meunier, A., de Pollak, C., Bourguignon, M., Oudina, K., Sedel, L., Guillemin, G., 2000. Tissue-engineered bone regeneration, Nature Biotechnology 18: 959-963.

Pfeiler, T.W., Sumanasinghe, R.D., Loboa, E.G., 2008. Finite element modeling of 3D human mesenchymal stem cell-seeded collagen matrices exposed to tensile strain. Journal of Biomechanics 41(10): 2289-2296.

Pillarisetti, A., Desai, JP., Ladjal, H., Schiffmacher, A., Ferreira, A., Keefer, C.L., 2011. Mechanical phenotyping of mouse embryonic stem cells: increase in stiffness with differentiation. Cell Reprogram 13(4): 371-80.

Pittenger, M.F., Mackay, A.M., Beck, S.C., Jaiswal, R.K., Douglas, R., Mosca, J.D., Moorman, M.A., Simonetti, D.W., Craig, S., Marshak, D.R., 1999. Multilineage potential of adult human mesenchymal stem cells. Science 284(5411): 143-147.

Pontikoglou, C., Deschaseaux, F., Sensebe, L., Papadaki, H.A., 2011. Bone marrow mesenchymal stem cells: biological properties and their role in hematopoiesis and hematopoietic stem cell transplantation. Stem Cell Reviews 7(3): 569-589.

Postacchini, F., Gumina, S., Perugia, D., De Martino, C., 1995. Early fracture callus in the diaphysis of human long bones. Histologic and ultrastructural study. Clinical Orthopaedics and Related Research 218-228.

Pradhan, S., and Sumpio, B., 2004. Molecular and biological effects of hemodynamics on vascular cells. Frontiers in Bioscience 9: 3276-3285.

Prendergast, P.J., Huiskes, R., Soballe, K., 1997. ESB Research Award 1996. Biophysical stimuli on cells during tissue differentiation at implant interfaces. Journal of Biomechanics 30: 539-548.

Prendergast, P. J., 1997. Finite element models in tissue mechanics and orthopaedic implant design. Clinical Biomechanics 12(6): 343-366.

Prendergast, P. J., 2001. An analysis of theories in biomechanics. Engineering Transactions (Rozprawy Inzynierskie) 49: 117-133.

Prendergast, P. J., 2002. Mechanics applied to skeletal ontogeny and phylogeny. Meccanica 37: 317-334.

Radmacher, M., Cleveland, J.P., Fritz, M., Hansma, H.G., Hansma, P.K., 1994. Mapping interaction forces with the atomic force microscope. Biophysical Journal 66(6): 2159-2165.

Reinhart-King, C.A., Dembo, M., Hammer, D.A., 2008. Cell-Cell Mechanical Communication through Compliant Substrates. Biophysical Journal 95: 6044-6051.

Riley, G.P., Curry, V., DeGroot, J., van El, B., Verzijl, N., Hazleman, B.L., Bank, R.A., 2002. Matrix metalloproteinase activities and their relationship with collagen remodelling in tendon pathology. Matrix Biology 21(2):185-195.

Ross, R., 1986. The pathogenesis of atherosclerosis-an update. The New England Journal of Medicine 314(8):488-500

Ruiz, S.A., Chen, C.S., 2008. Emergence of patterned stem cell differentiation within multicellular structures. Stem Cells 26: 2921-2927.

Sadoshima, J., Izumo, S., 1997 The cellular and molecular response of cardiac myocytes to mechanical stress. Annual Review of Physiology 59: 551-571.

Sandberg, M.M., Aro, H.T., Vuorio, E.I., 1993. Gene expression during bone repair. Clinical Orthopaedics and Related Research 292-312.

Sarraf, C.E., Otto, W.R., Eastwood, M., 2011. In vitro mesenchymal stem cell differentiation after mechanical stimulation. Cell Proliferation 44(1): 99-108.

Sarasa-Renedo, A., Chiquet, M., 2005. Mechanical signals regulating extracellular matrix gene expression in fibroblasts. Scandinavian Journal of Medicine & Science in Sports 15: 223-230.

Saris, D.B., Vanlauwe, J., Victor, J., Almqvist, K.F., Verdonk, R., Bellemans, J., Luyten, F.P., Treatment of symptomatic cartilage defects of the knee: characterized chondrocyte implantation results in better clinical outcome at 36 months in a randomized trial compared to microfracture. The American Journal of Sports Injury 37(1): 10S-19S.

Sethe, S., Scutt, A., Stolzing, A., 2006. Ageing of mesenchymal stem cells. Age Research Reviews 5: 91-116.

Shin, D., Athanasiou, K., 1999. Cytoindentation for obtaining cell biomechanical properties. Journal of Orthopaedic Research 17: 880-890.

Silver, F. H., Freeman, J. W., Seehra, G. P., 2003. Collagen self-assembly and the development of tendon mechanical properties. Journal of Biomechanics. 36: 1529-1553.

Slomka, N, Gefen, A., 2011. Finite Element Modeling of Cellular Mechanics Experiments, Cellular and Biomolecular Mechanics and Mechanobiology Studies in Mechanobiology, Tissue Engineering and Biomaterials, 4: 331-334.

Smith, S.B., Cui, Y., Bustamante, C., 1996. Overstretching B-DNA: the elastic response of individual double-stranded and single-stranded DNA molecules. Science New Series. 271(5250): 795-799.

Stamenovic, D., Coughlin, M.F., 1999. The role of prestress and architecture of the cytoskeleton and deformability of cytoskeletal filaments in mechanics of adherent cells: a quantitative analysis. Journal of Theoretical Biology 201(1): 63-74.

Stamenovic, D., Fredberg, J.J., Wang, N., Butler, J.P., Ingber, D.E., 1996. A Micro-structural Approach to Cytoskeletal Mechanics based on Tensegrity. Journal of Theoretical Biology 181(2): 125-136.

Starodubtseva, M.N., 2011. Mechanical properties of cells and ageing. Ageing Brain Research Reviews 10(1): 16-25.

Stein, G.S.., Lian, J.B., van Wijnen, A.J., Stein, J.L., Javed, A., Montecino, M., Choi, J., Vradii, D., Zaidi, S.K., Pratap, J., Young, D., 2007. Organization of transcriptional regulatory machinery in nuclear microenvironments: implications for biological control and cancer. Advances in Enzyme Regulation 47: 242-250.

Stern, A.R., Nicolella, D.P., 2013. Measurement and estimation of osteocyte mechanical strain. Bone 54(2): 191-195.

Stolzing, A., Scutt, A., 2006. Age-related impairment of mesenchymal progenitor cell function. Ageing Cell 5: 213-224.

Stops, A.J., McMahon, L.A., O'Mahoney, D., Prendergast, P.J., McHugh, P.E., 2008. A finite element prediction of strain on cells in a highly porous collagen-glycosaminoglycan scaffold. Journal of Biomechanics 130(6): 061001.

Swanson, A.B., 1960. Surgery of the Hand in Cerebral Palsy and the Swan-Neck Deformity. Journal of Bone Joint Surgery 42(6): 951-964.

Tagil, M., Aspenberg, P., 1999. Cartilage induction by controlled mechanical stimulation in vivo. Journal of Orthopaedic Research 17 (2): 200-204.

Vandenburgh, H. H., 1992. Mechanical forces and their second messengers in stimulating cell growth in vitro. American Journal of Physiology 262: 350-355.

van der Meulen, M.C., Huiskes, R., 2002. Why mechanobiology? A survey article. Journal of Biomechanics 35: 401-414.

Verdonschot, N., Huiskes, R., 1997. Cement debonding process of total hip arthroplasty stems. Clinical Orthopaedics and Related Research 336: 297-307.

Wagner, W., Bork, S., Horn, P., Krunic, D., Walenda, T., Diehlmann, A., Benes, V., Blake, J., Huber, F., Eckstein, V., Boukamp, P., Ho, A.D., 2009. Ageing and replicative senescence have related effecs on human stem and progenitor cells. PLoSONE 4(6): e5846.

Wang, J. H., 2006. Mechanobiology of tendon. Journal of Biomechanics. 39: 1563-1582.

Wang, J. H., Thampatty, B. P., Lin, J. S., Im, H. J., 2007. Mechanoregulation of gene expression in fibroblasts. Gene 391: 1-15.

Wang, N., Stamenovic, D., 2000. Contribution of intermediate filaments to cell stiffness, stiffening, and growth. American Journal of Physiology - Cell Physiology 279(1): 188-194.

Wang, N., Stamenovic, D., 2002. Mechanics of vimentin intermediate filaments. Journal of Muscle Research and Cell Motility 23(5-6): 535-540.

Wang, N., Naruse, K., Stamenovic, D., Fredberg, J.J., Mijailovich, S.M., Tolic-Norrelykke, I.M., Polte, T., Mannix, R., Ingber, D.E., 2001. Mechanical behavior in living cells consistent with the tensegrity model. Proceedings of the National Academy of Sciences; USA. 98(14): 7765-7770.

Wang, N., Tytell, J.D., Ingber, D.E., 2009. Mechanotransduction at a distance: mechanically coupling the extracellular matrix with the nucleus. Nature Reviews Molecular Cell Biology 10(1): 75-82.

Waugh, R.E., Agre, P., 1988. Reductions of erythrocyte membrane viscoelastic coefficients reflect spectrin deficiencies in hereditary spherocytosis. The Journal of Clinical Investigation 81(1): 133-141.

Weinans, H., Prendergast, P.J., 1996. Tissue adaptation as a dynamical process far from equilibrium, Bone 19: 143-149.

Wendling, S., Oddou, C., Isabey, D., 1999. Stiffening response of a cellular tensegrity model. Journal of Theoretical Biology 196(3): 309-325.

Zheng, H., Martin, J.A,, Duwayri, Y., Falcon, G., Buckwalter, J.A., 2007. Impact of ageing on rat bone marrow-derived stem cell chondrogenesis. The Journals of Gerontology Series A: Biological Sciences and Medical Sciences 62(2): 136-148.

Zhou, S., Greenberger, J.S., Epperly, M.W., Goff, J.P., Adler, C., LeBoff, M.S., Glowacki, J., 2008. Age-related intrinsic changes in human bone marrow-derived mesenchymal stem cells and their differentiation to osteoblasts. Ageing Cell 7(3): 335-343.

Appendices

Appendix A

The predicted tissue differentiation patterns under force-control without debonding

The stiffness of cell membrane was altered from 10% (x0.1) to 10 times (x10) of the original young cell. The highlighted two lines, i.e. E_{mem} x1 (3T) and E_{mem} x2 (2T) are the young and aged cells, respectively.

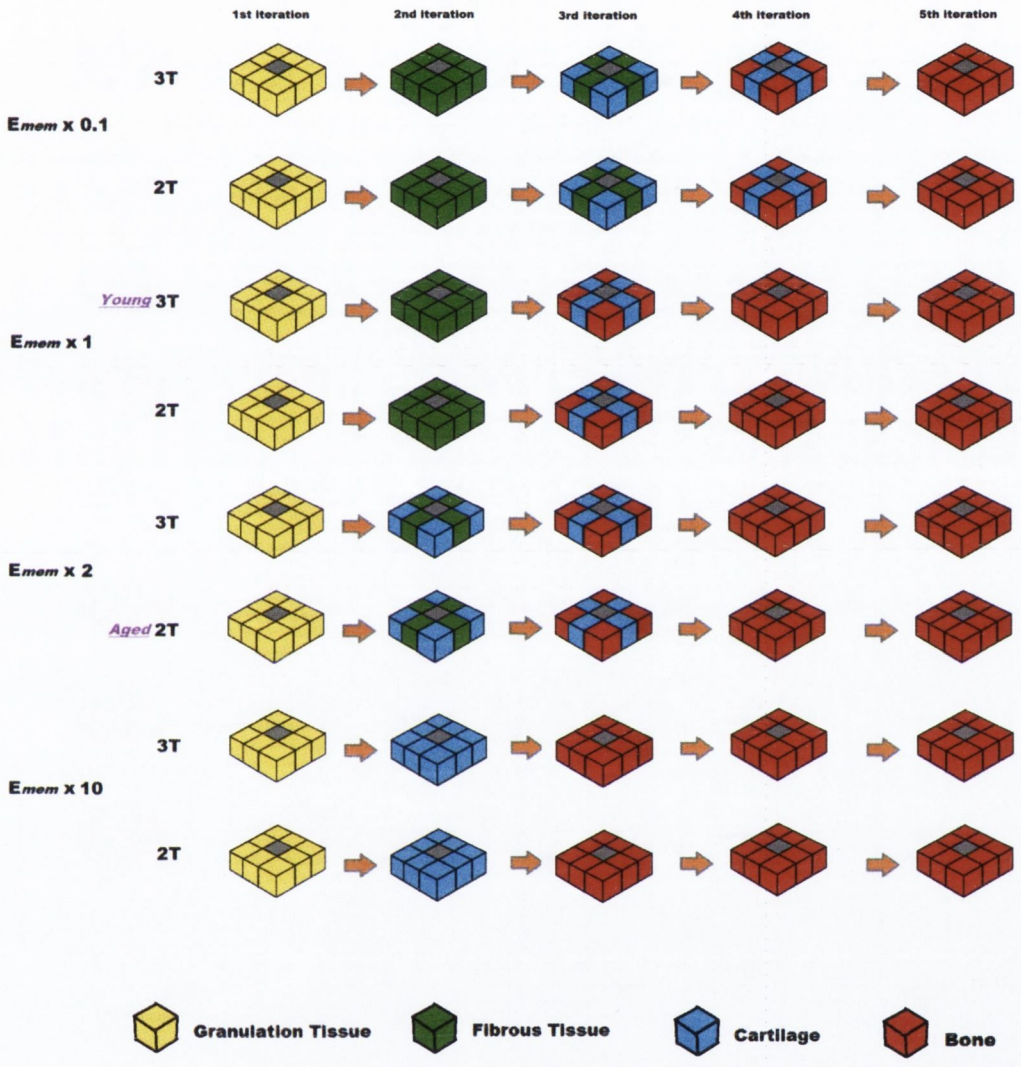


Figure A.1. Tissue differentiation patterns under force-control with a loading magnitude of 0.48 μN without debonding.

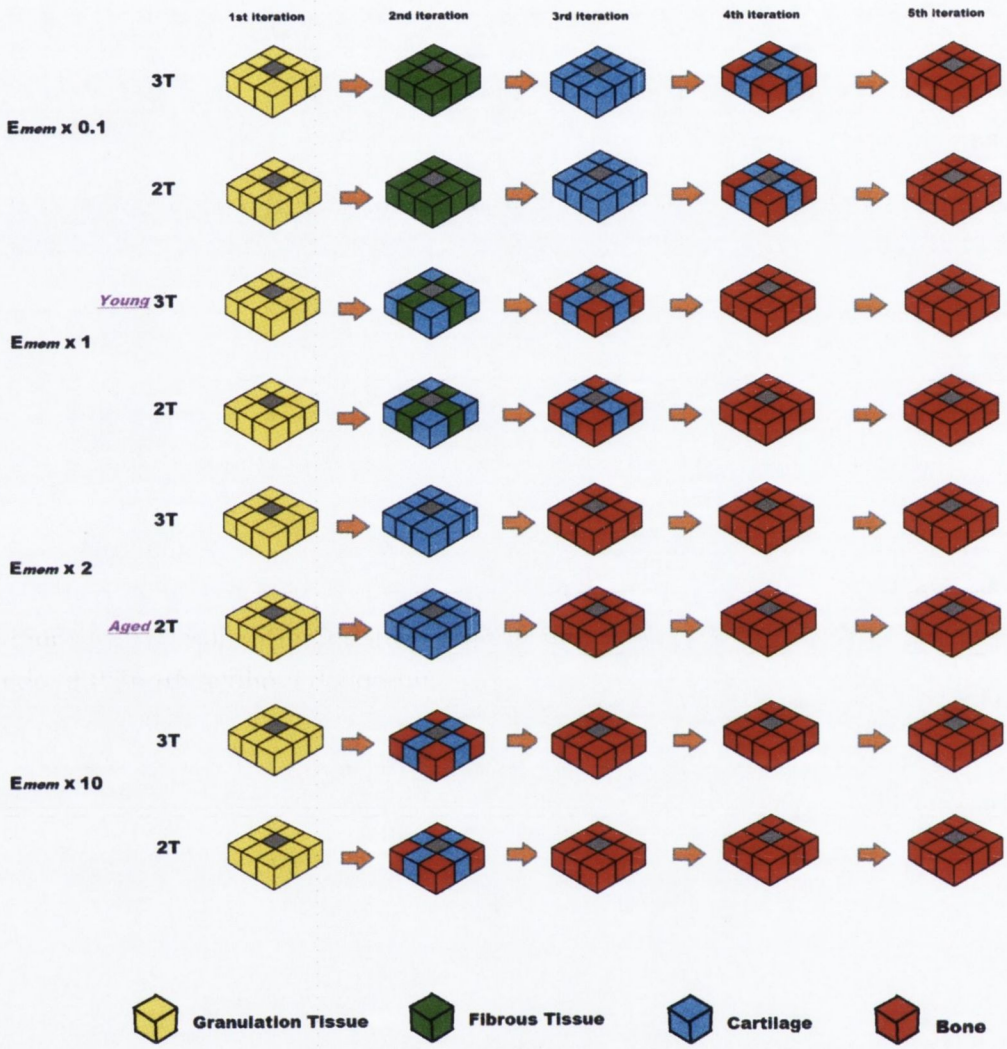


Figure A.2. Tissue differentiation patterns under force-control with a loading magnitude of 0.36 μN without debonding.

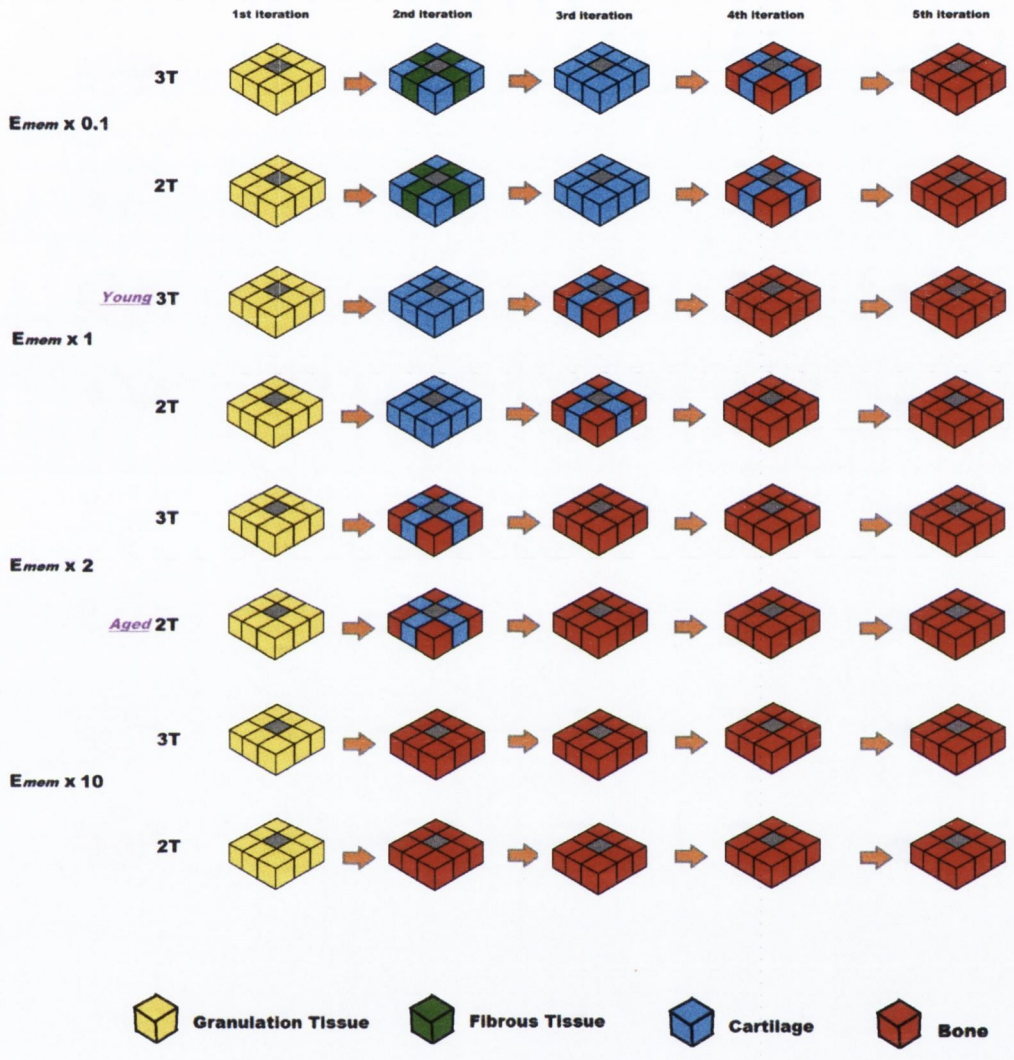


Figure A.3. Tissue differentiation patterns under force-control with a loading magnitude of 0.24 μN without debonding.

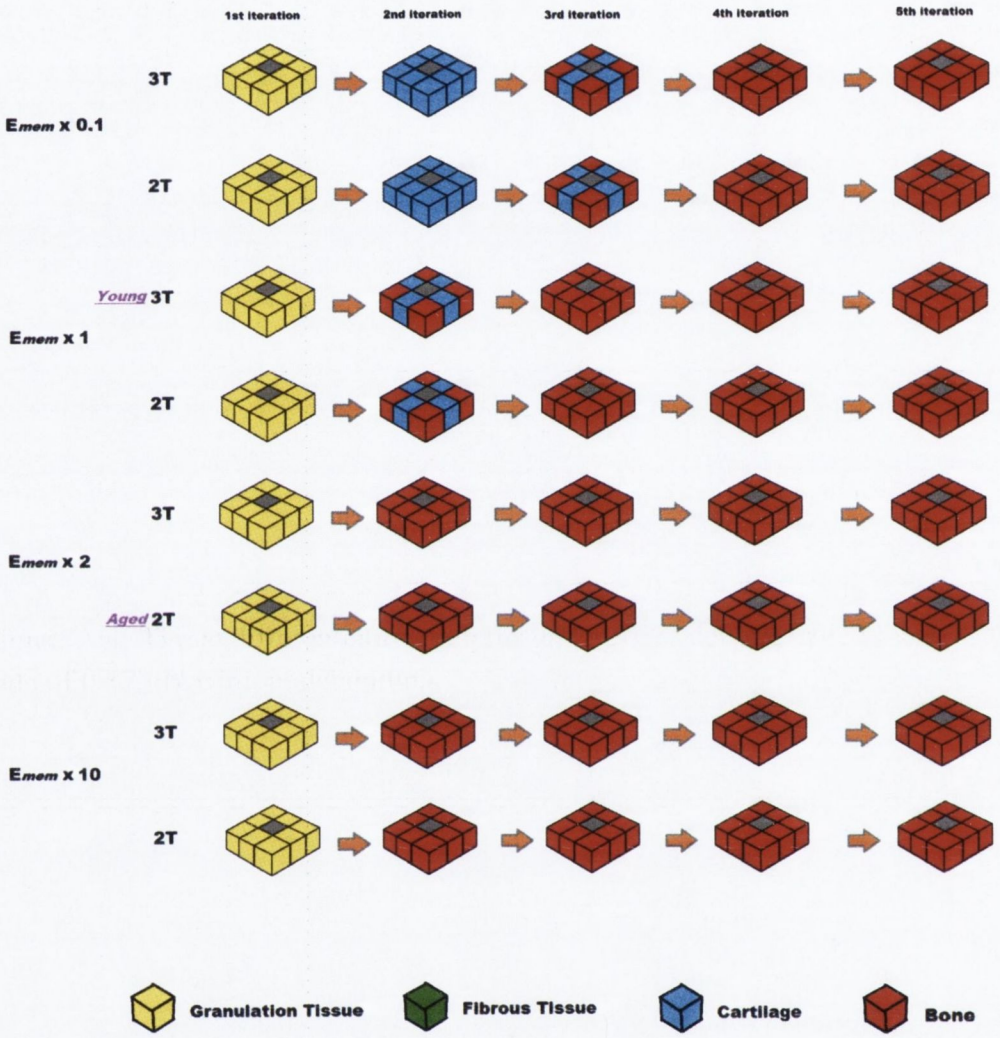


Figure A.4. Tissue differentiation patterns under force-control with a loading magnitude of 0.12 μN without debonding.

Appendix B

The predicted tissue differentiation patterns under force-control with one debonding surface (debonding case 1)

The stiffness of cell membrane was altered from 10% (x0.1) to 10 times (x10) of the original young cell. The highlighted two lines, i.e. E_{mem} x1 (3T) and $_{Emem}$ x2 (2T) are the young and aged cells, respectively.

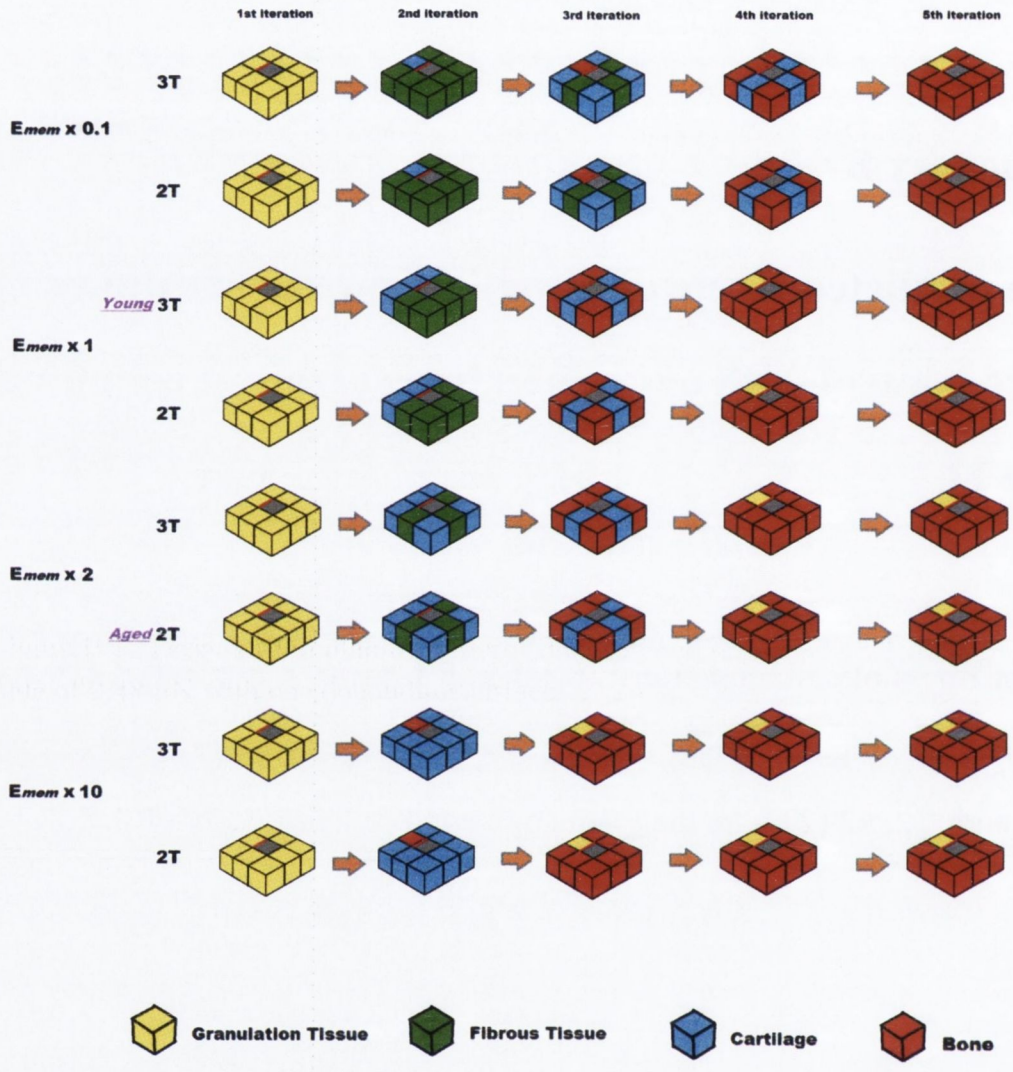


Figure B.1. Tissue differentiation patterns under force-control with a loading magnitude of 0.48 μN with one debonding surface.

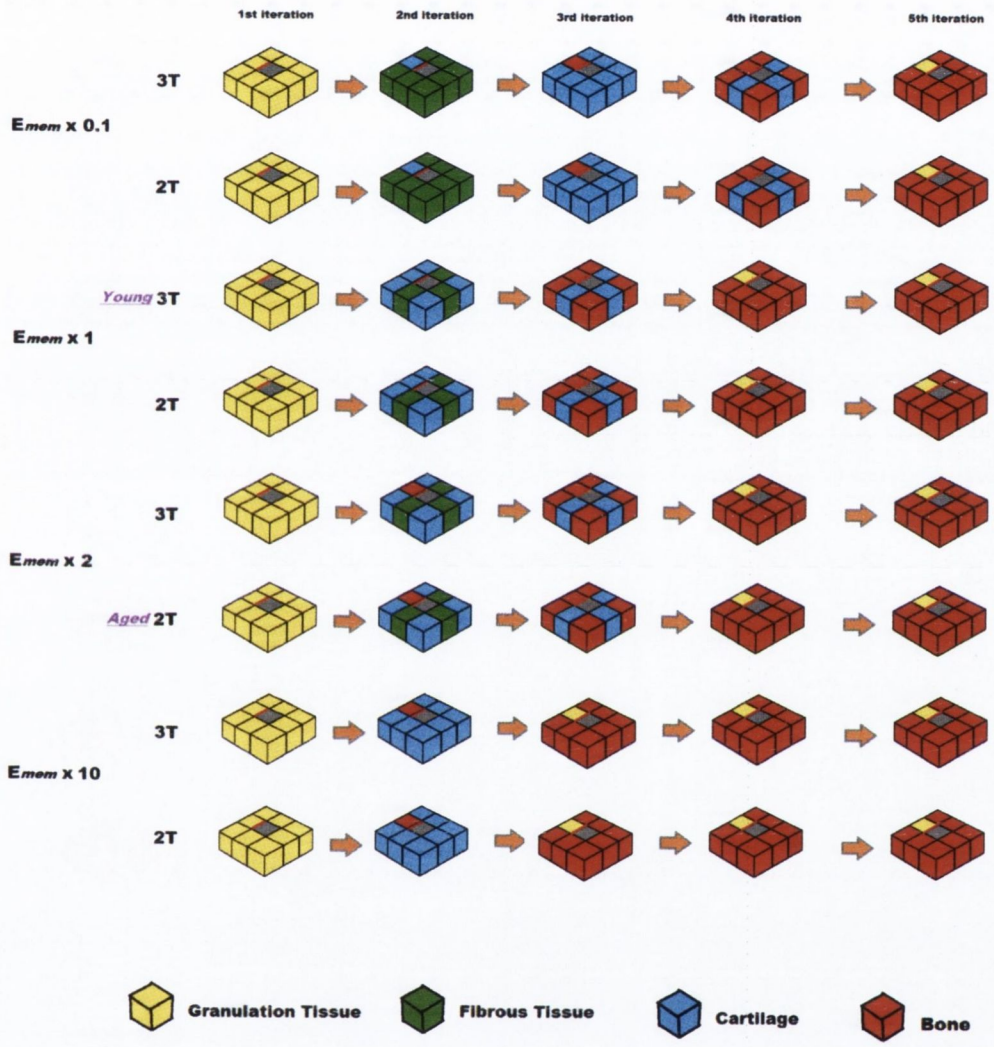


Figure B.2. Tissue differentiation patterns under force-control with a loading magnitude of 0.36 μN with one debonding surface.

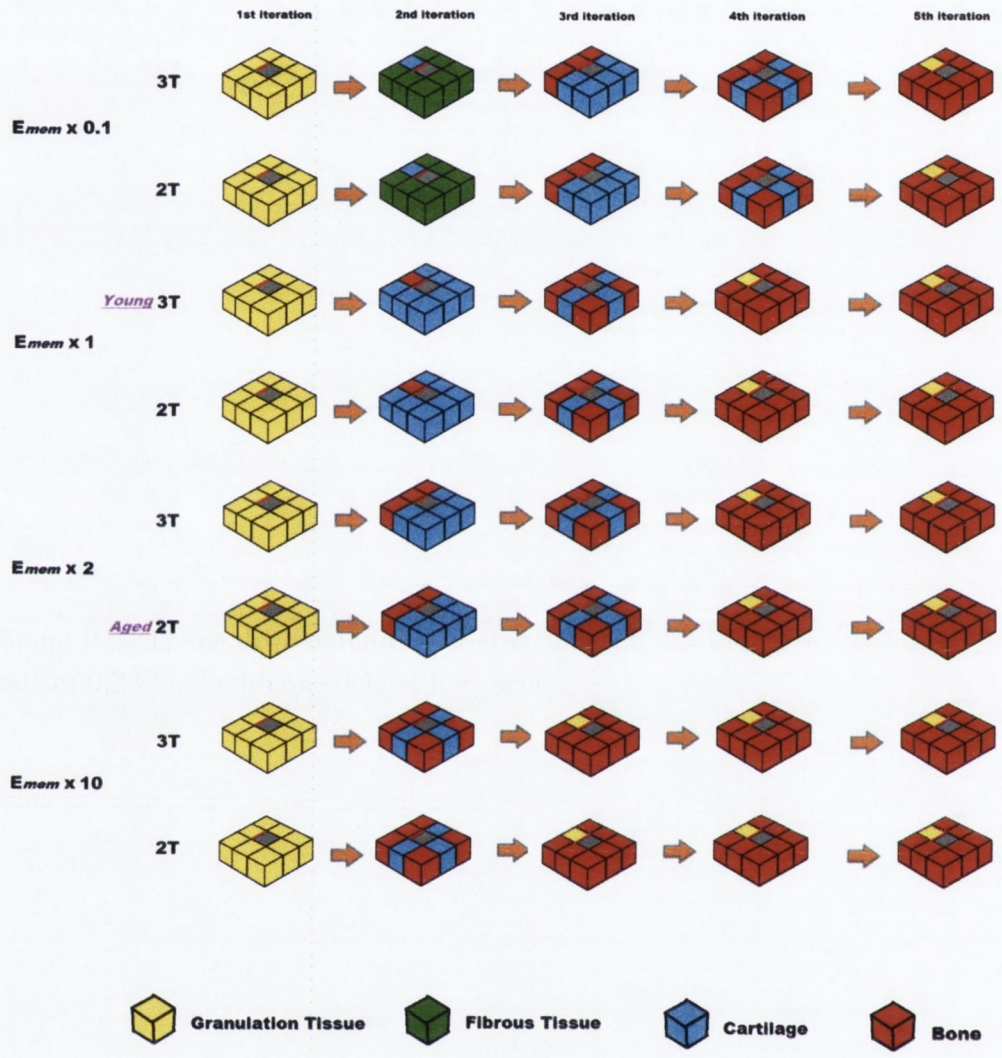


Figure B.3. Tissue differentiation patterns under force-control with a loading magnitude of 0.242 μN with one debonding surface.

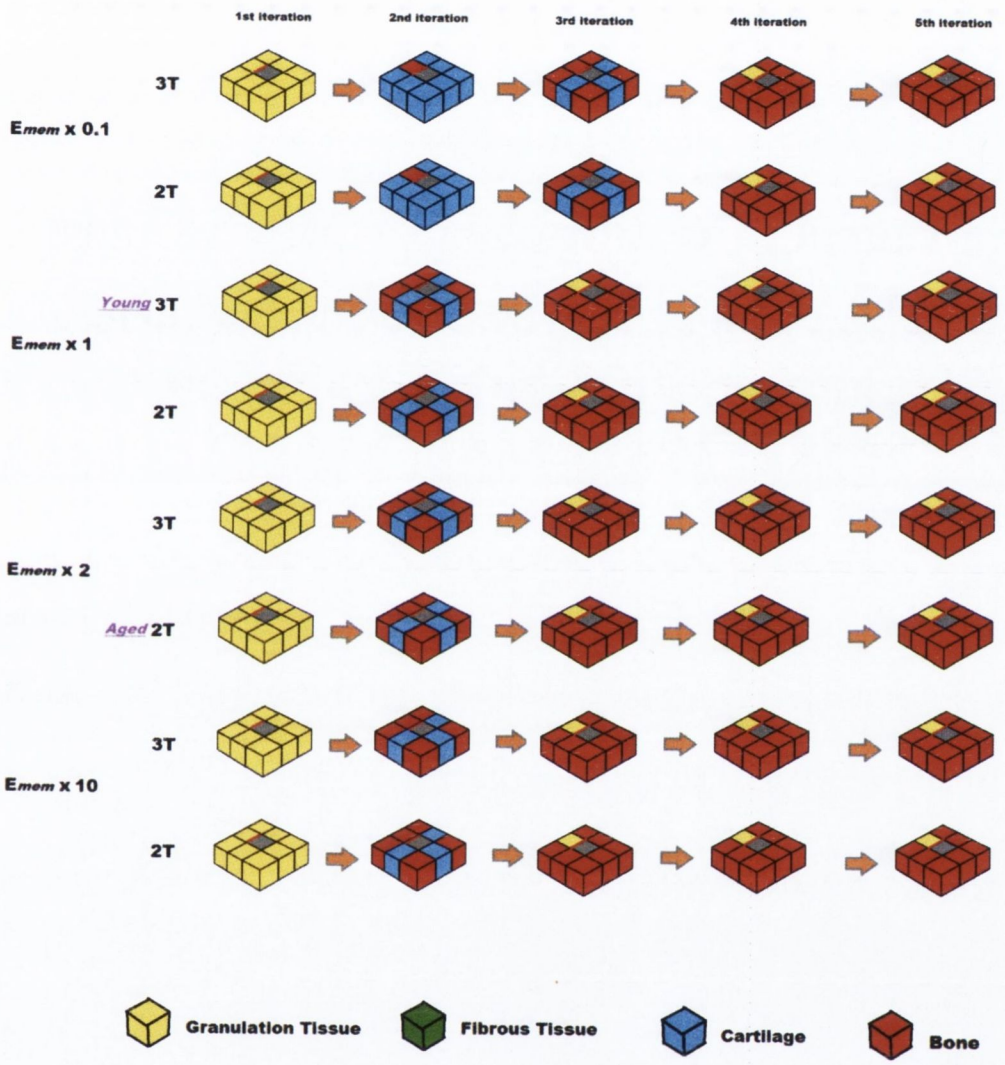


Figure B.4. Tissue differentiation patterns under force-control with a loading magnitude of 0.12 μN with one debonding surface.

Appendix C

The predicted tissue differentiation patterns under force-control with two opposite debonding surface (debonding case 2)

The stiffness of cell membrane was altered from 10% (x0.1) to 10 times (x10) of the original young cell. The highlighted two lines, i.e. E_{mem} x1 (3T) and E_{mem} x2 (2T) are the young and aged cells, respectively.

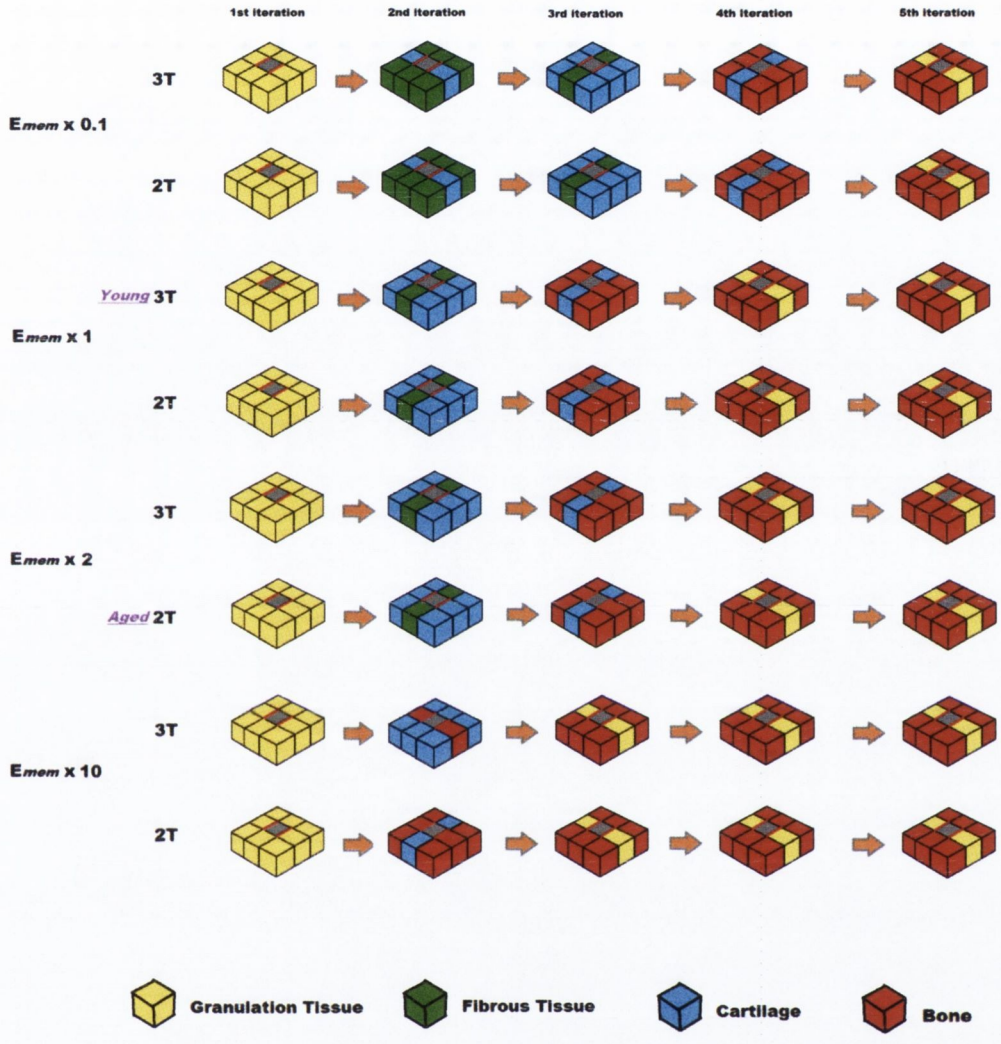


Figure C.1. Tissue differentiation patterns under force-control with a loading magnitude of 0.48 μN with two opposite debonding surfaces.

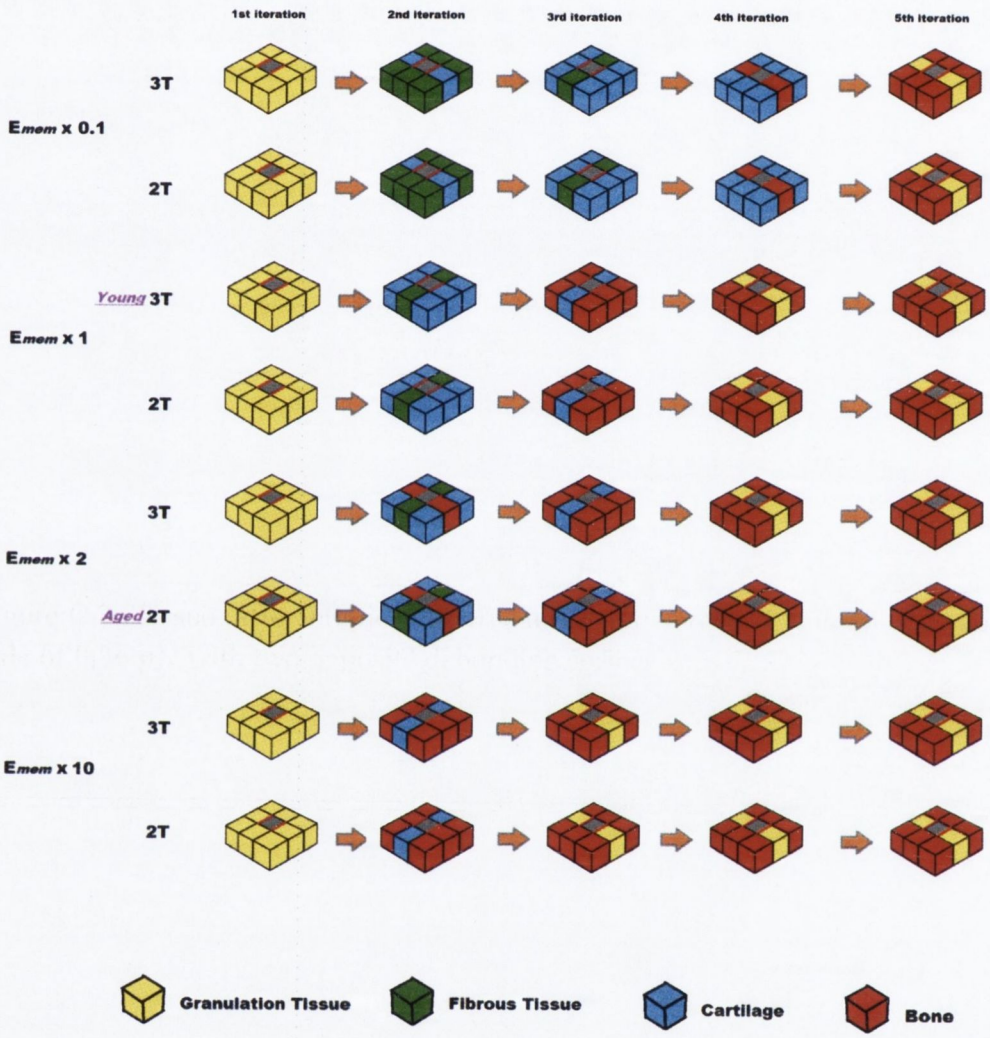


Figure C.2. Tissue differentiation patterns under force-control with a loading magnitude of 0.36 μN with two opposite debonding surfaces.

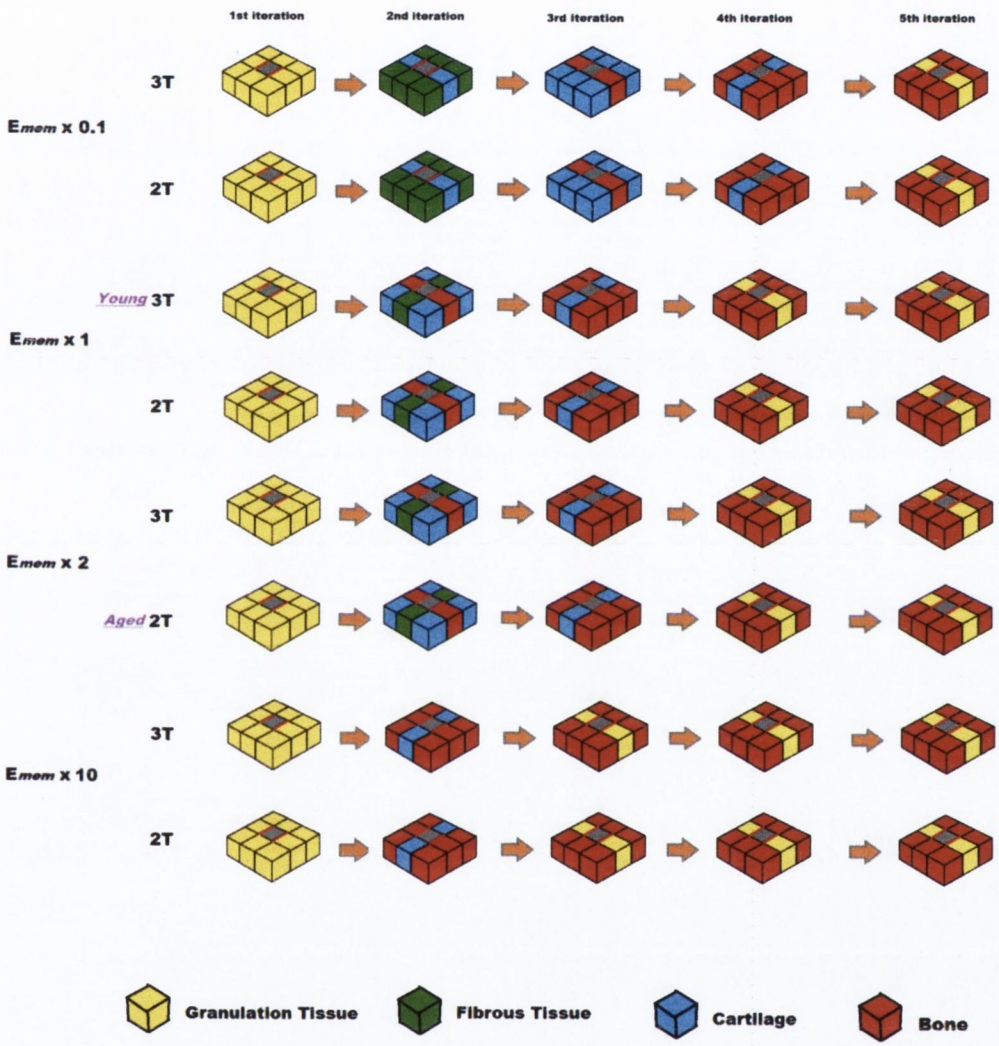


Figure C.3. Tissue differentiation patterns under force-control with a loading magnitude of 0.24 μN with two opposite debonding surfaces.

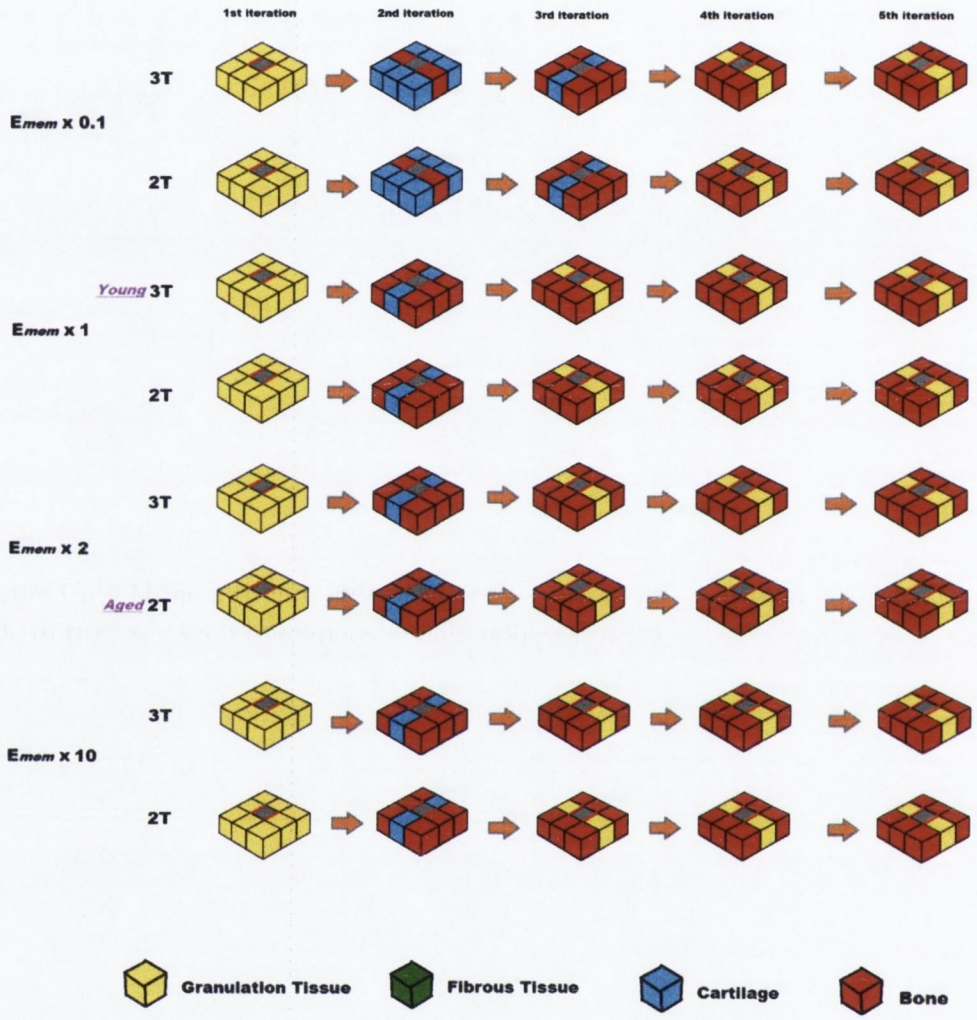


Figure C.4. Tissue differentiation patterns under force-control with a loading magnitude of 0.12 μN with two opposite debonding surfaces.

Appendix D

The predicted tissue differentiation patterns under force-control with two neighbouring debonding surfaces (debonding case 3)

The stiffness of cell membrane was altered from 10% (x0.1) to 10 times (x10) of the original young cell. The highlighted two lines, i.e. E_{mem} x1 (3T) and E_{mem} x2 (2T) are the young and aged cells, respectively.

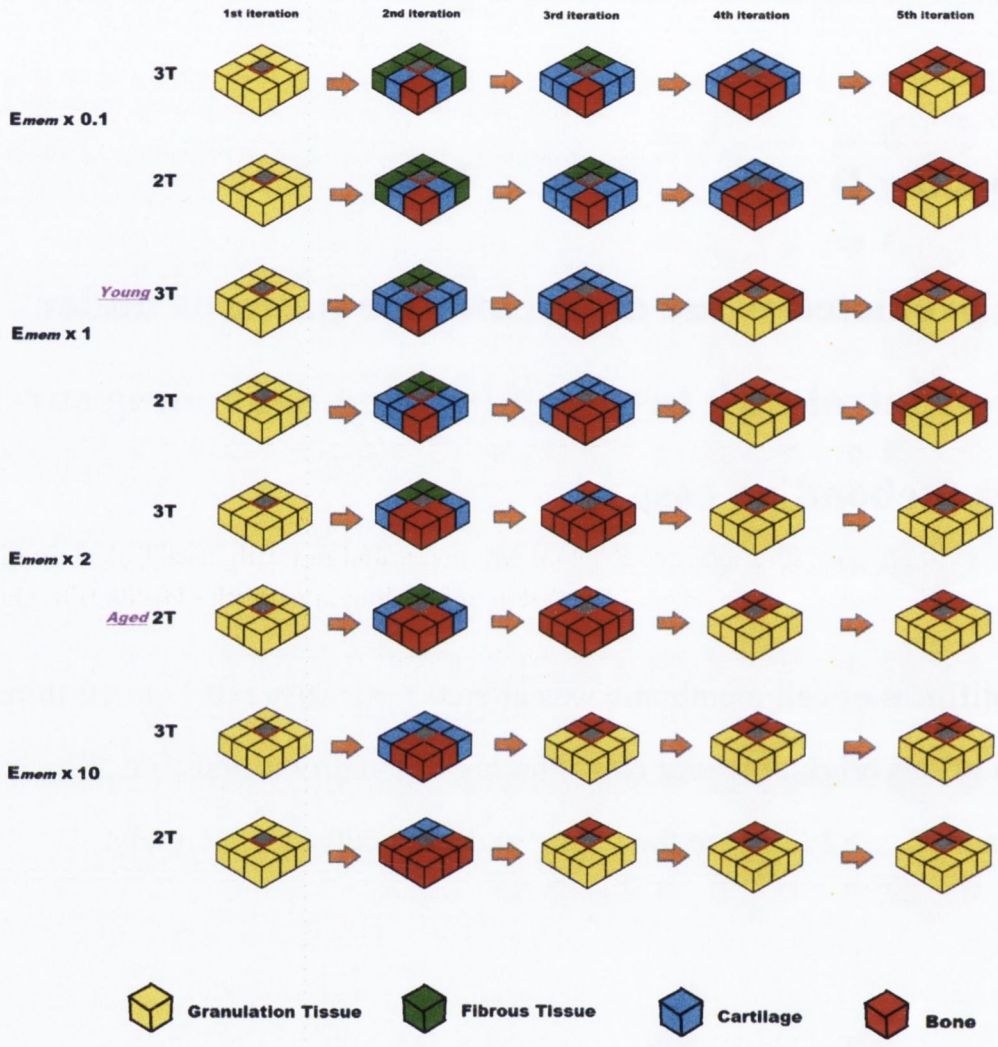


Figure D.1. Tissue differentiation patterns under force-control with a loading magnitude of 0.48 μN with two neighbouring debonding surfaces.

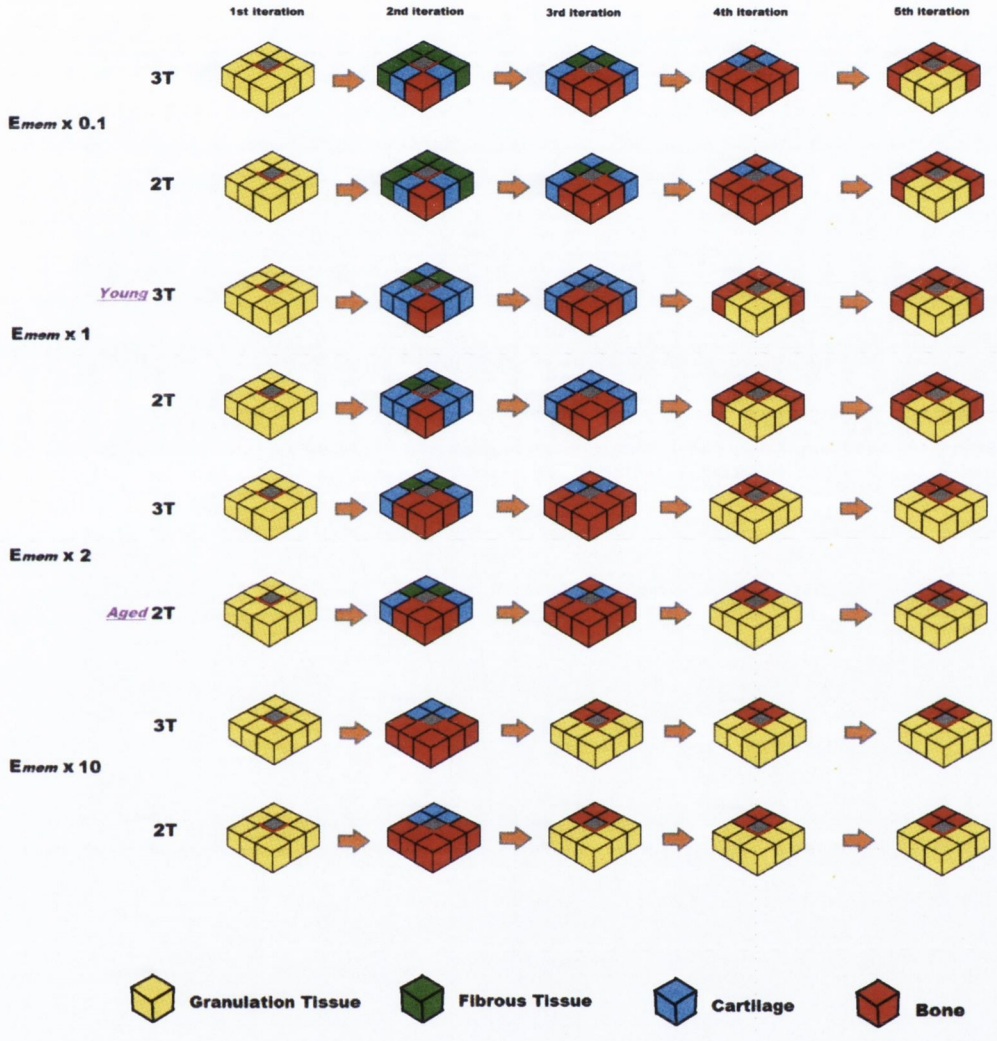


Figure D.2. Tissue differentiation patterns under force-control with a loading magnitude of 0.36 μN with two neighbouring debonding surfaces.

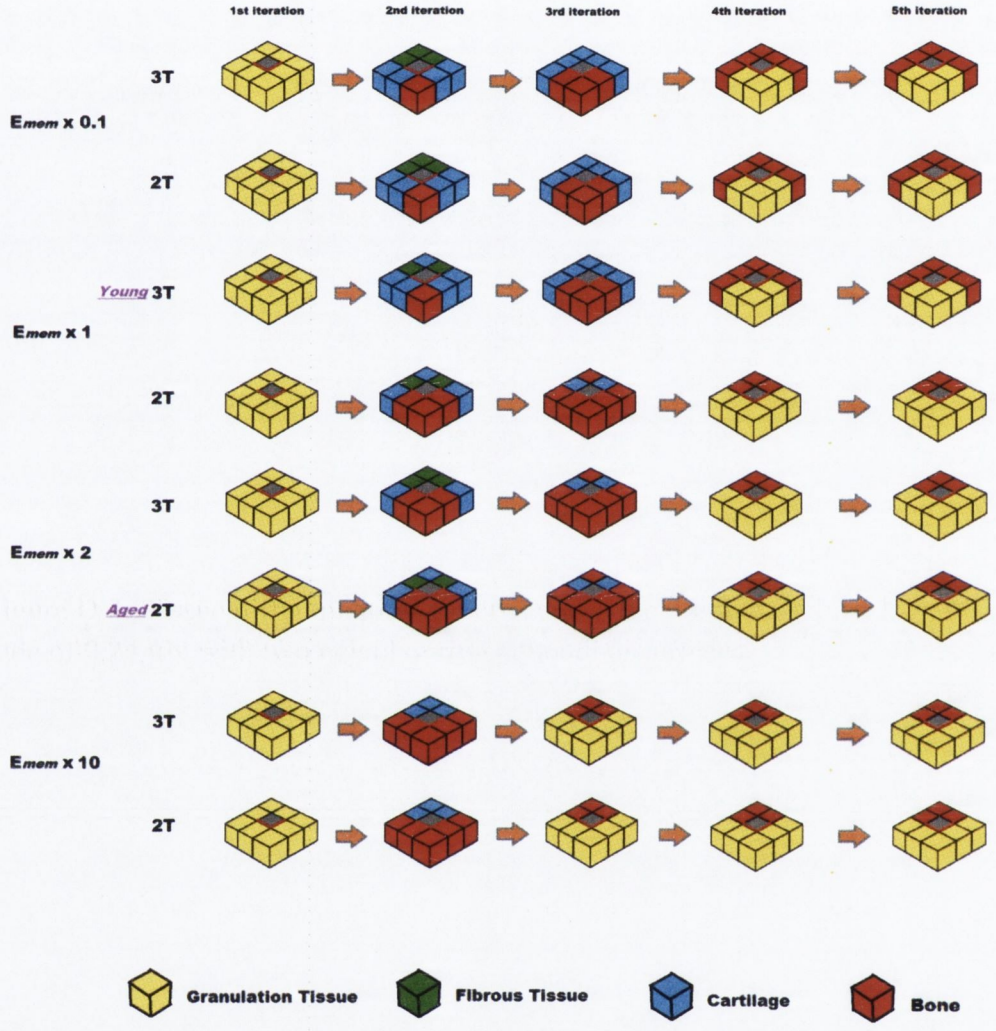


Figure D.3. Tissue differentiation patterns under force-control with a loading magnitude of 0.24 μN with two neighbouring debonding surfaces.

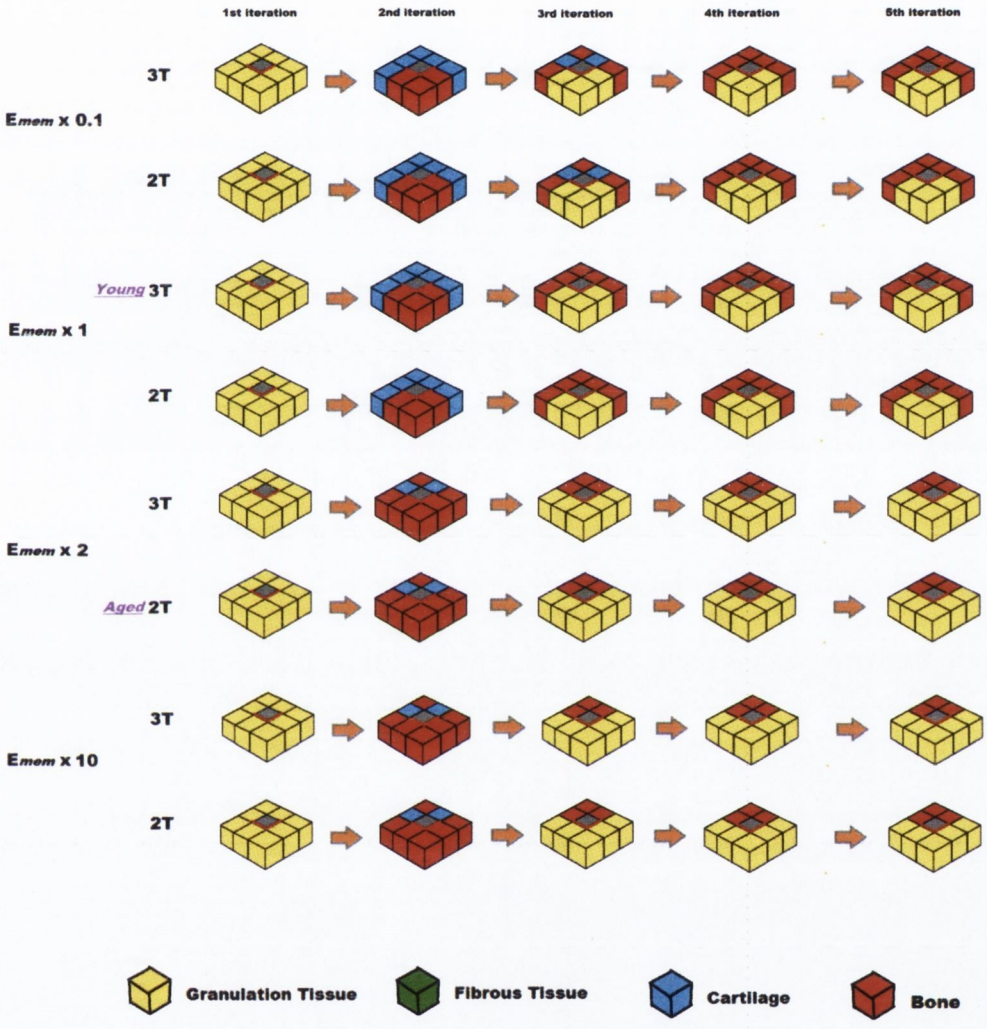


Figure D.4. Tissue differentiation patterns under force-control with a loading magnitude of 0.12 μN with two neighbouring debonding surfaces.

Appendix E

The predicted tissue differentiation patterns under force-control with three debonding surfaces (debonding case 4)

The stiffness of cell membrane was altered from 10% (x0.1) to 10 times (x10) of the original young cell. The highlighted two lines, i.e. E_{mem} x1 (3T) and E_{mem} x2 (2T) are the young and aged cells, respectively.

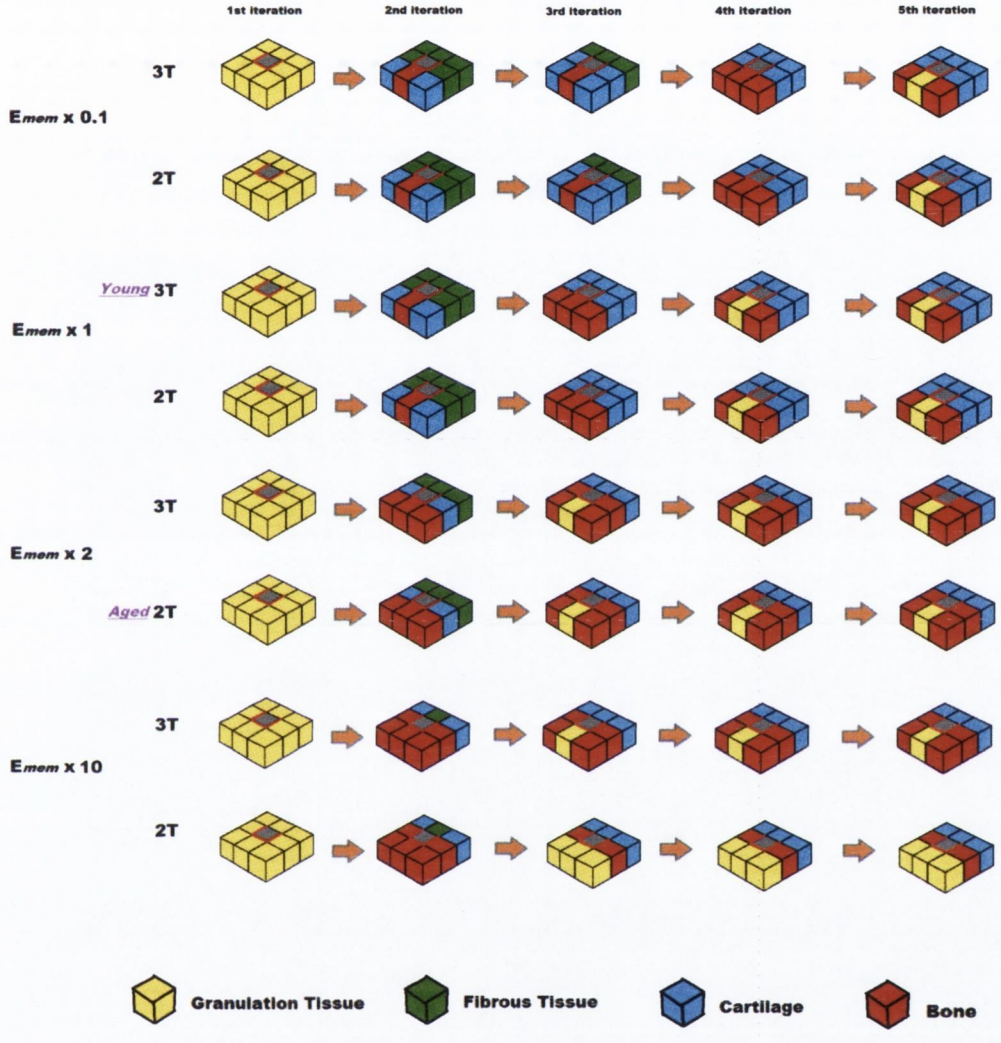


Figure E.1. Tissue differentiation patterns under force-control with a loading magnitude of 0.48 μN with three debonding surfaces.

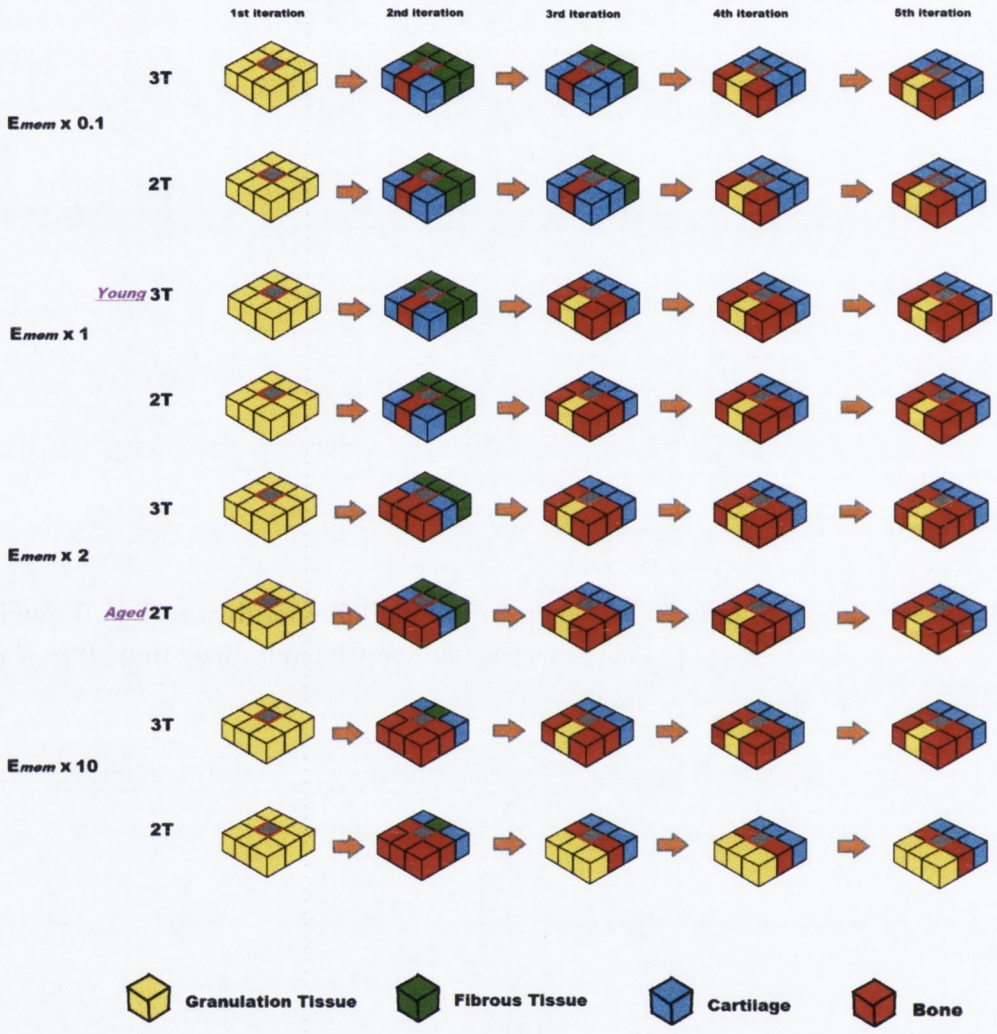


Figure E.2. Tissue differentiation patterns under force-control with a loading magnitude of 0.36 μN with three debonding surfaces.

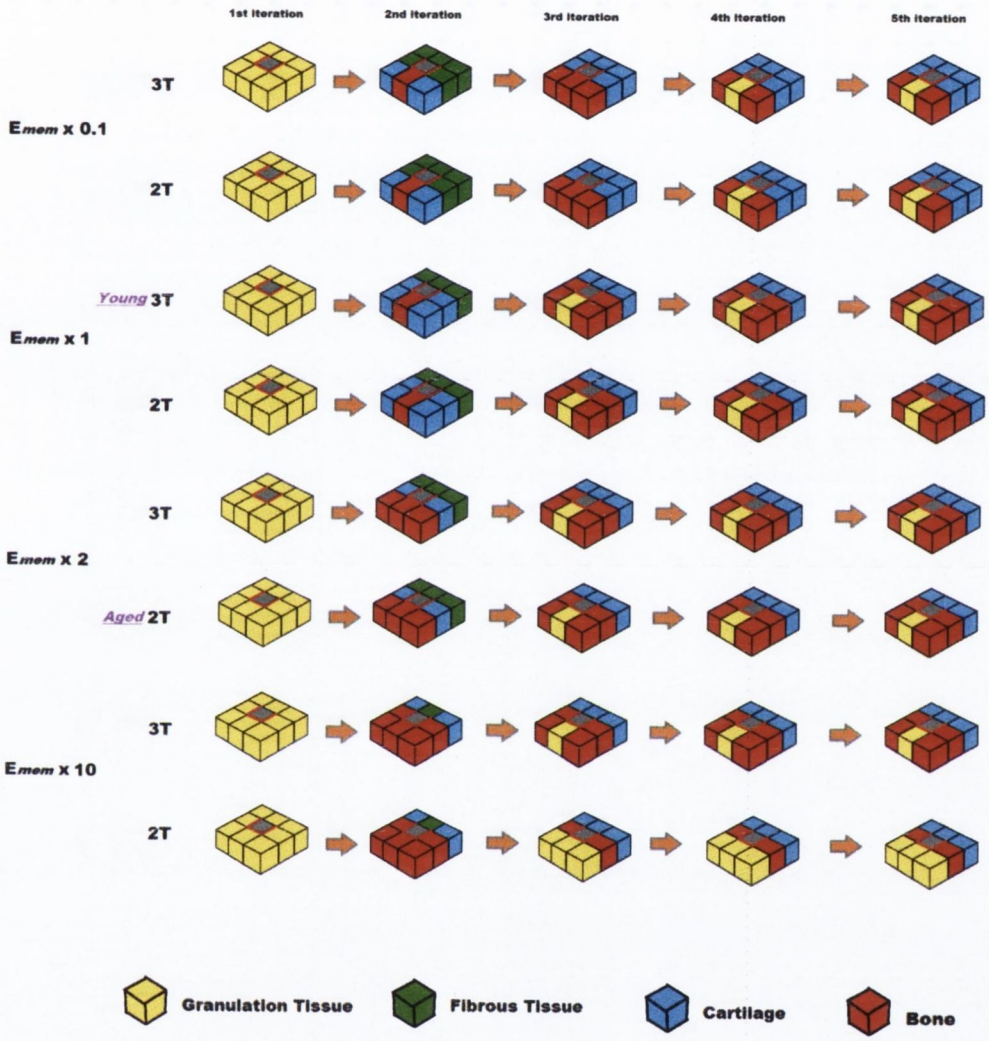


Figure E.3. Tissue differentiation patterns under force-control with a loading magnitude of 0.24 μN with three debonding surfaces.

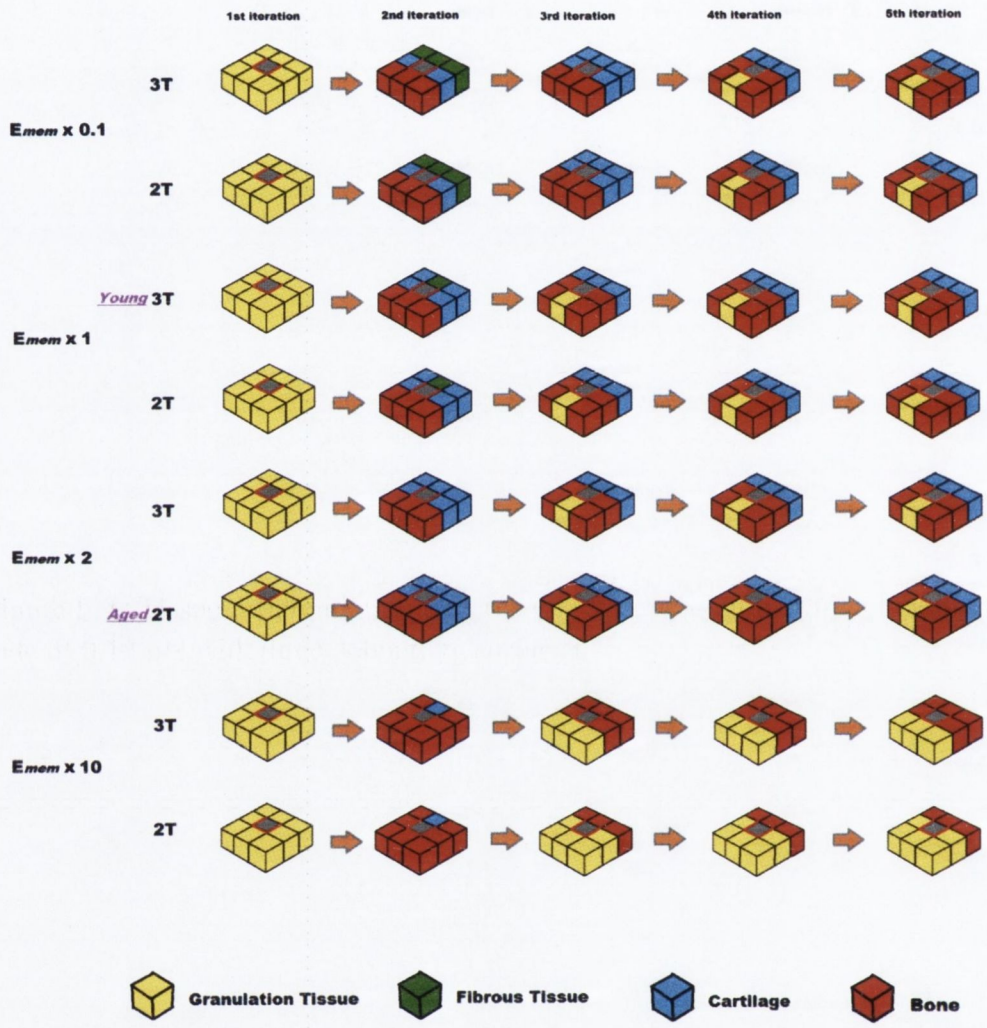


Figure E.4. Tissue differentiation patterns under force-control with a loading magnitude of 0.12 μN with three debonding surfaces.

Appendix F

The predicted tissue differentiation patterns under motion-control without debonding

The stiffness of cell membrane was altered from 10% (x0.1) to 10 times (x10) of the original young cell. The highlighted two lines, i.e. E_{mem} x1 (3T) and E_{mem} x2 (2T) are the young and aged cells, respectively.

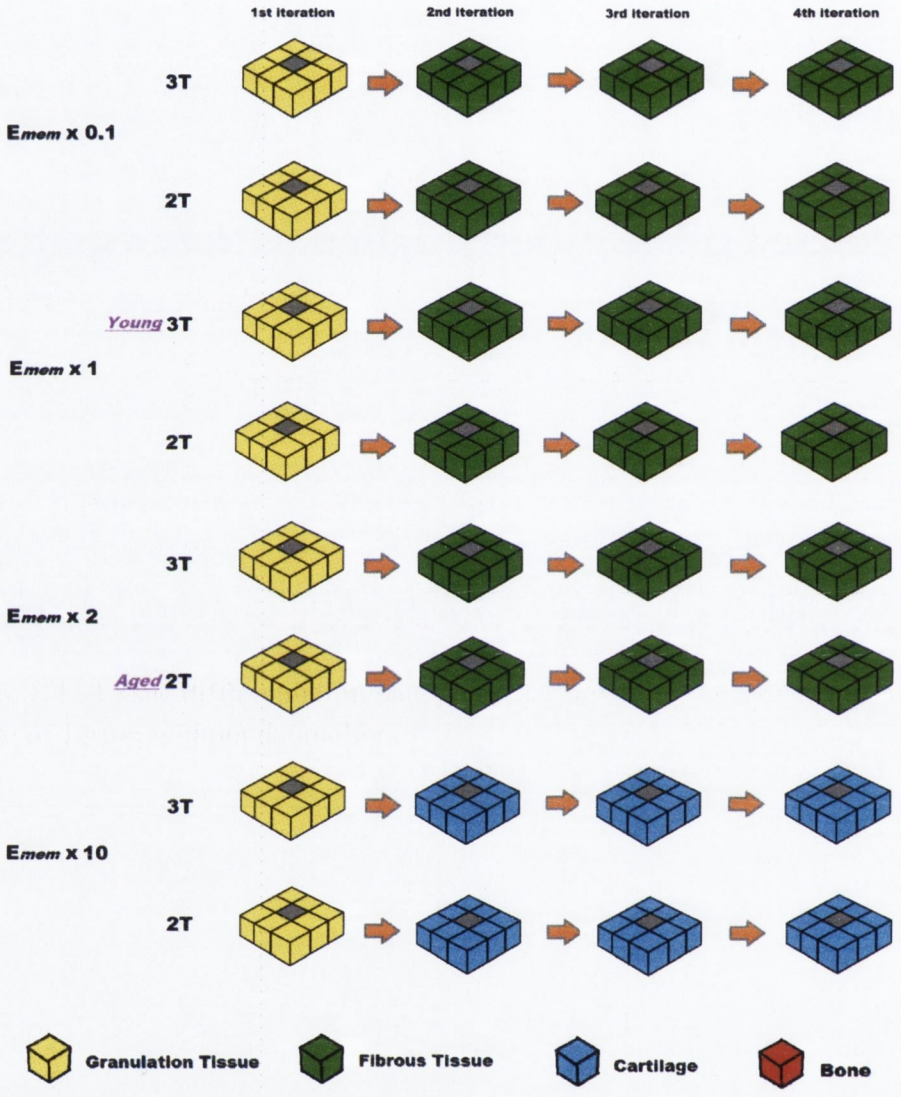


Figure F.1. Tissue differentiation patterns under motion-control with a loading magnitude of 12 μm without debonding.

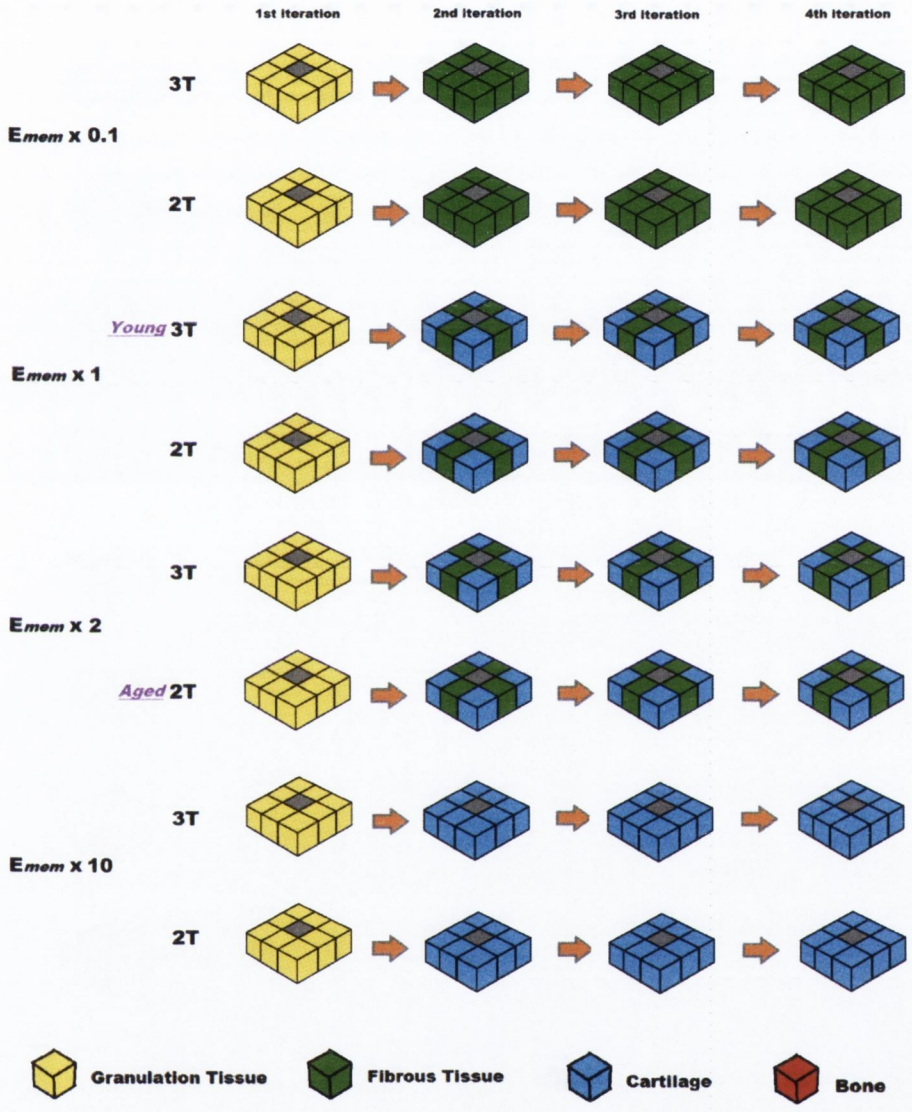


Figure F.2. Tissue differentiation patterns under motion-control with a loading magnitude of 9 μm without debonding.

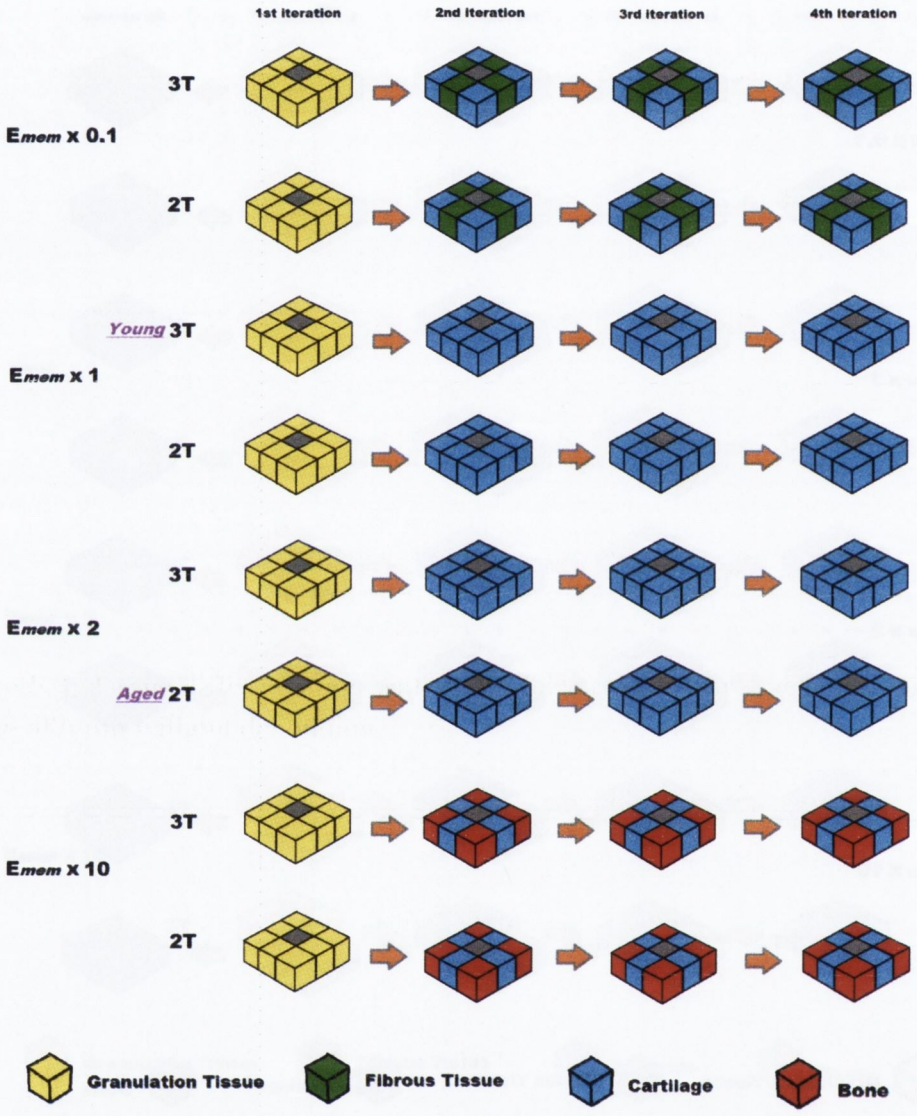


Figure F.3. Tissue differentiation patterns under motion-control with a loading magnitude of 6 μm without debonding.

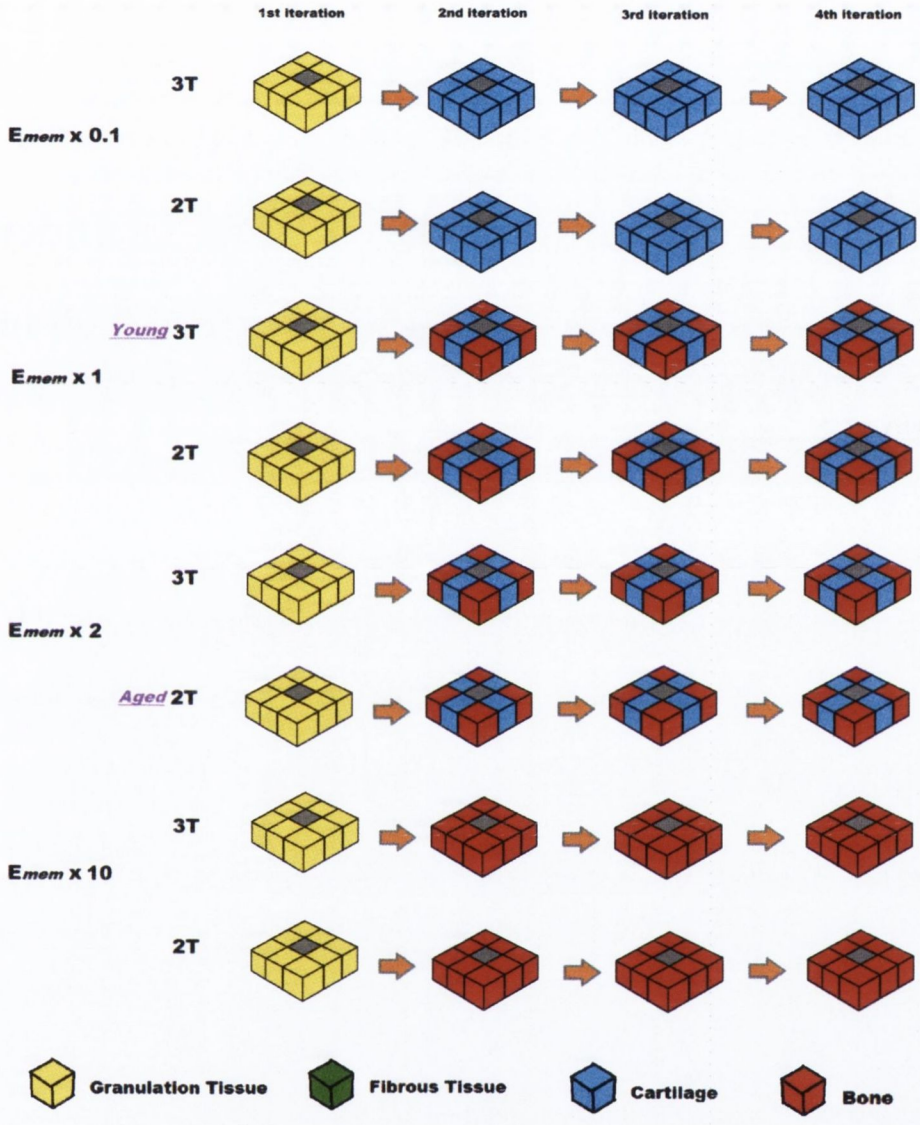


Figure F.4. Tissue differentiation patterns under motion-control with a loading magnitude of 3 μm without debonding.

Appendix G

The predicted tissue differentiation patterns under motion-control with one debonding surface (debonding case 1)

The stiffness of cell membrane was altered from 10% (x0.1) to 10 times (x10) of the original young cell. The highlighted two lines, i.e. E_{mem} x1 (3T) and E_{mem} x2 (2T) are the young and aged cells, respectively.

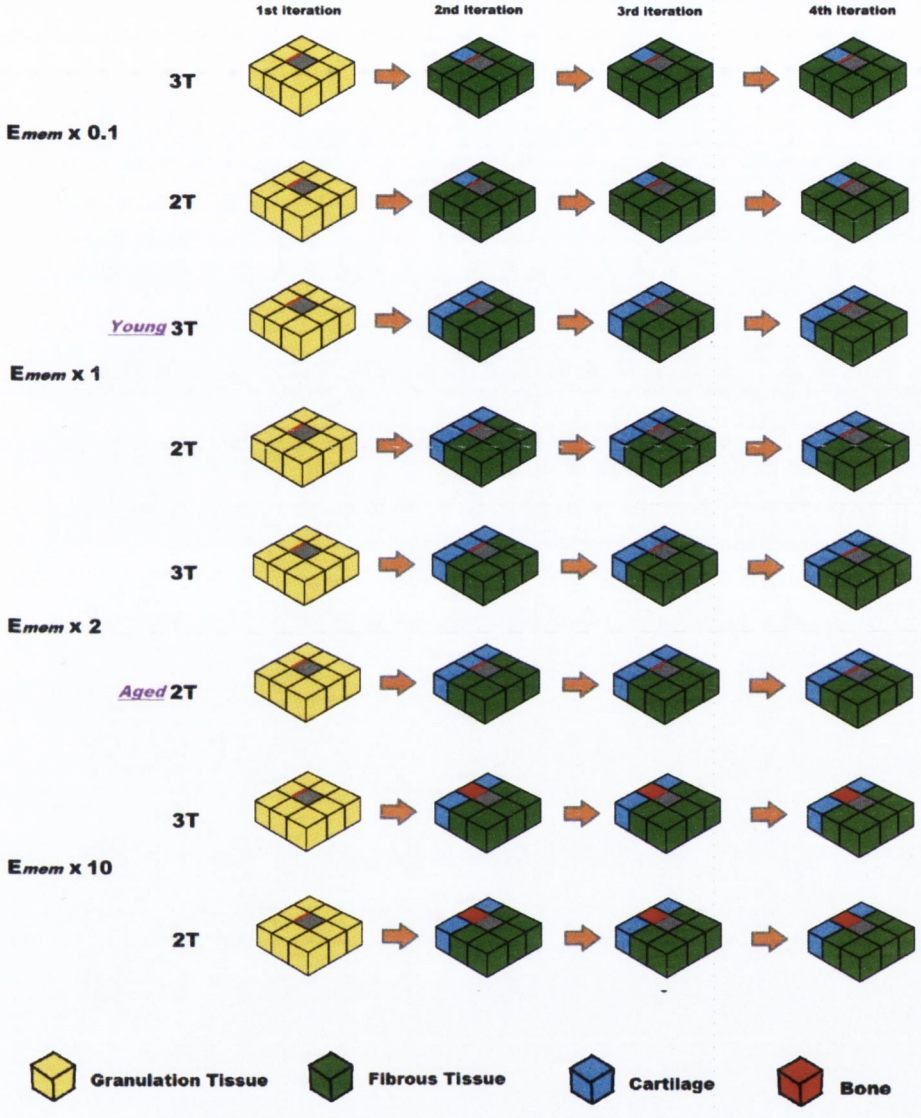


Figure G.1. Tissue differentiation patterns under motion-control with a loading magnitude of 12 μm with one debonding surface.

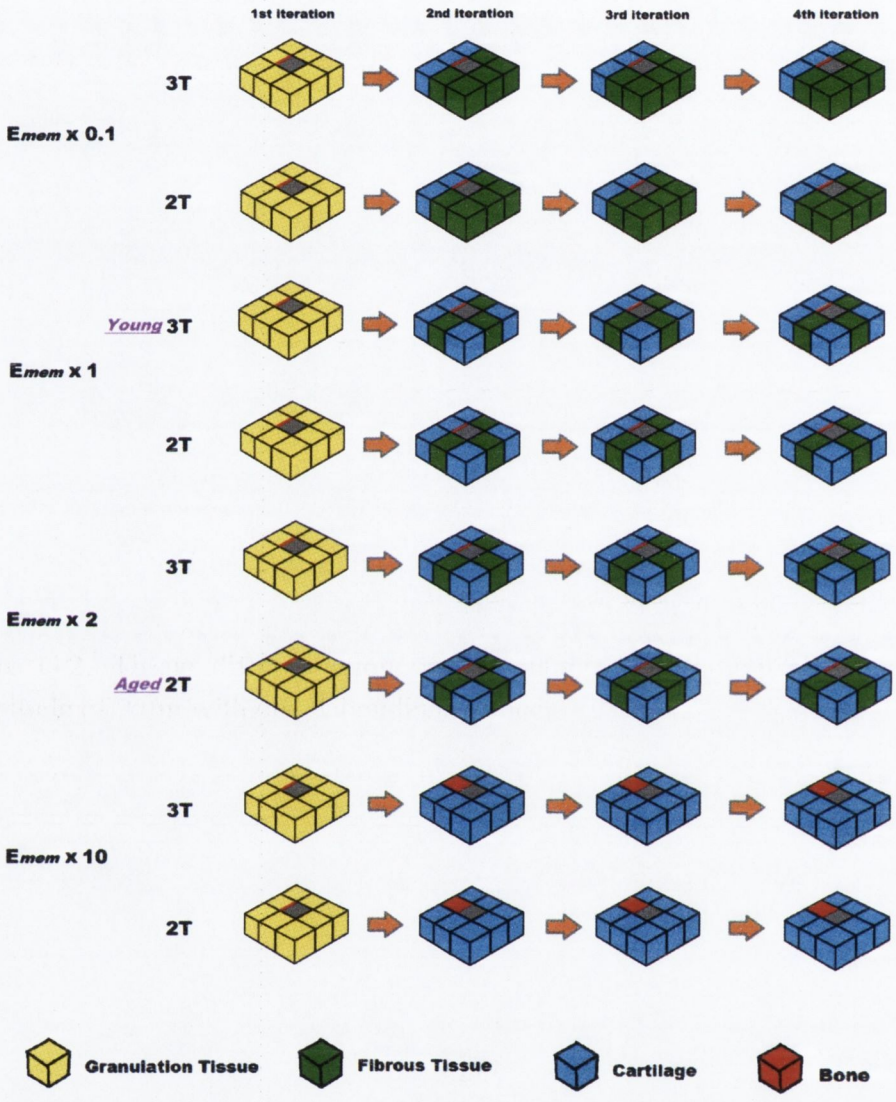


Figure G.2. Tissue differentiation patterns under motion-control with a loading magnitude of 9 μm with one debonding surface.

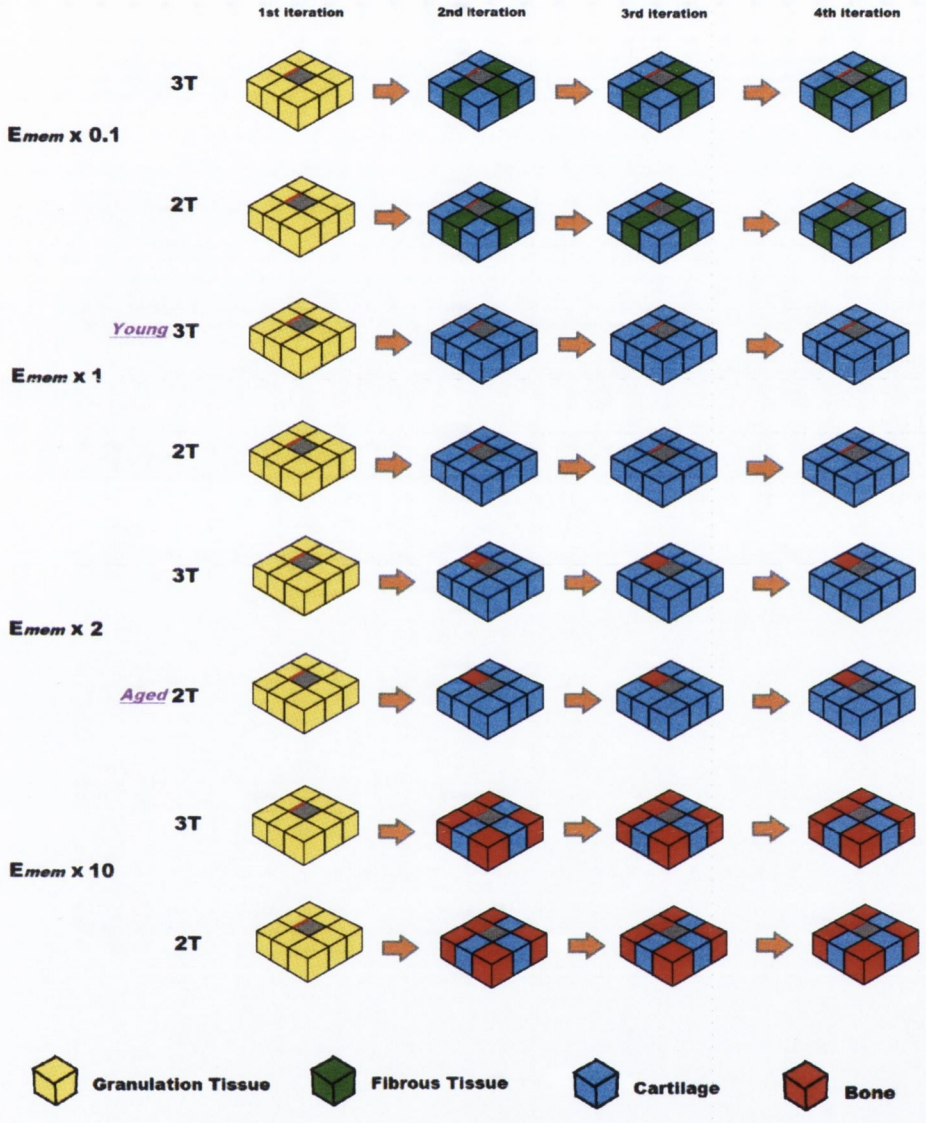


Figure G.3. Tissue differentiation patterns under motion-control with a loading magnitude of 6 μm with one debonding surface.

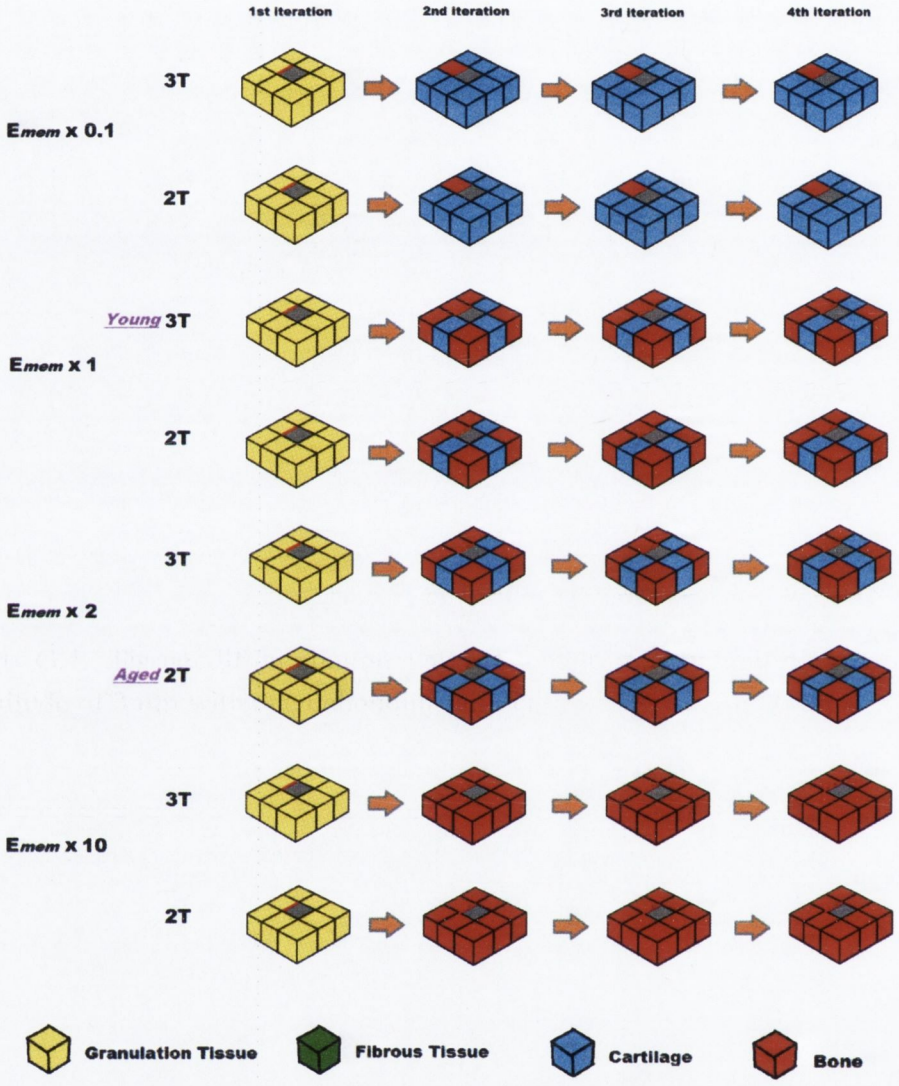


Figure G.4. Tissue differentiation patterns under motion-control with a loading magnitude of 3 μm with one debonding surface.

Appendix H

The predicted tissue differentiation patterns under motion-control with two opposite debonding surfaces (debonding case 2)

The stiffness of cell membrane was altered from 10% (x0.1) to 10 times (x10) of the original young cell. The highlighted two lines, i.e. E_{mem} x1 (3T) and E_{mem} x2 (2T) are the young and aged cells, respectively.

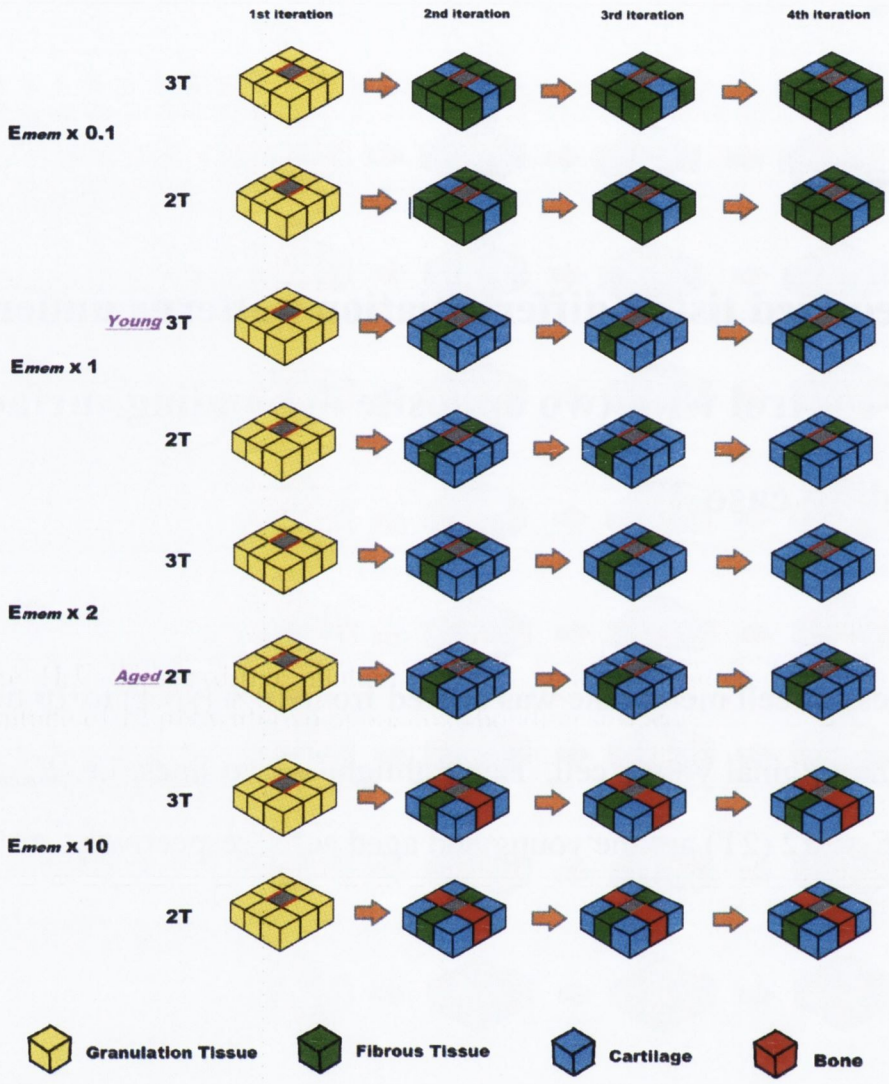


Figure H.1. Tissue differentiation patterns under motion-control with a loading magnitude of 12 μN with two opposite debonding surfaces.

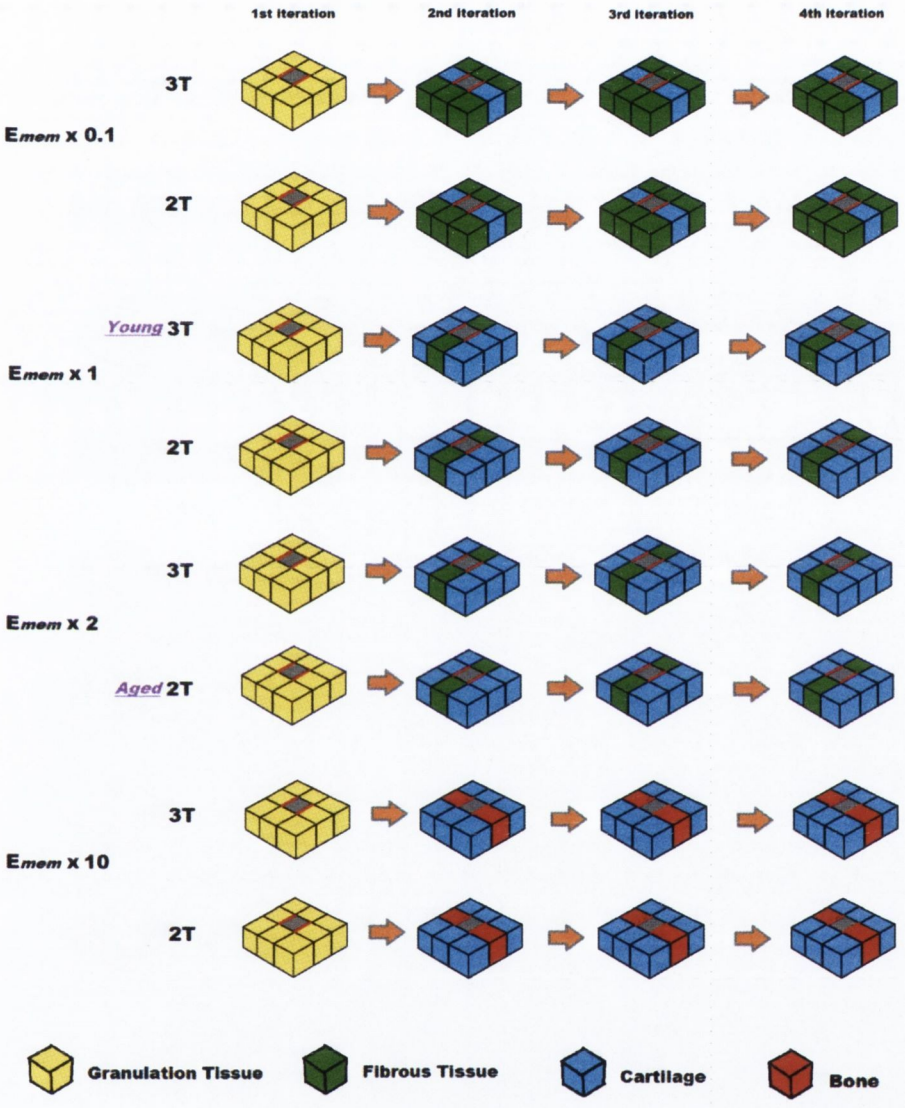


Figure H.2. Tissue differentiation patterns under motion-control with a loading magnitude of 9 μm with two opposite debonding surfaces.

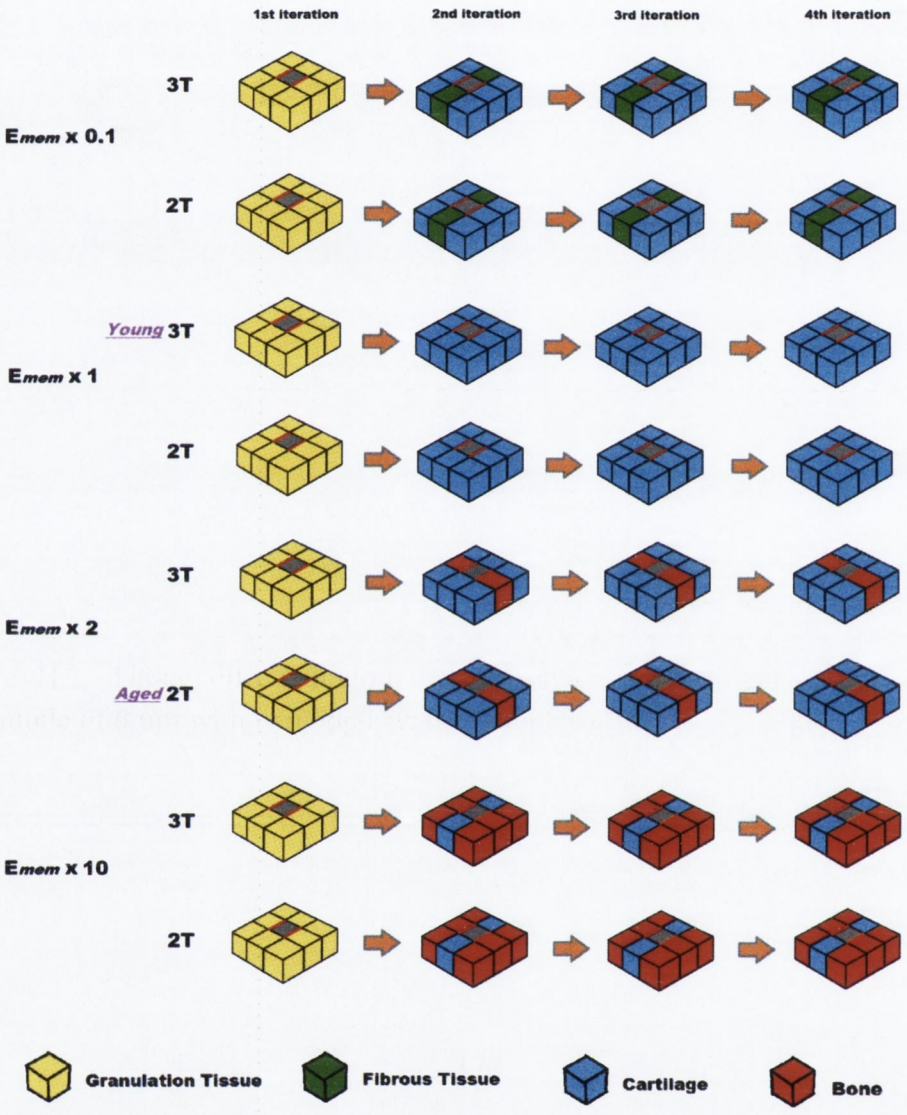


Figure H.3. Tissue differentiation patterns under motion-control with a loading magnitude of 6 μm with two opposite debonding surfaces.

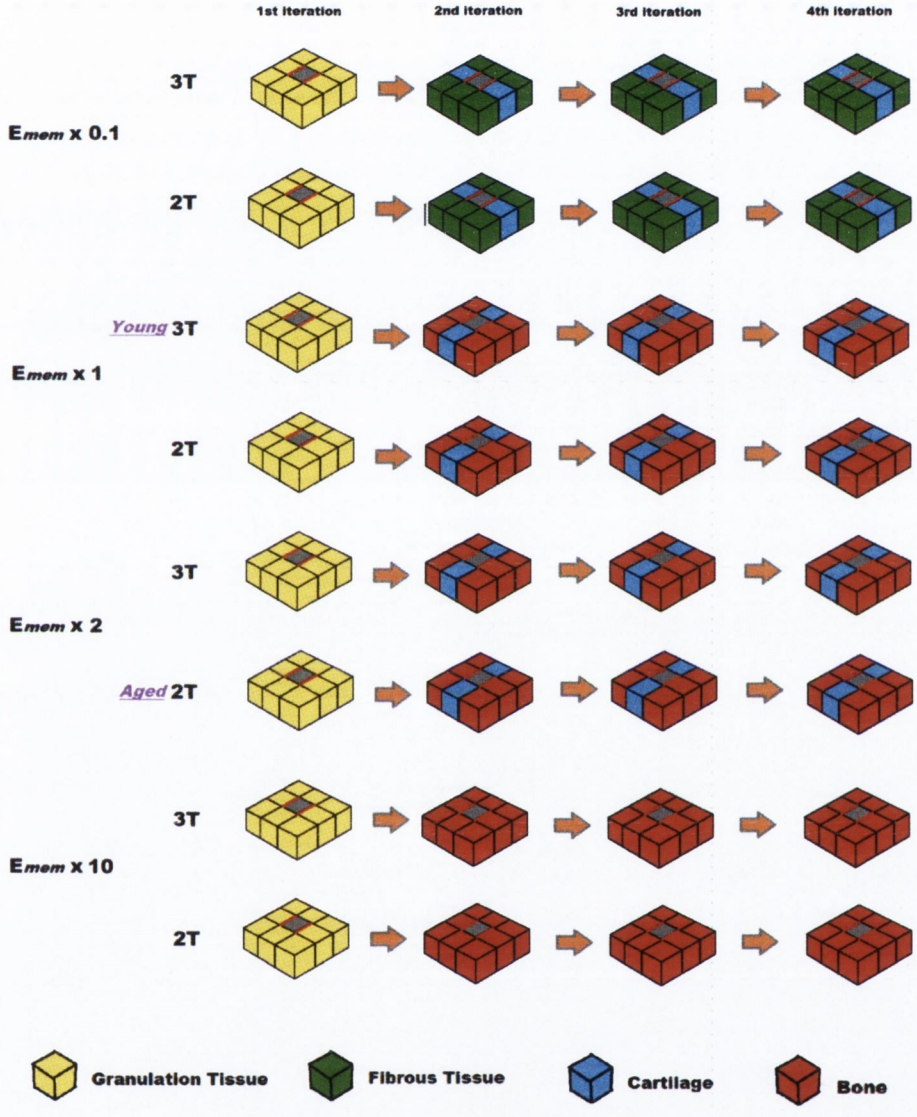


Figure H.4. Tissue differentiation patterns under motion-control with a loading magnitude of 3 μm with two opposite debonding surfaces.

Appendix I

The predicted tissue differentiation patterns under motion-control with two neighbouring debonding surfaces (debonding case 3)

The stiffness of cell membrane was altered from 10% (x0.1) to 10 times (x10) of the original young cell. The highlighted two lines, i.e. E_{mem} x1 (3T) and E_{mem} x2 (2T) are the young and aged cells, respectively.

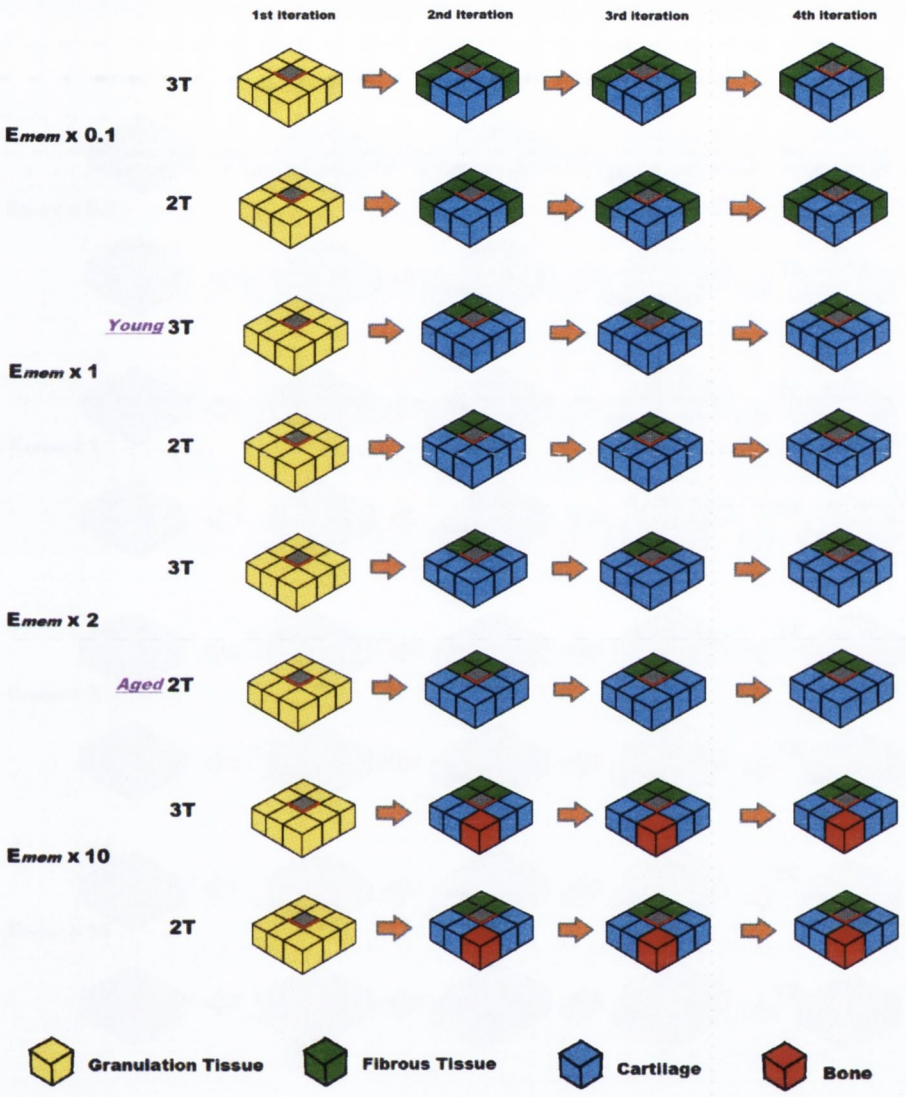


Figure I.1. Tissue differentiation patterns under motion-control with a loading magnitude of 12 μm with two neighbouring debonding surfaces.

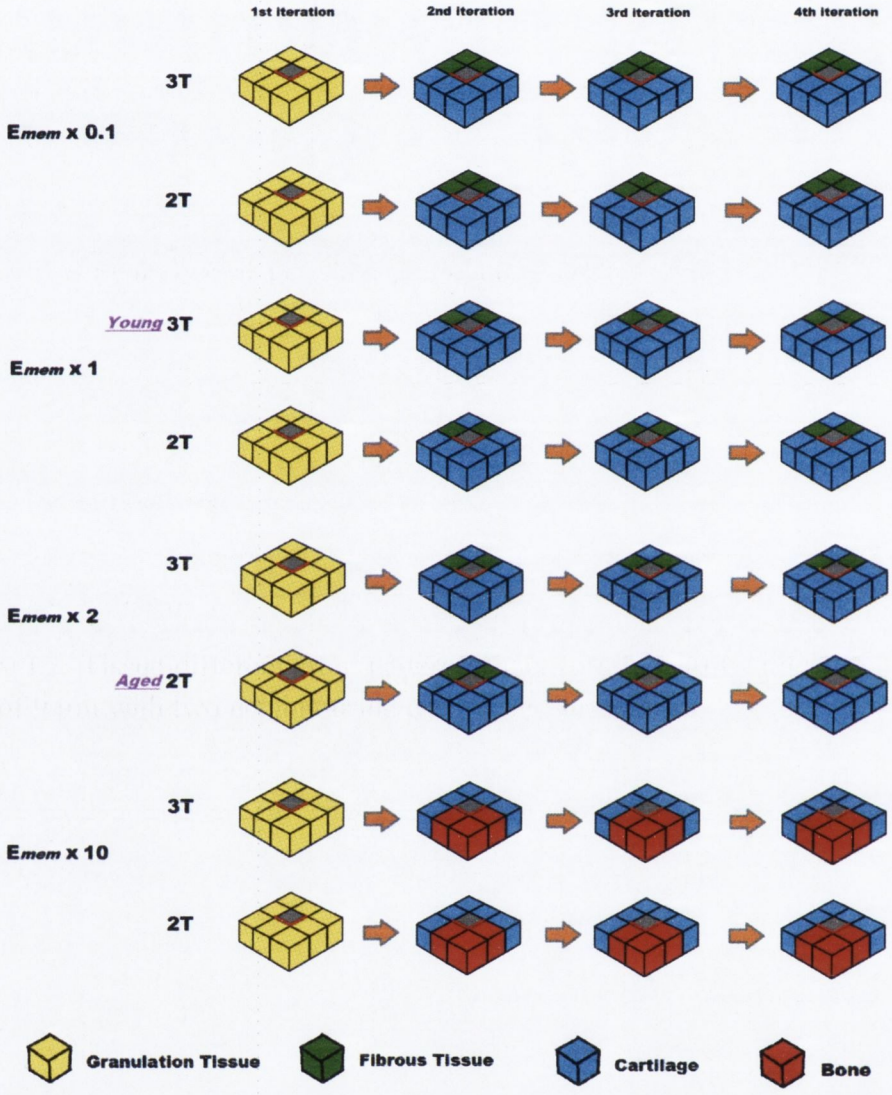


Figure I.2. Tissue differentiation patterns under force-control with a loading magnitude of 9 μm with two neighbouring debonding surfaces.

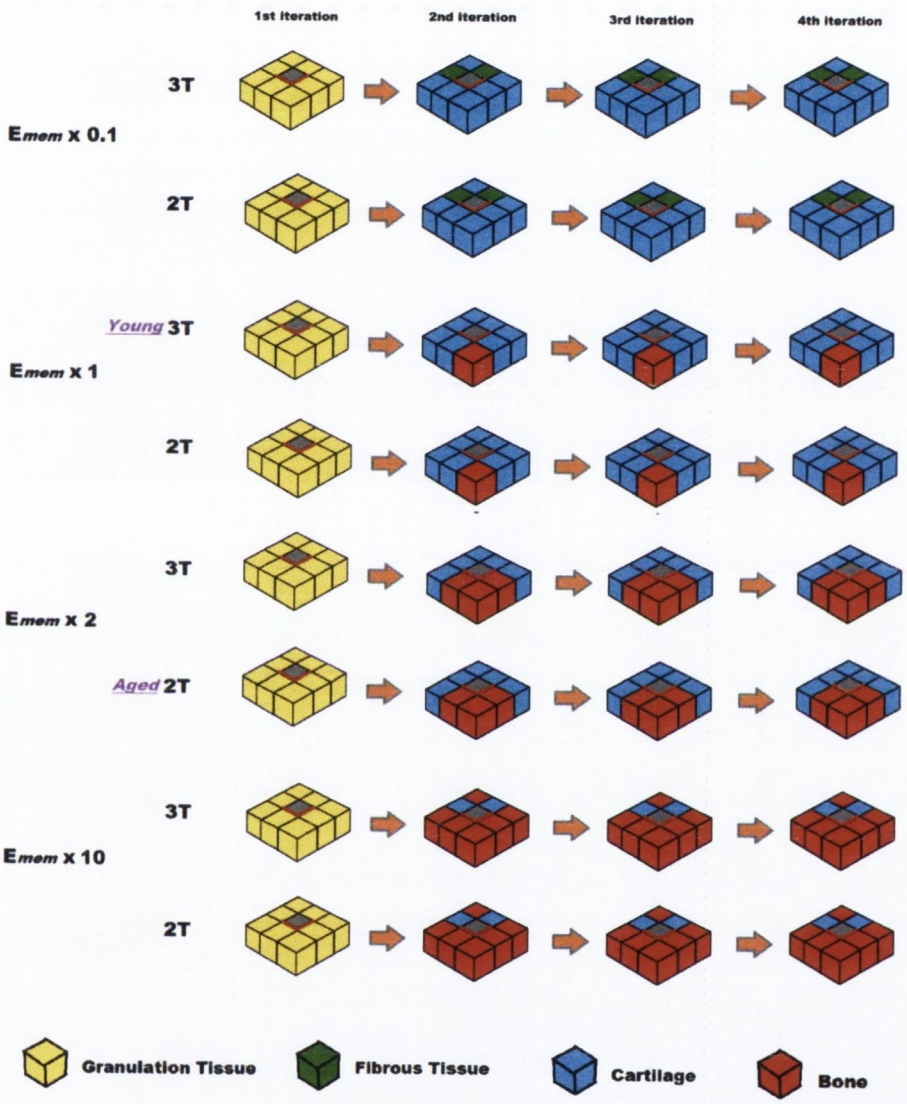


Figure I.3. Tissue differentiation patterns under motion-control with a loading magnitude of 6 μm with two neighbouring debonding surfaces.

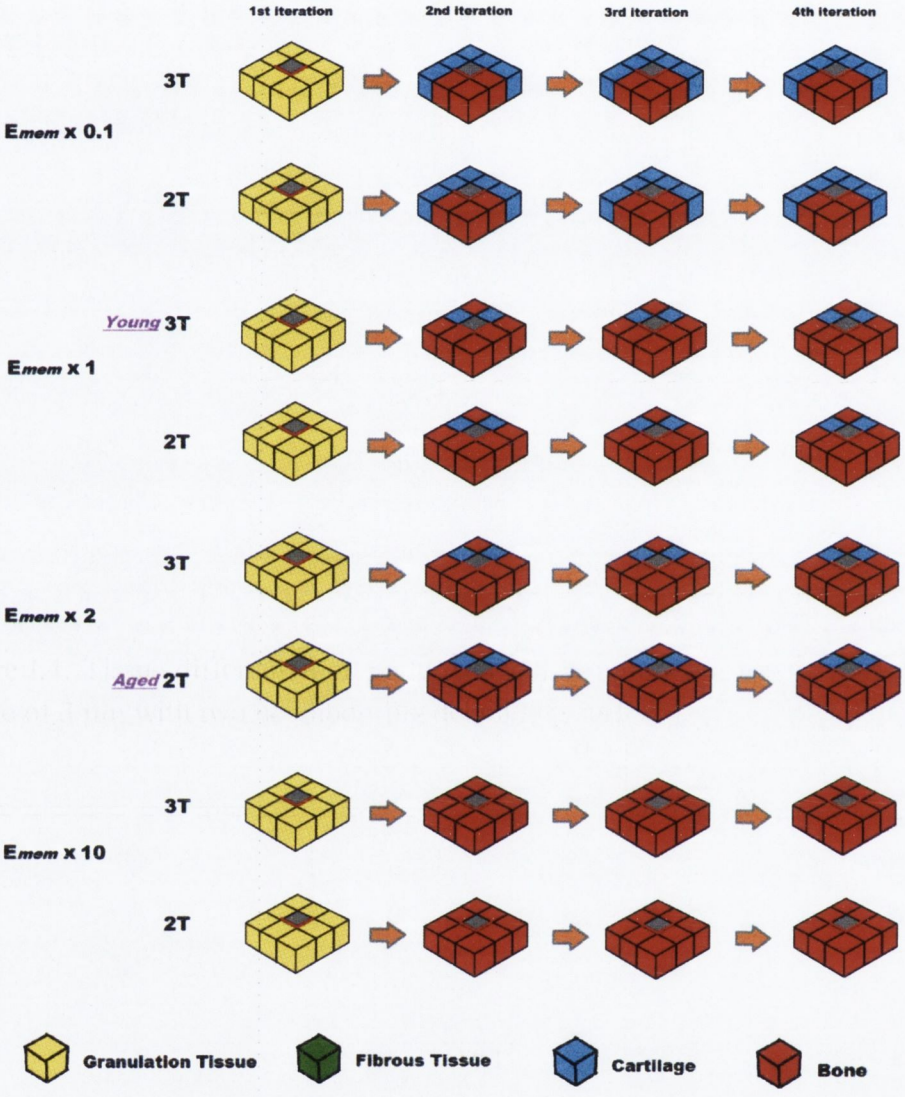


Figure I.4. Tissue differentiation patterns under motion-control with a loading magnitude of 3 μm with two neighbouring debonding surfaces.

Appendix J

The predicted tissue differentiation patterns under motion-control with three debonding surfaces (debonding case 4)

The stiffness of cell membrane was altered from 10% (x0.1) to 10 times (x10) of the original young cell. The highlighted two lines, i.e. E_{mem} x1 (3T) and E_{mem} x2 (2T) are the young and aged cells, respectively.

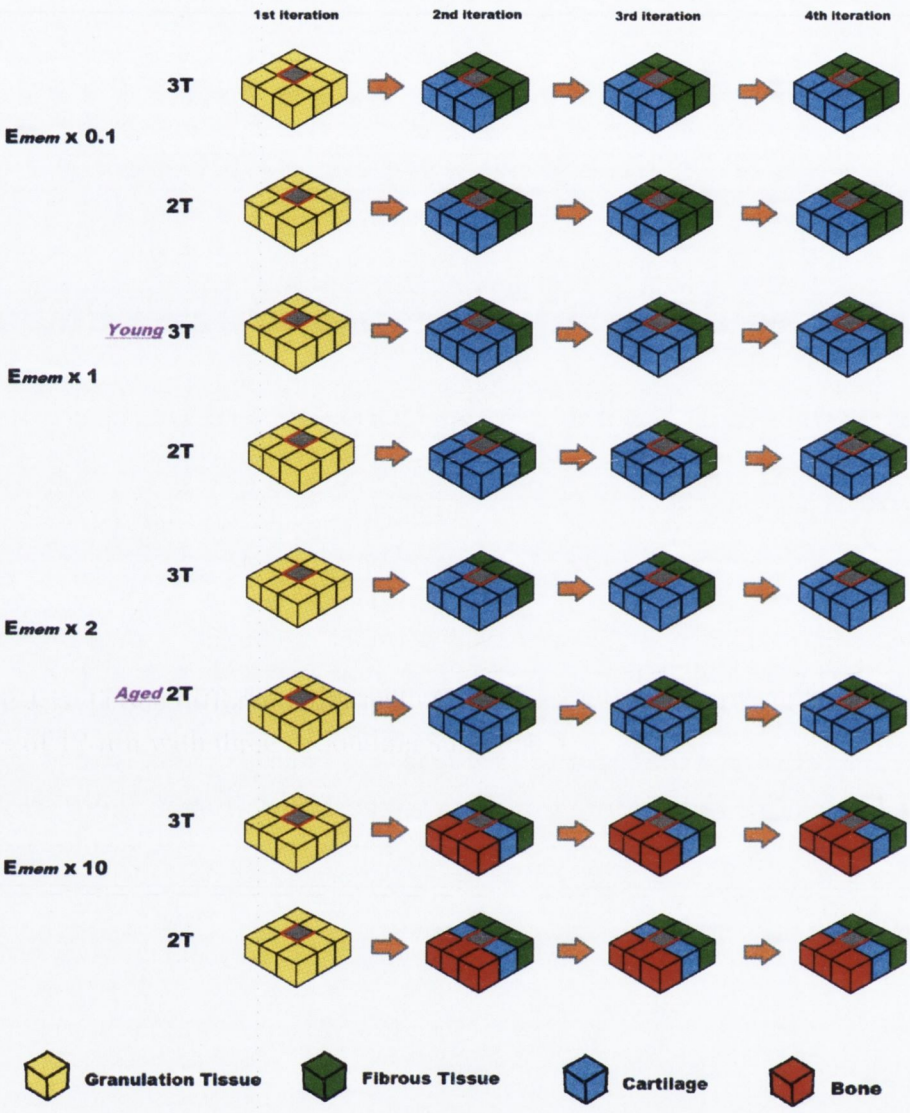


Figure J.1. Tissue differentiation patterns under motion-control with a loading magnitude of 12 μm with three debonding surfaces.

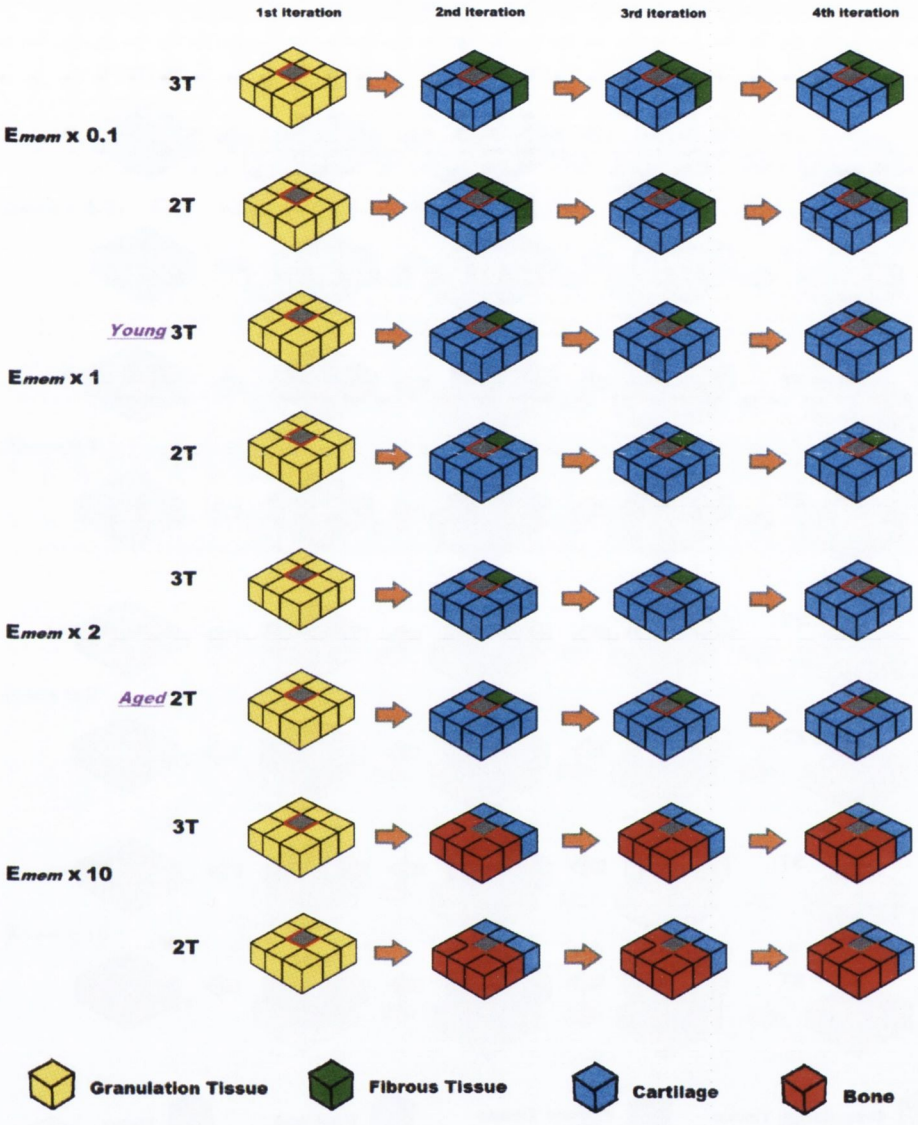


Figure J.2. Tissue differentiation patterns under motion-control with a loading magnitude of 9 μm with three debonding surfaces.

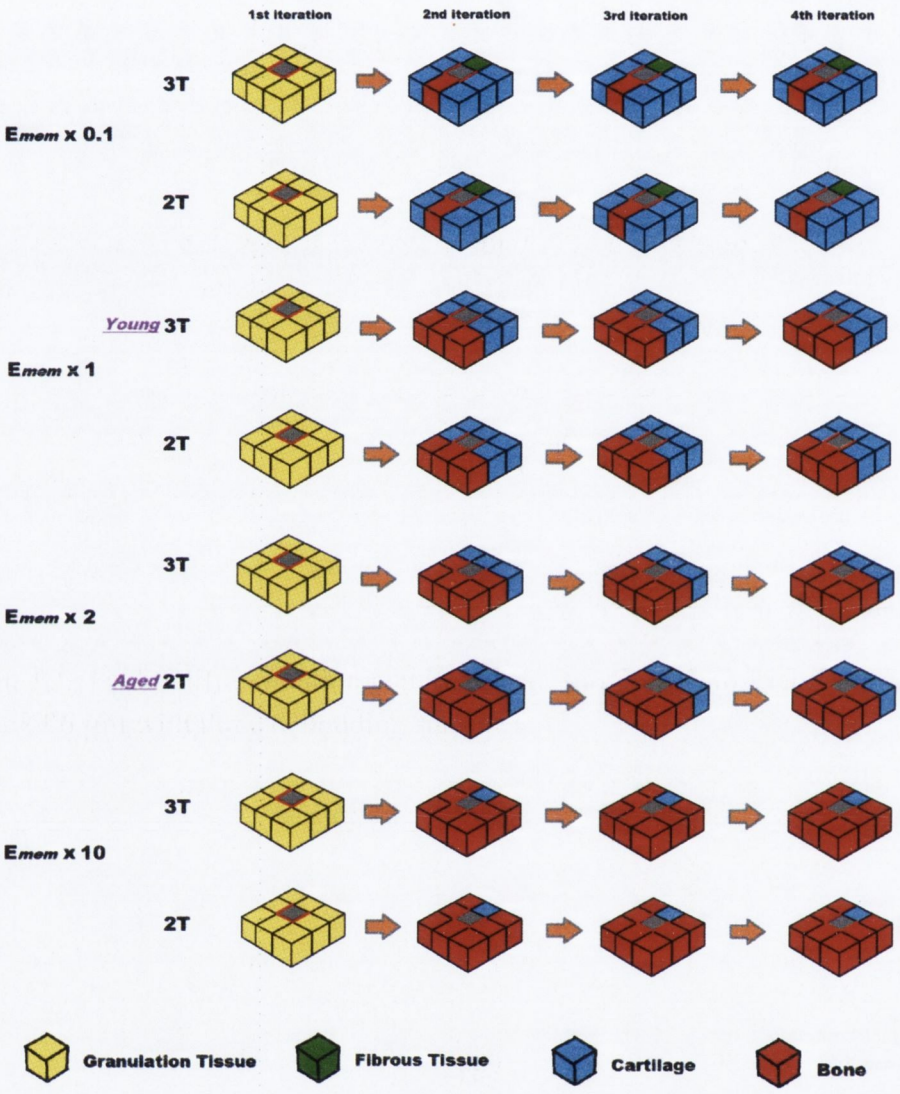


Figure J.3. Tissue differentiation patterns under motion-control with a loading magnitude of 6 μm with three debonding surfaces.

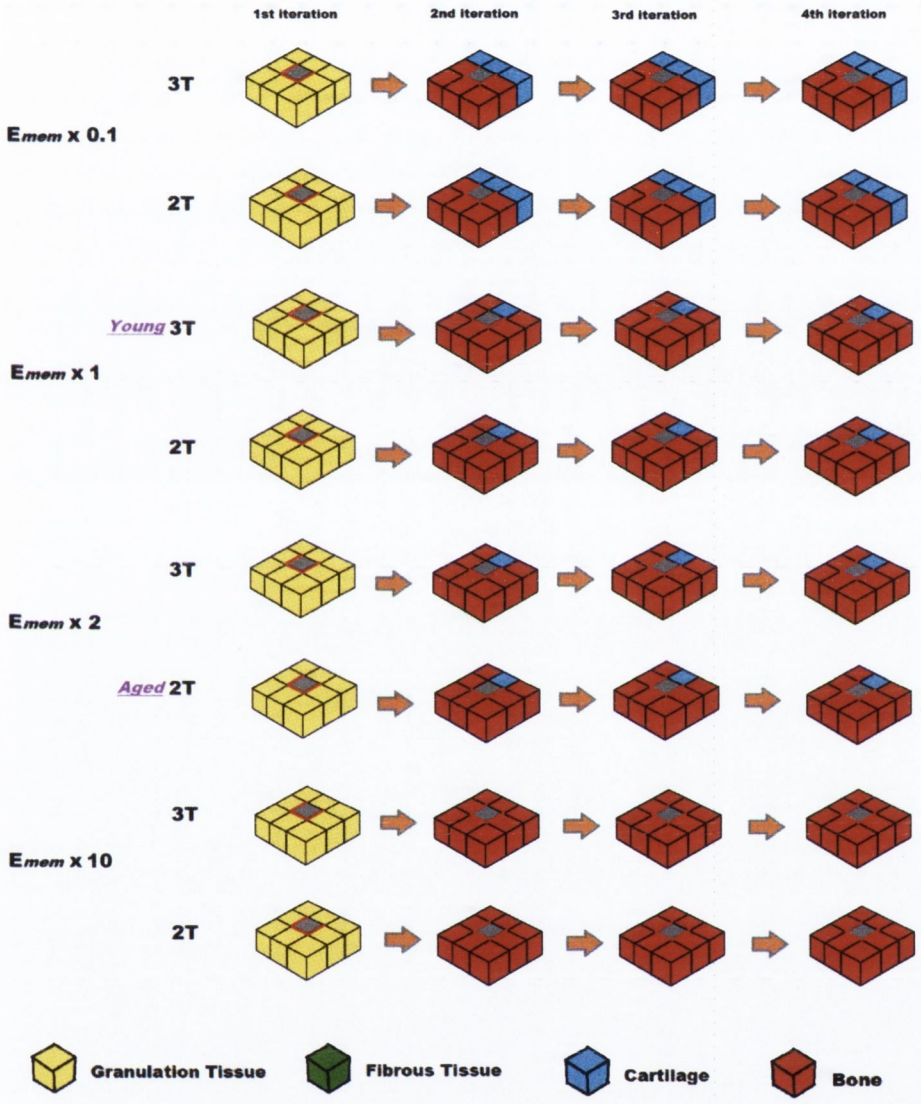


Figure J.4. Tissue differentiation patterns under motion-control with a loading magnitude of 3 μm with three debonding surfaces.